The 17th Baška Conference

GNSS

Global Navigation Satellite Systems

Green Navigation and Smart Systems

ISSN 3044-6171 (Online)
ISSN 3044-6112 (Print)

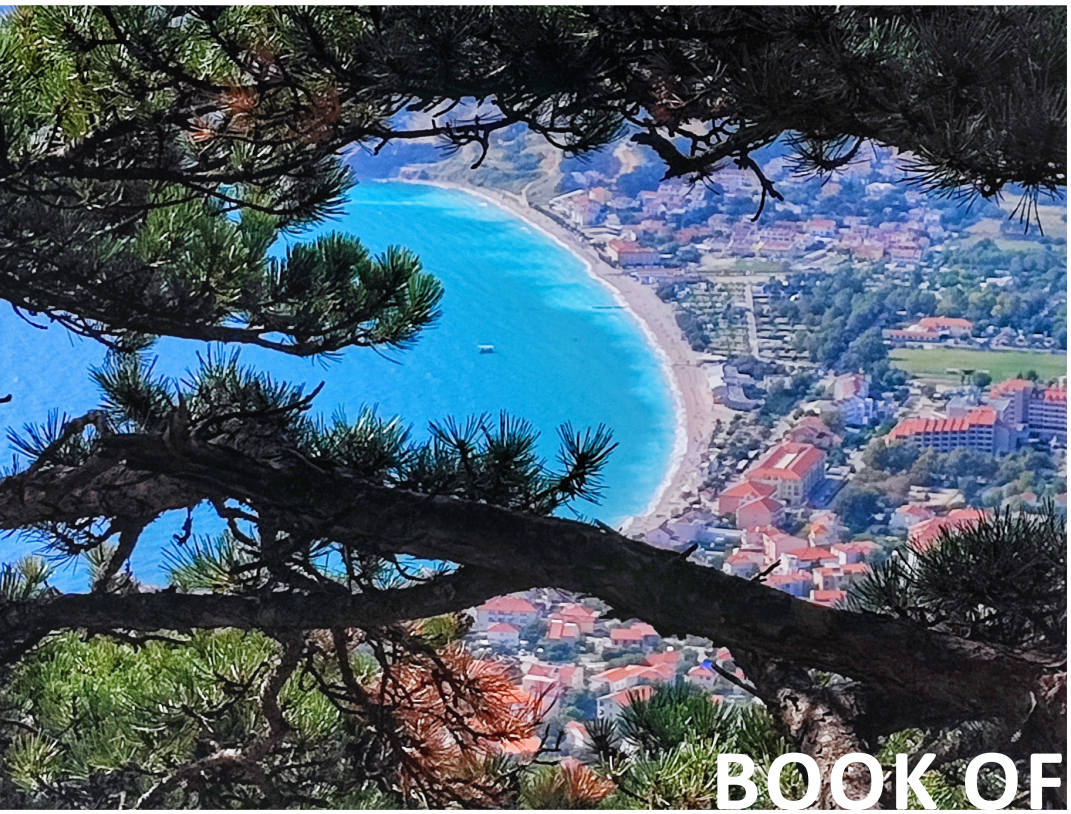

BOOK OF EXTENDED ABSTRACTS

17th Baška GNSS Conference:

Global Navigation Satellite Systems
and
Green Navigation and Smart Systems

Under the High Auspicies of

Baška, Krk Island, Croatia

11 – 15 May 2025

17th Baška GNSS Conference:

Global Navigation Satellite Systems and **Green Navigation and Smart Systems**

BOOK OF EXTENDED ABSTRACTS

17th Baška GNSS Conference: Global Navigation Satellite Systems and Green Navigation and Smart Systems – **BOOK OF EXTENDED ABSTRACTS**

ISSN 3044-6112 (Print) | ISSN 3044-6171 (Online)

Published by

University of Rijeka, Faculty of Maritime Studies, Rijeka, Croatia

For the Publisher

Assoc Prof Ana Perić Hadžić, PhD, Dean, University of Rijeka, Faculty of Maritime Studies, Rijeka, Croatia

Publishing Associates

Cynthia Robinson, OBE, FRIN, President, The Royal Institute of Navigation, London, UK
Ramsey Faragher, FRIN, Director, The Royal Institute of Navigation, London, UK

Editors-in-Chief

Assoc Prof David Brčić, PhD, University of Rijeka, Faculty of Maritime Studies, Rijeka, Croatia
Assoc Prof Marko Valčić, PhD, University of Zadar, Maritime Department, Zadar, Croatia

Editors

Assist Prof Nikola Lopac, PhD, University of Rijeka, Faculty of Maritime Studies, Rijeka, Croatia
Assoc Prof Mirjana Borucinsky, University of Rijeka, Faculty of Maritime Studies, Rijeka, Croatia
Prof Emer Serđo Kos, University of Rijeka, Faculty of Maritime Studies, Rijeka, Croatia

Proofreading

Assoc Prof Mirjana Borucinsky, University of Rijeka, Faculty of Maritime Studies, Rijeka, Croatia

Photo credits

Front page: *Stillness*, David Brčić

Text design

Tempora, Rijeka

Print

AKD d.o.o. Zagreb

Publisher's address

University of Rijeka, Faculty of Maritime Studies, Studentska 2, 51000 Rijeka, Croatia
Phone: +385 (0)51 338 411, Fax: +385 (0)51 336 755
URL: http://www.pfri.uniri.hr/, E-mail: dekanat@pfri.uniri.hr

Published biennially, in line with the conference schedule.

This edition published in 2025.

The 17th Baška Conference

GNSS

Global Navigation Satellite Systems

Green Navigation and Smart Systems

17th Baška GNSS Conference:

Global Navigation Satellite Systems and Green Navigation and Smart Systems

Under the High Auspicies of

BOOK OF EXTENDED ABSTRACTS

University of Zadar

Baška, Krk Island, Croatia

11 – 15 May 2025

ORGANISERS

Royal Institute of Navigation, London, United Kingdom; **University of Rijeka, Faculty of Maritime Studies**, Rijeka, Croatia; **University of Rijeka, Faculty of Engineering**, Rijeka, Croatia; **University of Zadar, Maritime Department**, Zagreb, Croatia; **University of Zagreb, Faculty of Transport and Traffic Sciences**, Zagreb, Croatia

MEDIA COVERAGE

Navigation News (London, UK), **Burza Nautike** (Rijeka, Croatia), **My Coordinates** (Delhi, India)

TECHNICAL CO-SPONSORS

University of Applied Sciences Hrvatsko Zagorje, Krapina,Croatia

INTERNATIONAL PROGRAM, SCIENTIFIC AND ORGANISING COMMITTEE

Conference chair:

John R Pottle, The Royal Institute of Navigation, London, UK

Conference co-chairs:

David Brčić, University of Rijeka, Faculty of Maritime Studies, Rijeka, Croatia; **Hrvoje Gold**, University of Zagreb, Faculty of Transportation and Traffic Sciences, Zagreb, Croatia; **Serdjo Kos**, University of Rijeka, Faculty of Maritime Studies, Rijeka, Croatia; **Jasna Prpić-Oršić**, University of Rijeka, Faculty of Engineering, Rijeka, Croatia; **Marko Valčić**, University of Zadar, Maritime Department, Zadar, Croatia

Programme chairs:

Marko Valčić, University of Zadar, Maritime Department, Zadar, Croatia; **David Brčić**, University of Rijeka, Faculty of Maritime Studies, Rijeka, Croatia

International Scientific and Organising Committee Members:

Clare Stead, Communications & Events Manager, The Royal Institute of Navigation, London, United Kingdom; **Đani Mohović**, University of Rijeka, Faculty of Maritime Studies, Rijeka, Croatia; **Danijel Šugar**, University of Zagreb, Faculty of Geodesy, Zagreb, Croatia; **Franc Dimc**, University of Ljubljana, Faculty of Maritime Studies and Transport, Portorož, Slovenia; **George Shaw**, General Lighthouse Authority, London, United Kingdom; **Gino Dardanelli**, The University of Palermo, Department of engineering, Palermo, Italy; **Helena Ukić Boljat**, University of Split, Faculty of Maritime Studies, Split, Croatia; **Josip Vuković**, University of Zagreb, Faculty of Electrical Engineering and Computing, Zagreb, Croatia; **Luca Braidotti**, University of Trieste, Department of Engineering and Architecture, Trieste, Italy; **Luka Grbić**, University of Zadar, Maritime Department, Zadar, Croatia; **Mario Muštra**, University of Zagreb, Faculty of Transportation and Traffic Sciences, Zagreb, Croatia; **Mariusz Specht**, Gdynia Maritime University, Gdynia, Poland;

Nenad Sikirica, Krapina University of Applied Sciences, Krapina, Croatia; **Neven Grubišić**, University of Rijeka, Faculty of Maritime Studies, Rijeka, Croatia; **Nikola Lopac**, University of Rijeka, Faculty of Maritime Studies, Rijeka, Croatia; **Ramsey Faragher**, Director, The Royal Institute of Navigation, London, United Kingdom; **Srđan Žuškin**, University of Rijeka, Faculty of Maritime Studies, Rijeka, Croatia; **Tomislav Josip Mlinarić**, University of Zagreb, Faculty of Transport and Traffic Sciences, Zagreb, Croatia; **Tomislav Kos**, University of Zagreb, Faculty of Electrical Engineering and Computing, Zagreb, Croatia; **Dea Aksentijević**, University of Rijeka, Faculty of Maritime Studies, Rijeka, Croatia; **Ivan Sulovsky,** University of Rijeka, Faculty of Engineering, Rijeka, Croatia; **Mirjana Borucinsky**, University of Rijeka, Faculty of Maritime Studies, Rijeka, Croatia; **Mario Bakota**, University of Split, Faculty of Maritime Studies, Split, Croatia; **Jana Kegalj**, University of Rijeka, Faculty of Maritime Studies, Rijeka, Croatia; **Marijana Balas**, University of Rijeka, Faculty of Engineering, Rijeka, Croatia; **Marko Strabić**, University of Rijeka, Faculty of Maritime Studies, Rijeka, Croatia; **Maro Car**, University of Dubrovnik, Maritime Department, Rijeka, Croatia; **Tomislav Krljan**, University of Rijeka, Faculty of Maritime Studies, Rijeka, Croatia

Reviewers:

Serdjo Kos, University of Rijeka, Faculty of Maritime Studies, Rijeka, Croatia; **Jasna Prpić-Oršić**, University of Rijeka, Faculty of Engineering, Rijeka, Croatia; **Nermin Hasanspahić**, University of Dubrovnik, Faculty of Maritime Studies, Dubrovnik, Croatia; **Đani Mohović**, University of Rijeka, Faculty of Maritime Studies, Rijeka, Croatia; **Franc Dimc**, University of Ljubljana, Faculty of Maritime Studies and Transport, Portorož, Slovenia; **Gino Dardanelli**, The University of Palermo, Department of engineering, Palermo, Italy; **Josip Vuković**, University of Zagreb, Faculty of Electrical Engineering and Computing, Zagreb, Croatia; **Luca Braidotti**, University of Trieste, Department of Engineering and Architecture, Trieste, Italy; **Mate Barić**, University of Zadar, Maritime Department, Zadar, Croatia; **Mario Muštra**, University of Zagreb, Faculty of Transportation and Traffic Sciences, Zagreb, Croatia; **Neven Grubišić**, University of Rijeka, Faculty of Maritime Studies, Rijeka, Croatia; **Nikola Lopac**, University of Rijeka, Faculty of Maritime Studies, Rijeka, Croatia; **Beldjiali Bilal**, Agence Spatiale Algerienne, Department of Space Geodesy, Algiers, Algeria

CONTENTS

PREFACE TO THE 17th EDITION

Welcome to the *17th Baška GNSS Conference: Global Navigation Satellite Systems and Green Navigation and Smart Systems*. Two GNSS acronyms in one title – both fully intentional. One points to the satellites above us, the other to the future paths we're building below: greener, smarter, more resilient.

This year's programme spans a wide range of research. Topics include GNSS receiver calibration, PNT as a service, performance of SBAS corrections, interference detection, and signal disruptions due to jamming and ionospheric activity. Several contributions explore mitigation strategies, including multi-sensor integration and the use of complementary technologies such as UWB and inertial systems. Maritime applications feature strongly, with work on AIS-based traffic modelling, ECDIS use, vessel detection, autonomous navigation, wind resistance estimation, and environmental risk assessment.

We are pleased to host six keynote talks that reflect both operational and strategic priorities: GNSS interference in the maritime domain, dynamic positioning for autonomy, mariners' reliance on GNSS, education and training, international cooperation, and PNT resilience. Two interactive workshops provide hands-on insight; one on discrete-event simulation in virtual reality, and another on GNSS positioning analysis.

And we're doing it all here in Baška – where the limestone cliffs meet the turquoise Adriatic, and where long days of sunshine make even complex algorithms feel a bit lighter. Take in the views, breathe in the sea air, and let the scenery inspire the science.

To our presenters, participants, supporters, and behind-the-scenes heroes – thank you. Let's make it a memorable one, again.

Editors

The 17th Baška Conference

GNSS

Global Navigation Satellite Systems

Green Navigation and Smart Systems

KEYNOTE ABSTRACTS

University of Zadar

UNINTENDED CONSEQUENCES OF GNSS INTERFERENCE IN THE MARITIME DOMAIN

Bridget Diakun

Lloyd's List Intelligence

Abstract. *Over the last year third-party interference with AIS data has become increasingly widespread and severe, particularly within the Black Sea. This is problematic not only from a safety point of view, but it also has serious repercussions in terms of risk and compliance.*

ARE MARINERS TOO DEPENDENT ON GNSS?

David Goddard

Marine navigation practitioner and Fellow of the Royal Institute of Navigation

Abstract. *GNSS has revolutionized marine navigation, by providing continuous accurate positioning. GNSS together with ECDIS has greatly improved spatial awareness at sea. However, GNSS is vulnerable to interference and denial, be it malicious or accidental. The case for the maintenance of alternative marine navigation systems and long-established traditional navigation skills remains strong. This presentation reminds mariners of the techniques available to ensure they can safely navigate independently of GNSS, both, to confirm GNSS positioning and as an alternative, should GNSS become unreliable.*

University of Zadar

LEVERAGING DYNAMIC POSITIONING TECHNOLOGIES FOR FUTURE AUTONOMOUS SHIPS: OPERATIONAL AND EDUCATIONAL PERSPECTIVES

Marko Valčić

University of Zadar, Maritime Department

Abstract. *The evolution of Dynamic Positioning (DP) systems offers a strong foundation for developing Maritime Autonomous Surface Ships (MASS). DP technologies, used for station-keeping and accurate low-speed manoeuvring, rely on advanced sensor fusion and control algorithms – key components also essential for autonomous navigation. Integrating LiDAR, SONAR, RADAR, GNSS, and AI-based decision-making within DP systems directly supports the situational awareness and positioning accuracy required for future MASS operations.*

Beyond technology, the transition to autonomous shipping requires skilled operators. DP Operator (DPO) certification programs, such as those by the Nautical Institute, provide structured system monitoring, emergency handling, and remote supervision training. These frameworks can be adapted to train Remote Vessel (RV) and MASS operators to oversee autonomous ships through Remote Operations Centres (ROCs). International efforts, including EMSA and Norway's Kongsberg-led initiatives, are already shaping standardized MASS training.

With IMO regulations for MASS expected by 2032, adapting DP expertise and training schemes will be crucial for a structured transition to autonomous maritime operations. Through initiatives like AGATI and DIH InnovaMare, Croatia is actively positioning itself in this technological shift.

University of Zadar

BUILDING ON THE SINGAPORE DECLARATION

Tom Southall

International Organization for Marine Aids to Navigation (IALA)

Abstract. *This address gives an update on the technical progress of IALA, whilst outlining the Organizations commitment to green navigation, highlighting its efforts to integrate environmentally responsible practices into Marine Aids to Navigation. The address will also cover the Singapore Declaration, marking IALA's transition to an IGO and provide an update on IALA's work in facilitating the development of enhanced decision support tools and digitization.*

YOUNG GNSS EDUCATION AND TRAINING (yGET): AN OVERVIEW

David Brčić

University of Rijeka, Faculty of Maritime Studies

Abstract. *As GNSS technologies continue to evolve, integrating GNSS education into nautical studies and maritime transport technology provides students with valuable insights into its principles, limitations, and practical applications. This keynote explores the development, structure, and future directions of an educational framework within Nautical Studies and Maritime Transport Technology, with a focus on the Satellite Navigation course. The course follows a progressive learning approach, gradually increasing task complexity to develop critical thinking, data interpretation skills, and problem-solving abilities. Students engage in hands-on exercises, acquiring and processing GNSS data while learning to present results using statistical, graphical, and descriptive methods. Special focus is given to reading and interpreting 'smart' visualizations that reveal key insights into GNSS performance. The curriculum starts with an introduction to GNSS fundamentals and essential programming tools for data processing. Students generate position records using GNSS ground truth data from reference networks and complement these with their own positioning solutions, recorded from mobile devices and other receivers. Step by step, they analyse accuracy degradation, satellite-receiver geometry effects, and error sources such as ionospheric and tropospheric delays, multipath interference, and clock biases. Throughout, they are encouraged to critically assess their findings, discuss sources of uncertainty, and refine their methodologies. In the final phase, students explore advanced positioning techniques like Precise Point Positioning (PPP) and Real-Time Kinematics (RTK), as well as various data formats, including*

University of Zadar

NMEA, commonly used in maritime navigation. By the end of the course, they are prepared to undertake and deliver independent research, applying their acquired skills to real-world GNSS challenges. This keynote highlights the pedagogical approach behind the course, emphasizing hands-on learning, structured discussions, and the integration of GNSS applications in everyday life. By progressively increasing task complexity and fostering inquiry-driven learning, the course equips students with the expertise needed for both professional practice and academic research in the area of satellite navigation.

The course was initially developed through a collaborative effort, reflecting shared expertise and contributions of people involved in shaping its content and methodology. Beside the lecturer, the initiators and developers are prof. Renato Filjar, PhD, FRIN, Prof. Emer. Serdjo Kos, PhD, FRIN, and Barbara Brčić, M.Eng. (Naut.)

LATEST "BEST PRACTICES" APPROACHES FOR ACHIEVING PNT RESILIENCE AND PREPAREDNESS

John Pottle

The Royal Institute of Navigation

Abstract. *It is more than two decades since the seminal 2001 Volpe report, which highlighted vulnerabilities in satellite-derived time and position. Over this time, the enticing accuracy from global navigation satellite systems (GNSS) has led to an uncomfortable over-reliance, with insufficient regard to resilience to all manner of vulnerabilities.*

Now, in 2025, governments around the world are beginning to respond. The responses that we are seeing vary widely. But why? And will they be effective? This talk analyses what is being done and compare and contrast the different approaches being taken. Is what we are seeing rational, based on expert assessment, driven by clear objectives? Or too-little-too-late and poorly thought through?

The 17th Baška Conference

GNSS

Global Navigation Satellite Systems

Green Navigation and Smart Systems

WORKSHOPS' ABSTRACTS

University of Zadar

DISCRETE-EVENT SIMULATION WITH VIRTUAL REALITY: COUPLING CFD AND VR FOR ADVANCED FIREFIGHTING TRAINING

Darko Glujić, Goran Vukelić

University of Rijeka, Faculty of Maritime Studies

Abstract. *Join us for an immersive workshop showcasing an advanced Virtual Reality (VR) maritime firefighting application. This cutting-edge simulation places participants inside a two-storey ship engine room, where realistic fire scenarios unfold. The fire behaviour in the VR environment is driven by Computational Fluid Dynamics (CFD) analysis, ensuring accurate and dynamic fire spread based on real-world physics. CFD results have been seamlessly integrated into the VR system, creating a highly authentic training experience. Participants will have the opportunity to test the application first hand using VR head-mounted devices, experiencing realistic emergency scenarios and engaging in critical firefighting decision-making.*

SELECTED TOPICS ON GNSS POSITIONING ANALYSIS WITH EXAMPLES IN R

David Brčić

University of Rijeka, Faculty of Maritime Studies

Abstract. *This hands-on workshop explores GNSS positioning through the lens of scientific data analysis using R and RStudio. Participants will work with RINEX data from global and local reference stations to develop both standard and advanced positioning solutions, including DGPS and RTK methods. The session builds on practical modules used in academic coursework, encouraging a seminar-style discussion of results, methods, and scientific reasoning. Emphasis is placed on data interpretation, error analysis, and the integration of programming with GNSS concepts for applied and research-focused use.*

The 17th Baška Conference

GNSS

Global Navigation Satellite Systems

Green Navigation and Smart Systems

EXTENDED ABSTRACTS

University of Zadar

The 17th Baška Conference
GNSS
Global Navigation Satellite Systems
Green Navigation and Smart Systems

GNSS RECEIVER ANTENNA CALIBRATION AND APPLICATION

Antonio Tupek*, Mladen Zrinjski, Krunoslav Špoljar, Karlo Stipetić

University of Zagreb, Faculty of Geodesy, Zagreb, Croatia

* *Corresponding author:* Antonio Tupek (antonio.tupek@geof.unizg.hr)

Abstract. *Carrier-phase observations are essential in high-accuracy Global Navigation Satellite Systems (GNSS) positioning applications. The quality of these observations is influenced by receiver antenna electrical signal reception characteristics. To eliminate the corresponding range errors, phase centre corrections (PCCs), determined through antenna calibration, need to be applied. In 2023, the Laboratory for Measurements and Measuring Technique (LMMT) of the University of Zagreb – Faculty of Geodesy developed a receiver antenna absolute field calibration system from the ground up. The system delivers meaningful and reliable dual-frequency GPS antenna calibration results. Within this study, the system has been further evaluated through a short-baseline test and a PPP test. Furthermore, it is investigated how the application of different PCC models (LMMT individual or IGS type-mean) impacts the performance of high-accuracy global positioning. The obtained results confirmed LMMT individual PCC models yield improved baseline accuracy, and that the application of type-mean models can result in millimetre-level station position offsets.*

Keywords: *absolute calibration; antenna; dual-frequency; GNSS; industrial robot; phase centre correction (PCC)*

University of Zadar

1. INTRODUCTION

To achieve high global positioning accuracy, Global Navigation Satellite Systems (GNSS) receivers and antennas are key sensors. However, it is crucial to address all influential factors and error sources appropriately. One critical factor affecting position accuracy is the variability of the receiver antenna phase centre (PC) [1], which necessitates the introduction of phase centre corrections (PCCs). PCCs are essentially direction- and frequency-dependent range corrections, predetermined through antenna calibration, and applied to carrier-phase observations within the GNSS data processing workflow. Several antenna calibration methods and approaches are developed, but the *absolute calibration* approach represents the state-of-the-art methodology [2].

Recognizing the significance of this field of research, several institutions have developed or are advancing their GNSS receiver antenna robotic calibration system [2–5]. Due to a strong scientific and practical impetus, in 2023, the development of a new GNSS receiver antenna absolute field calibration system began at the Laboratory for Measurements and Measuring Technique (LMMT) of the University of Zagreb – Faculty of Geodesy [2]. Published studies have demonstrated that the system delivers meaningful and reliable dual-frequency GPS calibration results [6,7].

This contribution concisely presents the calibration system developed at LMMT. Also, the system was further evaluated through a short-baseline test, and a PPP test the results and conclusions of which are summarized in the following sections. The primary research question concerns how the application of different PCC models (LMMT individual or IGS type-mean) impacts the performance of high-accuracy global positioning.

2. METHODOLOGY

The LMMT GNSS receiver antenna calibration system is an absolute field calibration system grounded in the principles of absolute antenna calibration [8]. The system comprises a six degrees of freedom (DOF) robot arm Mitsubishi MELFA RV-4FLM-Q. An on-site calibration set-up is shown in **Figure 1**. The PCC modelling is founded on the principles of the triple-difference (TD) methodology. Raw carrier-phase observations that are registered by the antenna-under-test (AUT) and the reference (REF) antenna are spatially and temporally differentiated to form time-differences of the double-difference (DD) observations [9]. The resulting

Figure 1. On-site set-up of the LMMT antenna calibration system [7]. The industrial robot Mitsubishi MELFA RV-4FLM-Q with the installed antenna-under-test (AUT) Leica Geosystems AX1202 GG and the reference (REF) antenna Trimble Zephyr 2 Geodetic. Baseline length is approx. 5 m. Both antennas are connected to Trimble NetR5 GNSS receivers.

TDs are parametrised by spherical harmonic (SH) expansion, converted to phase centre offset (PCO) and phase centre variations (PCVs), and exported to the ANTEX file format. A full system's description is provided in [2].

To further substantiate the validity of the developed system, two GNSS receiver antennas have been individually calibrated at LMMT: a Trimble Zephyr 2 Geodetic antenna (TRM571971.00 NONE) and a Leica Geosystems AX1202 GG antenna (LEIAX1202GG NONE). Dual-frequency GPS calibration results (GPS L1 – G01 and GPS L2 – G02) have been estimated. Initially, a short-baseline validation utilizing known ground truth was performed, followed by a PPP test. The primary goal of this study is to analyse how the application of different PCC models (LMMT individual or IGS type-mean) reflects on coordinate determination and high-accuracy global positioning.

Within the short-baseline test, on a 10-meter-long short-baseline both GNSS antennas have been positioned and a 6-hour-long static GNSS (GPS) survey was performed with an observation interval of 1 s. Reference values of baseline components have been previously determined. In data processing, short-baseline components are determined twice in relative positioning approach and under identical processing parameters except for the PCC models applied, i.e., firstly IGS type-mean and secondly, LMMT individual. Knowing the reference values, the impact of the PCC model on baseline accuracy is evaluated. Furthermore, in the second PPP test, the impact of antenna model on single station position is evaluated. For that purpose, based on the collected GNSS (GPS) observations on one station, two separate PPP GPS-only runs have been performed by identical processing parameters except for the antenna PCC models applied.

3. RESULTS AND DISCUSSION

Figure 2 shows individual dual-frequency GPS (G01 and G02) calibration results, i.e., PCO components and PCV grids, estimated at LMMT for the Trimble Zephyr 2 Geodetic GNSS antenna. A notable difference of 7.72 mm in the PCO Up component between the G01 and G02 frequencies warrants emphasis. Both PCC models show dominant elevation angle dependency with PCV values in total range of 11 mm.

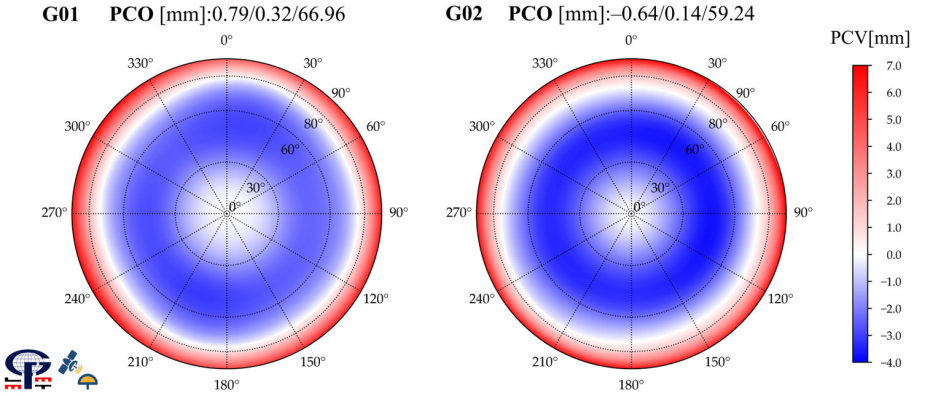

Figure 2. Individual calibration results (PCO and PCV) by LMMT for the Trimble Zephyr 2 Geodetic GNSS antenna at frequencies GPS L1 (G01) and GPS L2 (G02).

According to the short-baseline test methodology, topocentric coordinate differences and corresponding errors are determined and are presented in **Table 1**. The results show that the application of LMMT individual PCC models led to higher baseline accuracy for both analysed frequencies (G01 and G02).

Table 1. Topocentric coordinate errors (per component and spatial) per frequency and PCC model.

Freq.	PCC model	East [mm]	North [mm]	Up [mm]	3D [mm]
G01	IGS (*igs20_2283.atx*)	–0.6	–1.3	–2.1	2.5
	LMMT	–1.2	0.1	1.3	1.8
G02	IGS (*igs20_2283.atx*)	0.0	2.7	0.0	2.7
	LMMT	–1.1	1.5	0.1	1.8

In addition, station position offsets obtained within the PPP test are given in **Table 2**. The resulting offsets are directly attributable to the applied antenna PCC model with the total spatial (3D) offset measuring 9.1 mm.

Table 2. Station position offsets expressed in topocentric frame.

East [mm]	North [mm]	Up [mm]	3D [mm]
–2.8	5.7	6.5	9.1

4. CONCLUSIONS

This study investigates the influence and extent to which different receiver antenna calibration models, specifically LMMT individual and IGS type-mean models, transfer to the coordinate domain and reflect on high-accuracy global positioning. Short-baseline analysis confirmed that LMMT individual PCC models yield improved baseline accuracy. Furthermore, because of different PCC models, single station position offsets reach up to 6 mm in both the horizontal (2D) and vertical component. In conclusion, our results demonstrated limitations of type-mean antenna models, proving that these models do not universally represent actual receiver antenna signal reception properties.

REFERENCES

[1] Maqsood, M., Gao, S., Montenbruck, O. (2017). Antennas. In: Teunissen, P. J. & Montenbruck, O. (eds.) *Springer Handbook of Global Navigation Satellite Systems,* pp. 505–534. Springer Handbooks. Springer, Cham. https://doi.org/10.1007/978-3-319-42928-1_17.

[2] Tupek, A. (2024). *Development of an Absolute GNSS Antenna Field Calibration System*. Doctoral dissertation. Zagreb: University of Zagreb – Faculty of Geodesy.

[3] Hu, Z., Zhao, Q., Chen, G., Wang, G., Dai, Z., Li, T. (2015). First Results of Field Absolute Calibration of the GPS Receiver Antenna at Wuhan University. *Sensors*, 15, pp. 28717–28731. doi: 10.3390/s151128717.

[4] Willi, D., Lutz, S., Brockmann, E., Rothacher, M. (2020). Absolute Field Calibration for Multi-GNSS Receiver Antennas at ETH Zurich. *GPS Solutions*, 24 (28), pp. 1–15. doi: 10.1007/s10291-019-0941-0.

[5] Kröger, J., Kersten, T., Breva, Y., Schön, S. (2021). Multi-frequency multi-GNSS receiver antenna calibration at IfE: Concept—Calibration results—Validation. *Advances in Space Research*, 68 (12), pp. 4932–4947. doi: 10.1016/j.asr.2021.01.029.

[6] Tupek, A., Zrinjski, M., Švaco, M., Barković, Đ. (2023). GNSS Receiver Antenna Absolute Field Calibration System Development: Testing and Preliminary Results. *Remote Sensing*, 15, pp. 1–21. doi: 10.3390/rs15184622.

[7] Tupek, A., Zrinjski, M., Špoljar, K., Stipetić, K. (2025). Experimental Validation of a GNSS Receiver Antenna Absolute Field Calibration System. *Remote Sensing*, 17, pp. 1–22. doi: 10.3390/rs17010064.

[8] Wübbena, G., Schmitz, M., Menge, F., Seeber, G., Völksen, C. (1997). A New Approach for Field Calibration of Absolute GPS Antenna Phase Center Variations. *Navigation*, 44 (2), pp. 247–255. doi: 10.1002/j.2161-4296.1997.tb02346.x.

[9] Hauschild, A. (2017). Combinations of Observations. In: Teunissen, P. J. & Montenbruck, O. (eds.) *Springer Handbook of Global Navigation Satellite Systems,* pp. 583–604. Springer Handbooks. Springer, Cham. https://doi.org/10.1007/978-3-319-42928-1_20.

The 17th Baška Conference
GNSS
Global Navigation Satellite Systems
Green Navigation and Smart Systems

AUTOMATED CHARACTERIZATION OF JAMMING EFFECTS ON LOW-COST GNSS RECEIVER PERFORMANCE

Staš Dolinšek[1*], Polona Pavlovčič Prešeren[2], Boštjan Batagelj[1], Aljaž Blatnik[1]

[1] University of Ljubljana, Faculty of Electrical Engineering, Slovenia
[2] University of Ljubljana, Faculty of Civil and Geodetic Engineering, Slovenia
[*] *Corresponding author:* Aljaž Blatnik (aljaz.blatnik@fe.uni-lj.si)

Abstract. *Unpredictable intermittent GNSS signals complicate receiver evaluation. Simulations, using controlled jamming, isolate interference effects. We assessed low-cost receiver behaviour in jamming conditions, revealing signal and positioning degradation. Significant variations, even in simulation environment, emphasize the need for statistical analysis of GNSS measurements. This study evaluates receiver responses through repeated measurements under identical conditions.*

Keywords: *GNSS; jamming; GNSS simulator; GNSS receiver*

University of Zadar

1. INTRODUCTION

Testing GNSS receivers in real-world conditions provides insight into their performance in different environments, such as urban areas, open spaces, forests, or underground structures. However, field testing has significant limitations, primarily due to the non-repeatability of measurements, the inability to control environmental parameters, and limited options for interference assessment [1].

GNSS satellites are constantly moving, causing measurement parameters like satellite positioning, observation geometry, and signal quality to change over time. Atmospheric conditions and signal reflections add further unpredictability, making identical measurements impossible, even for a stationary receiver. Achieving true repeatability in the field is nearly impossible. Even with back-to-back tests, conditions continuously change [2]. Let us assume that we conduct 50 three-minute measurements to analyse receiver performance. While the first few may occur under similar conditions, satellite geometry, ionospheric and tropospheric effects, and multipath interference shift over time. By the final test, conditions may differ significantly, making direct comparisons unreliable.

Using multiple identical receivers can reduce temporal variability but introduces logistical challenges, costs, and potential discrepancies from receiver processing or local reflections [3]. These limitations highlight why field testing alone is insufficient for evaluating GNSS performance, as variability in satellite geometry, environmental effects, and receiver behaviour makes repeatable testing unfeasible.

2. GNSS SIMULATION FOR REPEATABLE TESTING

A GNSS simulator provides a controlled environment where all parameters can be precisely set and repeated. The process starts by defining the date, time, and receiver location. Using almanac data, the simulator accurately reproduces satellite positions and movements. It then transmits simulated signals that mimic real satellite transmissions.

This ensures identical test conditions—same satellites, signal strengths, and modelled atmospheric effects—allowing direct performance comparisons without environmental interference. Simulators also introduce controlled impairments like multipath, signal loss, and interference, making them essential for systematic GNSS receiver testing [4].

This research examined how different interference types and power levels affect GNSS receivers. Field tests showed high variability in receiver behaviour, making it unclear whether fluctuations in C/N_0 and position estimates were due to interference or changing conditions. A controlled test environment was needed to isolate interference effects. To achieve this, an automated system was implemented with a GNSS signal generator, an interference generator, a directional coupler, and a computer. High-end GNSS simulators offer built-in interference generation but at a high cost. Our mid-range Keysight system lacked this, except for basic CW interference. By adding a directional coupler and a standard lab signal generator, we enabled advanced interference testing, bringing mid-range simulators closer to high-end capabilities while maintaining flexibility. The directional coupler combined GNSS and interference signals with minimal loss and prevented unintended interactions. This setup ensured signal integrity while avoiding leakage that could disrupt nearby devices, eliminating regulatory constraints of real-world jamming tests. Each test began by restarting the GNSS simulation and cold-resetting receiver for identical starting conditions. After a two-minute stabilization, data collection started, introducing interference at specific times to analyse receiver response. Unlike field tests, this controlled setup ensured repeatability, enabling precise assessment of jamming effects. A similar approach was used by Craven et al. [5], who analysed GNSS interference under controlled conditions. Our research builds on this by incorporating repeated measurements, providing a more detailed assessment of receiver variability.

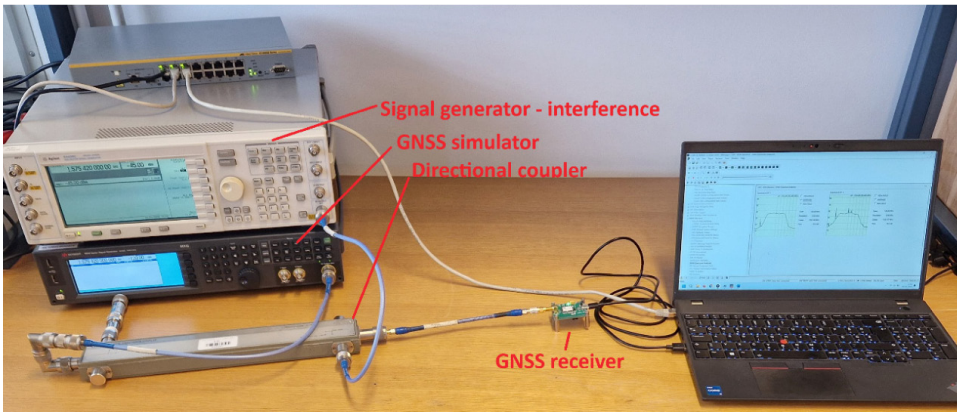

Figure 1. Measurement setup.

Each measurement had three phases: 100 seconds without interference for receiver stabilization, 100 seconds with controlled interference to assess its impact on positioning and signal reception, and 100 seconds for recovery. This scenario simulated operation under normal conditions, interference effects, and recovery, enabling systematic evaluation of jamming impact. The simulator reproduced the full GPS, Galileo, and BeiDou constellations throughout testing. Measurements included three interference types at various power levels. Continuous wave (CW) interference used a single-frequency signal at 1575.42 MHz (GPS L1). Frequency modulation (FM) interference applied an FM-modulated signal at the same frequency, with 8 MHz deviation and 1 kHz modulation. Frequency hopping switched every 0.01 seconds between 1575.42 MHz and ±735 kHz, affecting GPS L1 and potentially Galileo E1.

3. RESULTS AND DISCUSSION

The following graph presents the carrier-to-noise ratio (C/N_0) of individual satellites over 50 test runs. Each line represents a satellite in a given test. If used for position calculation, it appears in the blue-yellow spectrum; otherwise, it is shown in grey. The red line represents interference power, with values shown on the right scale.

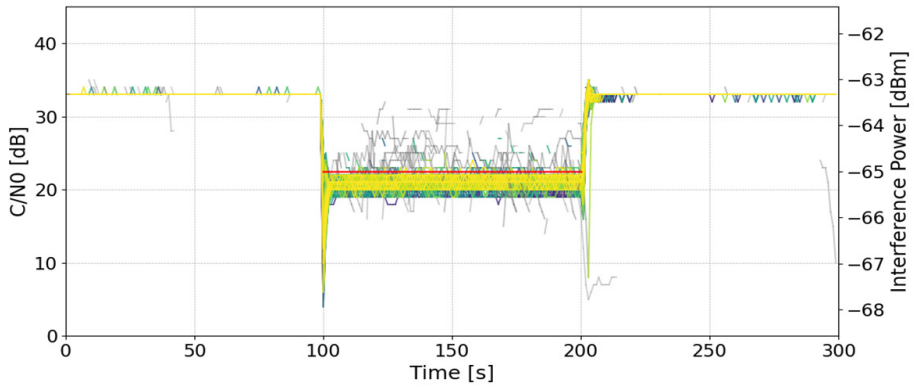

Figure 2. BeiDou CW interference -65 dBm.

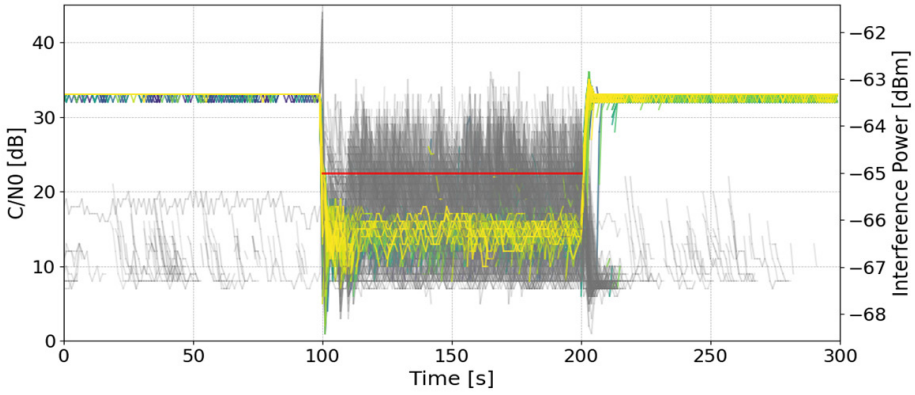

Figure 3. GPS CW interference -65 dBm

Only repeated measurements under identical conditions fully capture the range of C/N_0 values a receiver may experience under interference. A single test might suggest a specific outcome, but multiple trials reveal the full variability in signal reception. In the first 100 seconds without interference, satellites maintain stable C/N_0 values, often overlapping in the graph. However, during the 100 – 200 second interval, interference causes significant fluctuations. CW interference at 1575.42 MHz affects GPS satellites more than BeiDou, as it directly overlaps with GPS L1. Many GPS satellites drop out of position calculations, while their C/N_0 values decrease significantly, whereas BeiDou remains less affected.

The next graphs show latitude (top) and longitude (bottom) deviations over time, with standard deviation values marked at 50s, 150s, and 250s to assess accuracy. A black dashed line represents the mean position estimate, while the red line indicates interference power in dBm. Interference increases position deviations, as seen in higher standard deviation values and greater dispersion. The position was calculated based on signals from GPS, Galileo, and BeiDou constellations. As jamming power rises, accuracy decreases, fluctuations grow, and GNSS positioning becomes increasingly unstable.

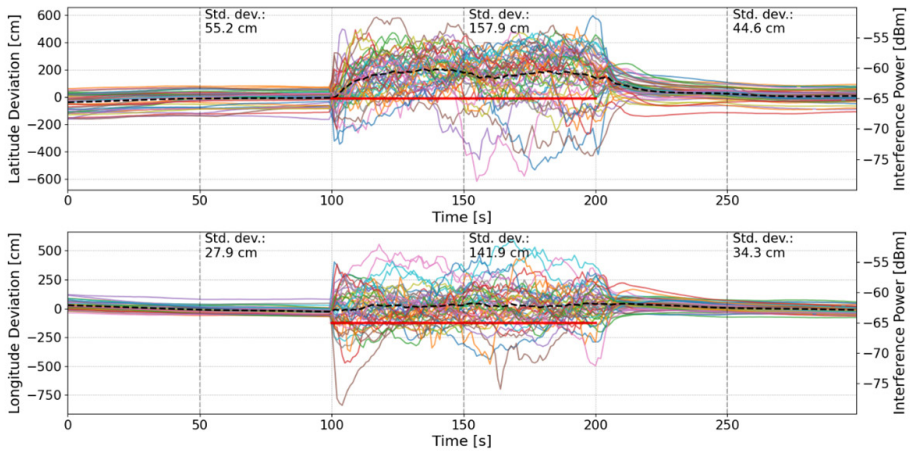

Figure 4. Latitude and longitude deviation with -65 dBm FM interference.

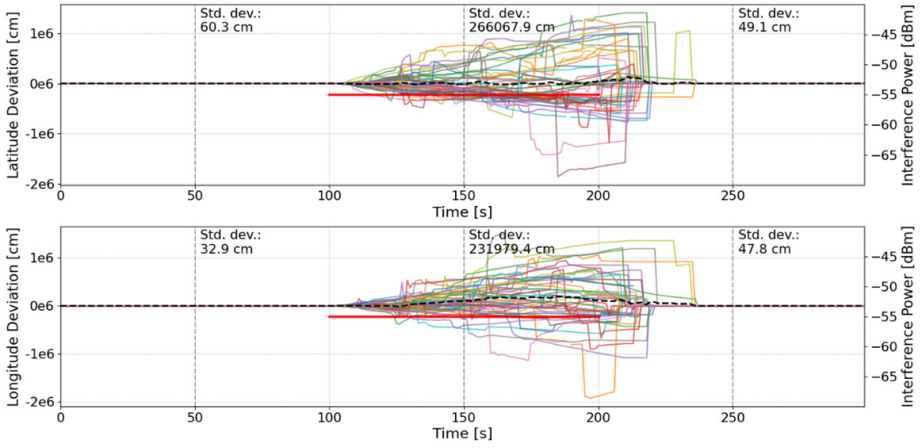

Figure 5. Latitude and longitude deviation with -55 dBm FM interference.

4. CONCLUSION

This level of insight into receiver behaviour is only possible in a controlled simulation environment, where identical conditions enable precise evaluation. Without such a setup, interference effects would be nearly impossible to isolate due to environmental variability. GNSS simulation remains the most reliable method for systematically analysing receiver performance and defining its limits.

Acknowledgements: This work was supported by the Slovenian Research and Innovation Agency (ARIS) under grant V2-2342 and L7-60164.

REFERENCES

[1] T. Morong, P. Puričer, and P. Kovář, "Study of the GNSS Jamming in Real Environment," Int. J. Electron. Telecommun., pp. 65–70, Jan. 2019, doi: 10.24425/ijet.2019.126284.

[2] H. Elghamrawy, M. Karaim, M. Tamazin, and A. Noureldin, "Experimental Evaluation of the Impact of Different Types of Jamming Signals on Commercial GNSS Receivers," Appl. Sci., vol. 10, no. 12, p. 4240, Jun. 2020, doi: 10.3390/app10124240.

[3] D. Borio, F. Dovis, H. Kuusniemi, and L. Lo Presti, "Impact and Detection of GNSS Jammers on Consumer Grade Satellite Navigation Receivers," Proc. IEEE, vol. 104, no. 6, pp. 1233–1245, Jun. 2016, doi: 10.1109/JPROC.2016.2543266.

[4] L. Biagi, F. Grec, and M. Negretti, "Low-Cost GNSS Receivers for Local Monitoring: Experimental Simulation, and Analysis of Displacements," Sensors, vol. 16, no. 12, p. 2140, Dec. 2016, doi: 10.3390/s16122140.

[5] P. Craven, R. Wong, N. Fedora, and P. Crampton, "Studying the Effects of Interference on GNSS Signals," in Proceedings of the 2013 International Technical Meeting of The Institute of Navigation, San Diego, California, Jan. 2013.

The 17th Baška Conference
GNSS
Global Navigation Satellite Systems
Green Navigation and Smart Systems

GNSS SIGNAL INTERFERENCE MEASUREMENT IN THE PORT OF KOPER

Matej Bažec[1*], Franc Dimc[1], Gianmarco Baldini[2], Polona Pavlovčič-Prešeren[3]

[1] University of Ljubljana, Faculty of Maritime and Transportation Studies, Portorož, Slovenia

[2] Joint Research Center, Ispra, Italy

[3] University of Ljubljana, Faculty of Civil Engineering and Geodesy, Ljubljana, Slovenia

[*] *Corresponding author:* Matej Bažec (matej.bazec@fpp.uni-lj.si)

Abstract. *Unintentional electromagnetic interference affecting GNSS signals was detected in the Port of Koper. Although the interference is relatively weak, it poses a risk to the continuous functioning of certain modern systems that rely on precise positioning, such as automated cranes. A spectrum survey around the GPS L1 frequency band was conducted in a section of the port, revealing several areas with significant, time-stable interference. This suggests that the source is stationary rather than mobile, e.g., a ship or truck. The collected data was analysed to assist port authorities in identifying the origin of the interference.*

Keywords: *GNSS; electromagnetic interference*

University of Zadar

1. INTRODUCTION

Modern positioning, radio navigation, and timing systems rely on global navigation satellite systems (GNSS). Efficient port operations require dependable infrastructure services. For instance, GNSS plays a crucial role in optimizing container movement by automated cranes, ensuring both spatial and temporal efficiency. However, GNSS signals are inherently weak at the Earth's surface, making them highly vulnerable to electromagnetic interference. Improperly configured communication systems can unintentionally generate such interference, potentially disrupting operations.

The GNSS spectrum is densely populated, with four independent global systems sharing frequency bands between 1156 and 1605 MHz. As GNSS usage expands in the civilian sector, unintentional interference has become a growing security concern. This makes interference detection and mitigation essential to maintaining infrastructure integrity. Even properly configured smartphones can assist in detecting interference by leveraging their location data to identify and mitigate potential disruptions.[1]

Research on electromagnetic interference detection and localization is extensive, particularly in the context of GNSS. A comprehensive review of all available studies would be too broad, so this survey focuses on recent research utilizing state-of-the-art equipment, ranging from high-end to low-budget solutions. A widely used method for detecting interference involves monitoring the carrier-to-noise density ratio (CNR), as most GNSS receivers can provide this data (e.g., via the GSV (satellites in view) sentence in the NMEA (National Marine Electronic Association) standard). [2, 3] Additionally, automatic gain control (AGC) can serve as an indicator if supported by the device, though it is rarely used independently. [4, 5]

Interference detection can also be achieved through crowdsourcing, leveraging either low-cost receivers in handheld devices or an array of geodetic instruments to estimate the location of the source of interference. [6,7] Another increasingly popular approach is the use of software-defined radio (SDR) to detect and even classify interference. This method has gained traction due to the significant drop in SDR receiver cost, making it more accessible for practical applications.

2. METHODOLOGY

The spectrum was acquired with the UBlox ZED-F9P that can monitor the spectrum around the GPS L1 (1519.46 MHz - 1646.96 MHz) and the L5 (1127.47 MHz - 1254.97 MHz) frequency. For this purpose, the MON-SPAN messages of the UBlox proprietary UBX protocol were recorded to a computer. The original provided patch antenna within UBlox evaluation kit was used for this purpose. It should be stressed out that the built-in spectral analyser is meant only for a coarse overview of the spectrum to rapidly identify a possible presence of an interfering signal.

To detect anomalies, a baseline of the power distribution was needed for the calculation of discrepancies. For this purpose, the average over the acquired distributions of the presumably non-interfered samples was used. This was achieved using the following algorithm. First, a point by point (in the sense of a fixed frequency) average and standard deviation were calculated indiscriminately of whether a sample was interfered or not. In the second step, the same has been done, only that the samples that deviated more than three times the standard deviation (3σ) were not included in the calculation. The last step was repeated a few times up to the convergence.

The reasoning beyond the algorithm above was that the points that deviate more than 3σ are probably interfered. Of course, there is a probability that some omitted points were non-interfered (assuming the normal distribution there should be 0.3% such points) and some interfered points were included in the baseline calculation. However, since most samples were non-interfered, those should not significantly affect the result.

3. QUANTIFYING THE INTERFERENCE

In order to objectively measure the amount of interference, different metrics were used that can be grouped into three categories according to what a metric is based on:

- receiver parameters,
- spectrum variations from the baseline and
- carrier to noise density ratio (CNR) for a particular set of satellites.

In the first group the value of PGA (programmable gain amplification) of the AGC (automatic gain control) unit of the receiver was used as the metric. Receivers typically try to maximize the PGA to exploit the full resolution of the ADC (analogue to digital converter). If a strong interference is present, it typically saturates the ADC unless PGA is decreased. Such an approach has already been used.[8]

In the second group the following metrics were observed: the maximum discrepancy from the spectrum baseline, the average discrepancy and the number of excluded points of the current spectrum in the baseline calculation.

In the third group only GPS satellites were considered. The metrics involved were the average CNR for all the GPS satellites with the elevation above some threshold, 30° for the first and 50° for the second.

4. INTERFERENCE LOCALIZATION

The algorithm to localize the interference source was designed to locate one or more sources of interference in an urban area. The algorithm assumes that the interfering signal would degrade the CNR values of a GNSS receiver in a proportional way to the power of the source or its distance from the receiver. The problem is that there are three unknowns:

1. The power is not known
2. The location is not known
3. The orography of the urban city is not known. The interference power could be altered not by the distance to the GNSS receiver but by the presence of buildings and obstacles.

The data, which can be used to detect the interferences are the CNR values in addition to the radio frequency spectrum snapshots. Then, an empirical approach is adopted where circles are drawn around each position of the vehicle with a radius, which is inversely proportional to the value of CNR or directly proportional to the peak of the radio frequency spectrum snapshot. This approach is well documented in literature [9]. The proposed approach is composed of the following steps:

- Convert latitude and longitude to cartesian coordinates.
- Extract the L1 and L5 CNR.

- Find the intersections of circles starting from the moving point (vehicle or boat).

Due to the large number of points and the fact that we are only interested in identifying the presence of interference, only the CNR values less than 38dB were considered. The radius of the circle is another hyper-parameter, because the power of the source it is not known, which may impact its value. A scale of radius of 75 meters for dB-Hz of the CN/0 starting from 30 was chosen.

5. RESULTS

The survey was conducted on the following days:

- inside the port area on 5/7/24 and 6/14/24,
- in the vicinity water area on 5/29/24 and
- outside the port area yet adjacent to it on 5/27/24.

For the sake of brevity, only the combined map plots are shown with a few selected metrics: maximum and average spectrum distortion, AGC and CNR of satellites over 30°.

As can be seen from the **Figure 1**, the metrics show deviation from the expected values primarily in the same areas: north, south and north-east of the second basin and south of the first basin. There are, however, some differences in the amount of variation. For instance, the north-eastern part of the second basin has a strong maximum deviation from the spectrum baseline, but a weak average deviation. That indicates an interference source with a very narrow frequency peak.

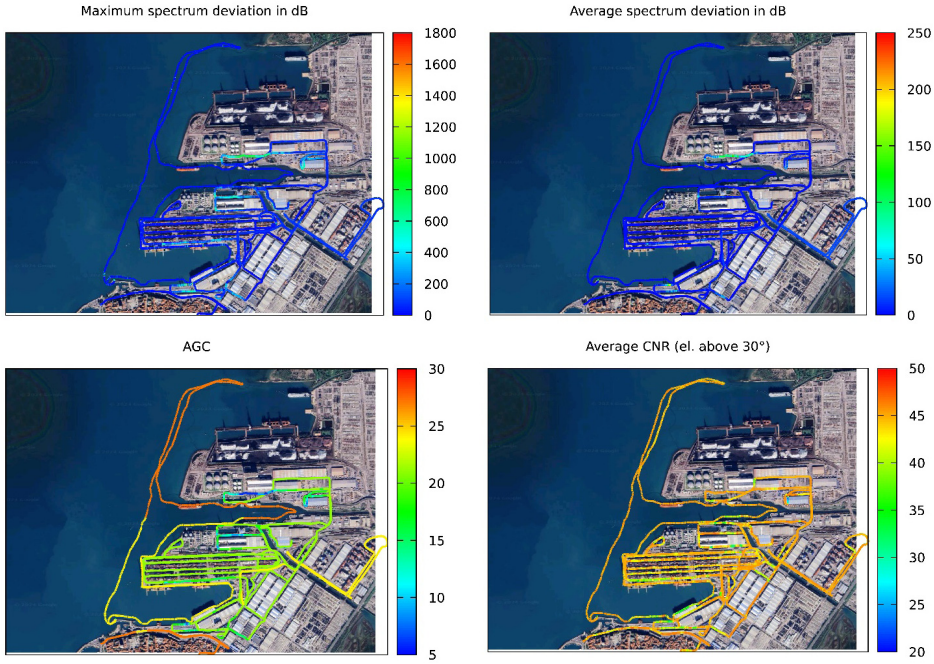

Figure 1. Different metrics values for the interference detection during the survey. The bottom left corner on the images is at the coordinate 399800, 46280 (in meters) of the Slovene National Grid EPSG 3794.

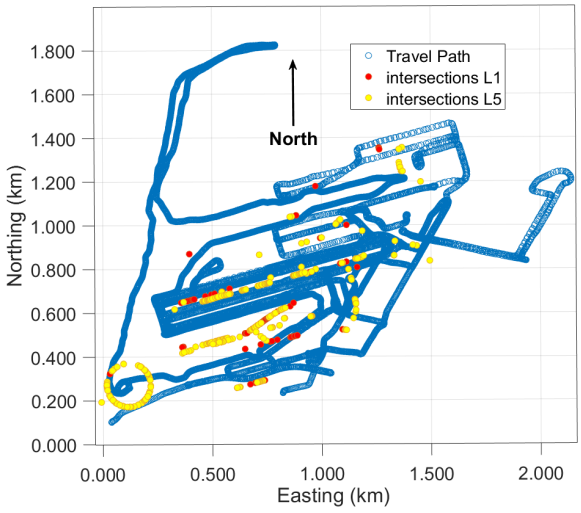

Figure 2. Calculated possible sources of the interference. The coordinate system is chosen in such a way that the origin is at position 400500, 46200 (in meters) in the Slovene National Grid EPSG 3794.

Figure 2 shows the results of the analysis of the localization attempt based on CNR. Generally, it gave reliable results in the sense that the position is approximately the same as it was expected to be. There are, however, some exceptions. For instance, the algorithm suggested a presence of an interference source in the middle of the first basin. On the other hand, there should have been a source north of the second basin that the algorithm missed.

6. CONCLUSIONS

The analysis showed a strong presence of various sources of interference, which corresponds to the reports of the port authorities. Although a rough map of the affected area was constructed, there is still a need to find the offending source. Further analysis with a directed antenna is expected to be performed shortly in order to precisely localize the source.

Additionally, an improvement to the localization algorithm is to be done to take into account the highly reflective area due to the high stacks of conducting steel containers.

REFERENCES

[1] N. Spens, D.-K. Lee, D. Akos, "An Application for Detecting GNSS Jamming and Spoofing," Proceedings of the 34th International Technical Meeting of the Satellite Division of The Institute of Navigation (ION GNSS+ 2021), St. Louis, Missouri, September 2021, pp. 1981–1988. doi: 10.33012/2021.18027.

[2] E. Valles et al., "Interference Detection Algorithms for GNSS-enabled Android Devices," Proceedings of the 28th International Technical Meeting of The Satellite Division of the Institute of Navigation.

[3] D. Miralles et al., "GNSS Threat Monitoring and Reporting with the Android Raw GNSS Measurements and STRIKE3," Proceedings of the 32nd International Technical Meeting of the Satellite Division of The Institute of Navigation.

[4] N. L. Raichur et al., "Machine Learning-assisted GNSS Interference Monitoring through Crowdsourcing," Proceedings of the 35th International Technical Meeting of the Satellite Division of The Institute of Navigation.

[5] L. Strizic et al., "Crowdsourcing GNSS Jammer Detection and Localization," Proceedings of the 2018 International Technical Meeting of The Institute of Navigation.

[6] G. Baldini et al., "Trapping the jammer: The Slovenian experiment," Coordinates 2016, 12, pp. 12–18.

[7] P. Pavlovčič-Prešeren et al., "Exploiting the Sensitivity of Dual- Frequency Smartphones and GNSS Geodetic Receivers for Jammer Localization," Remote Sens. 2023, 15(4), 1157.

[8] L. Scott, "Interference: Origins, Effects, and Mitigation," in Position, Navigation, and Timing Technologies in the 21st Century, vol. I, Y. Jade Morton, F. van Diggelen, J. J. Spilker and B. W. Parkinson, Eds. New Jersey: John Wiley, 2021, pp. 638–673.

[9] Schäfer, M., Soeruer, S., Kippak, T., Sadrak, E. (2023, September). Jammer on theHorizon: A Robust Method for GPS Jammer Localization Using ADS-B Data. In Proceedings of the 36th International Technical Meeting of the Satellite Division of The Institute of Navigation (ION GNSS+ 2023) (pp. 4183-4196).

The 17th Baška Conference
GNSS
Global Navigation Satellite Systems
Green Navigation and Smart Systems

GNSS-AIDED TROPOSPHERIC DELAY MITIGATION IN ADS-B MLAT

Neil Gogoi*, Paolo Dabove, Milad Bagheri

Politecnico di Torino, Torino, Italy

* *Corresponding author:* Neil Gogoi (neil.gogoi@polito.it)

Abstract. *ADS-B is surveillance technology in aviation in which aircrafts broadcasts their position, among other on-board information in real time. MLAT is a secondary surveillance technique where the position is determined by analysing the Time Difference of Arrival of ADS-B signals received at multiple ground stations. In this work, the authors firstly present the use of GNSS tropospheric delay estimation techniques to potentially refine ADS-B MLAT measurements. Further, the benefit of an extensive low-cost GNSS and ADS-B base station network to improve MLAT performances is presented.*

Keywords: *Global Navigation Satellite System (GNSS); Automatic Dependent Surveillance–Broadcast (ADS-B); Multilateration (MLAT); Zenith Tropospheric Delay (ZTD)*

University of Zadar

1. INTRODUCTION AND BACKGROUND

ADS-B was proposed to modernize Air Traffic Management by replacing ground-based surveillance [1]. While multilateration (MLAT) emerged separately, it became a robust alternative to GNSS-based navigation and ADS-B [2-4]. Previous MLAT studies [5] showed a sub-15m mean error with specific algorithms. This research, part of the SpaceItUp! project, assumes synchronized, interconnected receivers and focuses on mitigating atmospheric propagation delays affecting lower tropospheric ADS-B signals.

2. METHODOLOGY

Tropospheric delay is frequency-independent for signals in the microwave range, as it is caused by refraction and there is no dispersion like in the ionosphere [6]. The work presented will be as follows:

A. Modified GNSS Tropospheric Delay Model for ADS-B Signals

Only the standard Saastamoinen Model [7] for Zenith Hydrostatic Delay (ZHD) will be used considering the Wet Delay as comparatively negligible. This is modified with an exponential height scaling based on geodetic literature [8, 9], removing the portion of the troposphere above an aircraft and can be expressed as,

$$ZHD' = \left(\frac{0.0022767 \,.\, p}{1 - 0.00266 \,.\cos(2\emptyset) - 0.00028 \,.\, h_g} \right) \cdot \left(e^{\frac{-h_a}{H}} - e^{\frac{-h_g}{H}} \right) \quad (1)$$

where ZHD' is the modified, p, $\emptyset$ is the ellipsoidal latitude, h_g is the height of the aircraft derived from the ADS-B message and H is the scale height from the barometric pressure equation. A mapping function will be then applied to consider the slant of the incoming ADS-B signal.

B. Using GNSS Network Based ZTD Estimates for ADS-B Signals

The work in [10] integrates low-cost GNSS base station networks with a conventional geodetic network, namely Centipede-RTK (Real-time Kinematic Positioning) network with the SPIN3 inter-regional positioning service [11] achieved through GNSMART2 [12]. In it, the ZTD estimation analysis demonstrates that

the extended network can deliver dependable tropospheric delay observations, with estimations roughly corresponding to the Regional Reference Frame Sub-Commission for Europe (EUREF) ZTD reference product. These ZTD estimates on GNSS signals will be used to compute the delay on ADS-B signals.

3. RESULTS AND DISCUSSION

The results will primarily be post processed and consider an idealized scenario to isolate residual, system, and user errors. It will show the effectiveness or futility of adding tropospheric signal propagation delay mitigation to ADS-B based MLAT considering an extensive network of synchronized, interconnected receivers. Comparisons to similar MLAT accuracy and errors in literature will be provided.

4. CONCLUSIONS

The work explores the implementation of GNSS tropospheric delay estimation techniques with ADS-B MLAT to enhance positioning accuracy in aviation surveillance. The methodology presented includes modifying the Saastamoinen Model for ADS-B signals and using an extensive network of low-cost GNSS and ADS-B base stations to address the impact of tropospheric propagation delays. The upcoming results will evaluate the potential improvements in MLAT performance, benchmarked against existing literature, offering insights into a cost-effective approach for enhancing ADS-B surveillance in aviation, especially in high-traffic areas.

Acknowledgments: This study was carried out within the Space It Up project funded by the Italian Space Agency, ASI, and the Ministry of University and Research, MUR, under contract n. 2024-5-E.0 - CUP n. I53D24000060005.

REFERENCES

[1] RTCA. (1999). *Development and Implementation Planning Guide for Automatic Dependent Surveillance Broadcast (ADS-B) Applications*. Technical Report RTCA/DO-249, Washington, DC.

[2] Niles, F. A., Conker, R. S., El-Arini, M. B., O'Laighlin, D. G., & Baraban, D. V. (2012). *Wide area multilateration for alternate position, navigation, and timing (APNT)*. MITRE-CAASD, Tech. Rep.

[3] International Civil Aviation Organization. (2011). *ICAO/FAA Workshop on ADS-B and Multilateration Implementation*. Available from: http://www.marinemec.com/technology/fleet-management.htm, accessed 27 February 2025.

[4] Jheng, S. L., Jan, S. S., Chen, Y. H., & Lo, S. (2020). 1090 MHz ADS-B-based wide area multilateration system for alternative positioning navigation and timing. *IEEE sensors journal*, *20*(16), 9490-9501.

[5] Galati, G., Leonardi, M., Mantilla Gaviria, I., & Balbastre Tejedor, J. (2013). Comparison of Localization Algorithms for Mode–S Multilateration (MLAT) Systems in Airport Surface Surveillance. In *Proceedings of Symposium ESAVS 2013, Enhanced Solutions for Aircraft and Vehicle Surveillance Applications, 20-21 March 2013, Berlin, Germany* (Vol. 258). Deutsche Gesellschaft für Ortung und Navigation.

[6] Langley, R. B., Teunissen, P. J., & Montenbruck, O. (2017). Introduction to GNSS. *Springer handbook of global navigation satellite systems*, 3-23.

[7] Saastamoinen, J. (1972). Atmospheric correction for the troposphere and stratosphere in radio ranging satellites. *The use of artificial satellites for geodesy*, *15*, 247-251.

[8] Böhm, J., Heinkelmann, R., & Schuh, H. (2007). Short note: a global model of pressure and temperature for geodetic applications. *Journal of Geodesy*, *81*, 679-683.

[9] Tregoning, P., & Herring, T. A. (2006). Impact of a priori zenith hydrostatic delay errors on GPS estimates of station heights and zenith total delays. *Geophysical Research Letters*, *33*(23).

[10] Bagheri, M., Dabove, P. (2025). Assessing Low-Cost GNSS Network Performance for Atmospheric and Positioning Applications: A preliminary Multi-Station Analysis of a low-cost Network.To be published in the proceedings of *2025 IEEE/ION Position, Location and Navigation Symposium (PLANS)*.

[11] SPIN3 GNSS. *Servizio di Posizionamento Interregionale GNSS*. Available at: https://www.spingnss.it/. Accessed: 26 February 2025.

[12] GNSMART. *GNSMART Precise Satellite Positioning Software*. Available at: https://www.geopp.de/. Accessed: 26 February 2025.

The 17th Baška Conference
GNSS
Global Navigation Satellite Systems
Green Navigation and Smart Systems

CHARACTERISTICS AND PERFORMANCE ASSESSMENT OF CORRECTIONS TRANSMITTED BY THE ALGERIAN SBAS USING ALCOMSAT-1

Lahouaria Tabti*, Younes Ahmed Betchim, Hicham Dekkiche

Department of Space Geodesy, Centre of Space Techniques, Algerian Space Agency, Algeria

* *Corresponding author:* Lahouaria Tabti (ltabti@cts.asal.dz, thouaria@yahoo.fr)

Abstract. *Satellite-Based Augmentation Systems (SBAS) enhance GPS positioning accuracy and integrity by providing real-time corrections. The Algerian Satellite-Based Augmentation System (AL-SBAS) was developed to improve positioning performance across Algeria. It relies on the geostationary satellite Alcomsat-1, which is primarily used for telecommunications, while AL-SBAS broadcasts corrections via PRN 148. The system has been operational since July 2020.*

To assess its performance, experimental tests were conducted at a site in northern Algeria throughout 2023. The collected data were processed using RTKLIB and MATLAB. Results demonstrated that AL-SBAS significantly improves positioning accuracy, showing performance comparable to EGNOS, which has been operational since October 1, 2009. RMS errors ranged from 2.87 m to 4.15 m for AL-SBAS, compared to over 10 m for GPS alone. EGNOS corrections provided even greater accuracy, with RMS values between 1.29 m and 2.03 m.

Keywords: *accuracy; AL-SBAS; EGNOS; GPS*

University of Zadar

1. INTRODUCTION

The Global Navigation Satellite System (GNSS) transmits signals that enable receivers to determine position, speed, and time, making it essential for various applications. However, the accuracy of GNSS-derived positions is often affected by multiple sources of error, potentially leading to inaccuracies exceeding 10 m in real time. Moreover, these systems do not guarantee the integrity of the information they provide. To address this issue, Satellite-Based Augmentation Systems (SBAS) have been developed. These systems can correct a significant portion of these errors, thereby enhancing the overall performance of GPS. SBAS improves GNSS accuracy by providing differential correction messages and can also alert users to potential malfunctions within the GNSS through integrity messages. This includes information on GPS satellite, such as confidence levels and alerts in case of anomalies [1].

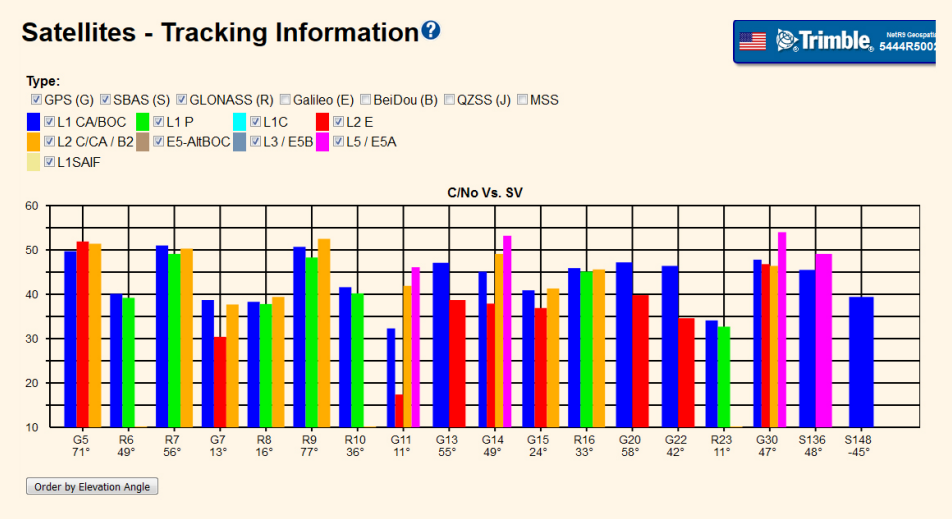

Figure 1. Satellite tracking information displaying signal strength for various satellites, including PRN 148.

Currently, several SBAS are operational, while others are in various stages of development. Algeria has demonstrated its interest in SBAS technology through the Algerian Space Agency (ASAL). The AL-SBAS system utilizes Alcomsat-1, which was launched on December 11, 2017, and is positioned in a geostationary orbit at 24.8° W. AL-SBAS consists of Reference Stations (RS) installed exclusively within

Algeria, ensuring full national coverage. Additionally, it includes a Data Processing Centre (DPC) and a Ground Uplink Land Station (GULS) located in Algiers [2][3]. Satellite tracking information, including the signal-to-noise ratio (C/N_0) for PRN 148, is presented in **Figure 1**, illustrating the signal strength of various satellites.

2. AL-SBAS CORRECTIONS

AL-SBAS corrections are broadcast to users within the service area at a rate of 250 bits per second using the L1 frequency (1575.42 MHz), transmitted via the geostationary SBAS satellite PRN 148 [4]. These corrections include fast corrections, long-term corrections, and ionospheric corrections. The information is structured into several message types (MT), as summarized in **Table 1**, which outlines the AL-SBAS messages used to improve positioning.

Table 1. Broadcast Message Types.

Message Type	Contents
1	PRN Mask
2 to 5	Fast Correction
24	fast/long-term satellite error correction
25	long-term satellite correction
18	Lonospheric grid point masks
26	Ionospheric delay correction

There are three main categories of messages: satellite information messages, ionospheric information messages, and additional messages. **Figure 2** presents the Message Types (MT) received from the AL-SBAS PRN 148 satellite on January 3, 2025, using the Trimble NetR9 receiver.

The figure presents the distribution of different message types in terms of percentage. The highest proportion is observed for message types 2, 3 and 4, which exceed 20%, indicating their dominant role in position correction, as they provide rapid corrections for GNSS satellites, improving positioning accuracy by quickly mitigating errors. Message type 26 also has a notable presence but at a lower percentage, as it contains ionospheric corrections.

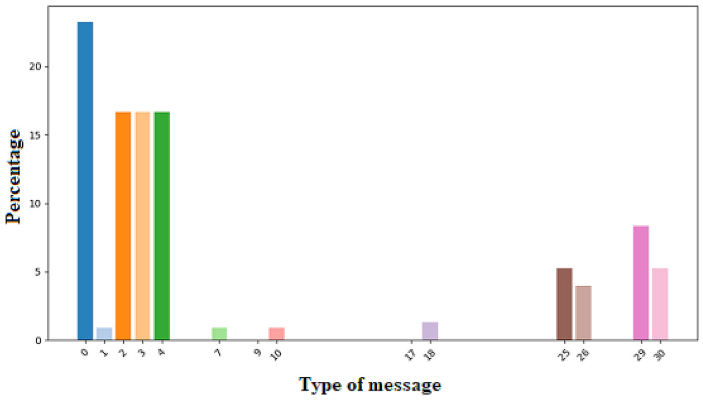

Figure 2. Message Type (MT) received from the AL-SBAS 148 satellite.

Meanwhile, other message types, such as 1, 9, 10, and 18, appear with minimal representation. This distribution suggests that certain message types are more frequently used or transmitted, while others have a limited occurrence.

3. APPLICATION OF CORRECTIONS

To apply EGNOS corrections to the GPS signal, a position must first be determined to identify the appropriate parameters. For each measurement taken, SBAS corrections are computed. The calculated parameters include fast/long-term corrections, corrected satellite positions, ionospheric and tropospheric delays. The corrected pseudo-range is calculated as follows [5][6]:

$$l_{corr}(t) = l_{mes}(t) + RC_{fast}(t) + RC_{clock} - RC_{iono}(t) + RC_{tropo}(t) \quad (1)$$

where l_{corr} is the corrected pseudo-range used for position determination, l_{mes} is the measured pseudo-range, RC_{fast} represents the fast corrections, RC_{clock} is clock corrections for the particular satellite, RC_{iono} is the Ionospheric corrections and RC_{tropo} is the Tropospheric corrections for the selected model.

4. RESEARCH EXPERIMENT

To assess the performance of AL-SBAS, a testing campaign was conducted using the Trimble NetR9 receiver, which was installed on the roof of the research block in Arzew (Oran), located in northern Algeria at latitude 35.85°N and longitude -0.31°E (**Figure 3**). The campaign covered several days, specifically from February 22 to 23 (DOY 53 to 54), March 5 to 9 (DOY 64 to 68), and March 12 to 16 (DOY 71 to 75).

Figure 3. Trimble NetR9 installed on the roof of the research block in Arzew.

The data were processed using RTKLIB and MATLAB. The RTKPOST library was utilized to determine the site position in Single Point Positioning (SPP) mode, both with and without AL-SBAS and EGNOS [7]. At this stage, corrections from AL-SBAS satellite S148 and EGNOS satellite S136 were applied. These corrections were downloaded from the CNES FTP server, as shown in **Figure 4**.

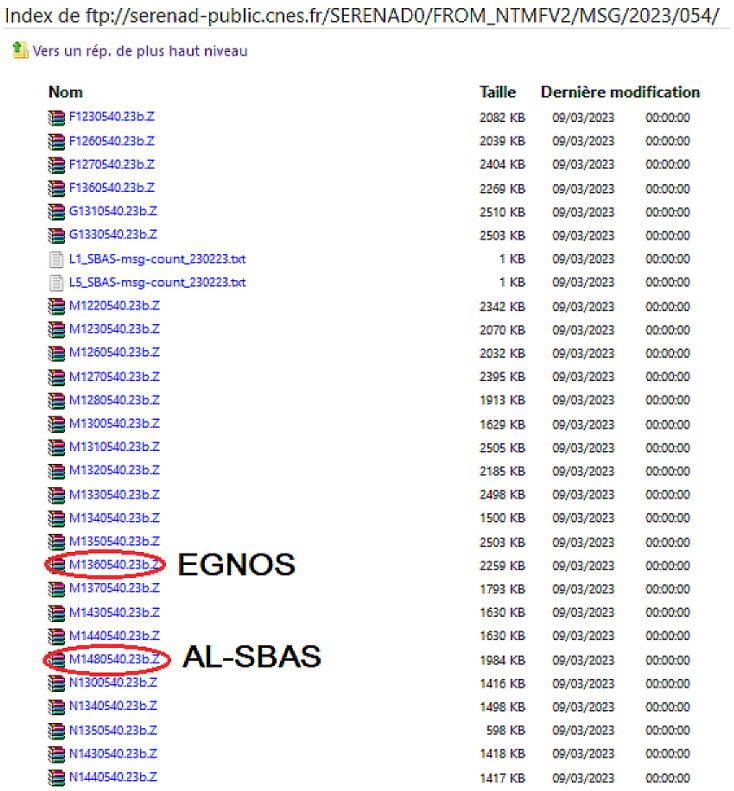

Figure 4. CNES FTP Directory for Downloading SBAS Corrections in RINEX-B Format.

The input data included RINEX GPS files (NAV, OBS) and SBAS corrections. Broadcast ionospheric corrections were applied using the Klobuchar model for GPS and the SBAS model for EGNOS and AL-SBAS. Tropospheric corrections were derived from the Saastamoinen model for GPS, while the SBAS model was used for both for both systems. Ephemeris and clock data were obtained from broadcast ephemeris for GPS, supplemented by SBAS corrections.

4. ASSESSMENT OF AL-SBAS ACCURACY

The precise position of the site is well known, allowing for an accurate assessment of positioning errors. Position errors (dX, dY, dZ) are calculated by comparing the estimated coordinates (Xi, Yi, Zi) with the reference coordinates (Xref, Yref, Zref) [8]. The three-dimensional (3D) positioning error (PE) is computed using the following equation:

$$3\ \text{D Error} = \sqrt{(dX)^2 + (\text{dY})^2 + (dZ)^2} \quad (2)$$

Table 2 present the statistics of the 3D PE obtained during the test campaign.

Table 2. Statistics of the 3D PE Using the Trimble NetR9 Receiver (m).

	Min	Max	Mean	STD
GPS	0.18	27.00	4.84	4.83
GPS+AL-SBAS	0.08	27.96	2.79	2.29
GPS+EGNOS	0.07	16.28	1.65	1.00

The results in **Table 2** indicate that both AL-SBAS and EGNOS significantly improve positioning accuracy compared to GPS alone. The standard deviations(STD), which measure the dispersion of the 3D PE, are below 2.29 m for GPS+AL-SBAS and 1 m for GPS+EGNOS, whereas GPS alone reaches 4.83 m. The minimum 3D PE is approximately 0.08 m for GPS+AL-SBAS and 0.07 m for GPS + EGNOS, while for GPS alone, it can reach 0.18 m. This demonstrates a clear improvement in positioning accuracy when SBAS corrections are applied. However, it is worth noting that the maximum 3D PE for AL-SBAS can be higher than for GPS alone. This could be due to occasional instability in the AL-SBAS system during the test campaign. To further analyse the results, the daily Root Mean Square (RMS) error of the 3D PE values are illustrated in **Figure 5**.

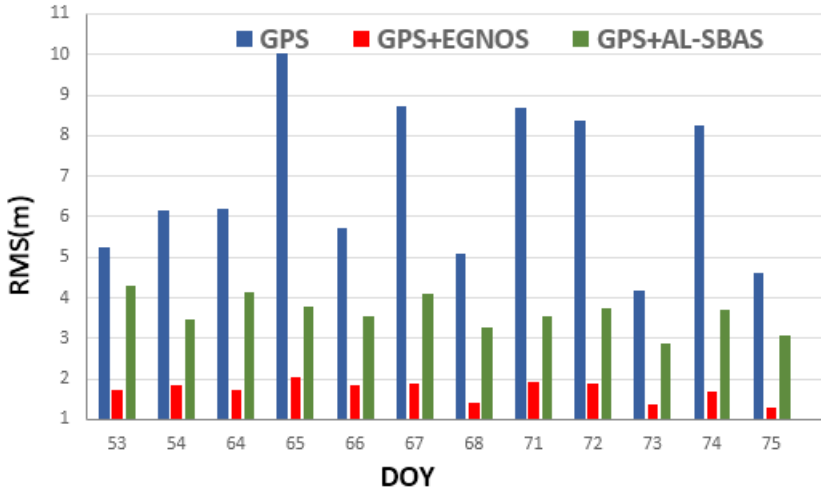

Figure 5. Daily RMS for Different Configurations (GPS, GPS+EGNOS, GPS+AL-SBAS).

Figure 5 clearly shows that using SBAS corrections significantly reduces positioning errors. GPS alone exhibits the highest RMS values, whereas EGNOS consistently provides the most stable and accurate results, followed by AL-SBAS. The results presented confirm that applying AL-SBAS and EGNOS corrections significantly improves absolute positioning accuracy compared to using GPS alone. To better interpret these results, **Figure 6** illustrates the temporal evolution of the 3D PE over a 24-hour period. These graphs provide a visual representation of the absolute 3D PE for two specific days March 12 (DOY 71) and 16 (DOY 75). The comparison highlights fluctuations in positioning accuracy over time and reinforces the effectiveness of SBAS corrections in reducing positioning errors.

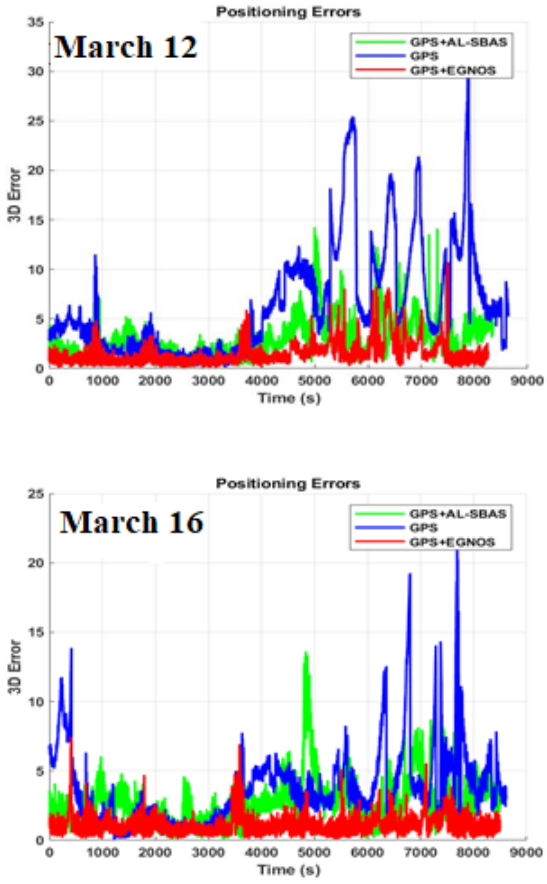

Figure 6. Temporal variation of the 3D PE over a 24-hour period for three configurations (GPS, GPS+AL-SBAS, GPS+EGNOS).

From **Figure 6**, the results demonstrate that applying SBAS corrections significantly improves positioning accuracy. The GPS-only solution exhibits large fluctuations, with errors occasionally exceeding 25 m, whereas GPS+EGNOS and GPS+AL-SBAS show reduced error amplitudes and greater stability. Notably, EGNOS corrections provide the best overall accuracy, while AL-SBAS also enhances positioning but exhibits slightly higher variations at certain times.

5. CONCLUSION

GNSS performance can be enhanced by regional Satellite-Based Augmentation Systems (SBAS). These systems improve the accuracy and integrity of GNSS data by correcting measurement errors. The integrity and accuracy of SBAS signals also enable the development of applications in various fields beyond aviation, including maritime and land transport (road and rail), cartography, and cadastral surveying. This study aimed to evaluate the accuracy of the Algerian augmentation system, AL-SBAS, for single-frequency positioning. Data were collected using a Trimble NetR9 receiver, processed with RTKLIB software, and analysed with MATLAB programs to compare three solutions: GPS-only solution: Without any correction, GPS+AL-SBAS solution: Applying AL-SBAS corrections and GPS+EGNOS solution: Applying EGNOS corrections.

The results showed that positioning accuracy using AL-SBAS or EGNOS is significantly better than when using GPS alone. The standard deviation of positioning errors with AL-SBAS corrections was 2.29 m, compared to 4.83 m without corrections. These findings provide a preliminary assessment of GPS+AL-SBAS positioning quality in northern Algeria. However, due to the limited duration of the test campaign, conducted over only a few days, these results do not allow for a comprehensive evaluation of AL-SBAS performance and quality. Moreover, this study did not assess integrity, which is a critical aspect of SBAS augmentation systems. As a next step, it is essential to conduct further analyses to evaluate the performance of AL-SBAS in terms of both accuracy and integrity across multiple sites in Algeria.

REFERENCES

[1] Grunwald, G., Ciećko, A., Krasuski, K., and Kaźmierczak, R. (2021). The GPS/EGNOS Positioning Quality in APV-1 and LPV-200 flight procedures. Communications-Scientific. Letters of the University of Zilina, 23(2), E23-E34.

[2] Kahlouche, S., Tabti, L., Benbouzid, A.B., and Outamazirt, F. (2022). Algerian satellite based augmentation system based on ALCOMSAT-1: characteristics and preliminary performance tests. International Meeting on the Applications of GNSS Systems, Vienna, Austria, 5 - 9 December.

[3] Li, R., Zheng, S., Wang, E., Chen, J., Feng, S., Wang, D and Dai, L. (2020). Advances in BeiDou Navigation Satellite System (BDS) and satellite navigation augmentation technologies, Satellite Navigation, vol. 1, issue (1), pp. 1-23, 2020.

[4] National Coordination Office for Space-Based Positioning. (2021). L1 C/A PRN Code Assignments. June 2021 edition. Washington D.C. (United States). Available at https://www.gps.gov/technical/prn-codes/L1-CA-PRN-code-assignments-2021-Jun.pdf.

[5] RTCA. (2001). Minimum Operational Performance Standards for Global Positioning System/wide area augmentation system airborne equipment. Washington, DC 20036. Supersedes DO-229B.

[6] Eurocontrol. (2003). Technical Notes on SBAS Doc No: PEG-TN-SBAS. Issue: I, Project: PEGASUS.

[7] RTKLIB Website. Available online: http://rtklib.com/.

[8] Tabti, L., Kahlouche, S., Benadda, B and Beldjilali, B. (2020). Improvement of a single-frequency GPS positioning performance based on EGNOS corrections in Algeria. Journal of Navigation, Cambridge University, UK. https://doi.org/10.1017/S037346331900095X.

The 17th Baška Conference
GNSS
Global Navigation Satellite Systems
Green Navigation and Smart Systems

VLM – AIDED EXPERIMENTATION: CASE STUDY OF GNSS SIGNAL TRANSMISSION UNDER FADING AND INTERFERENCE CONDITIONS

Dragana Krstic[1*], Suad Suljovic[2], Nenad Petrovic[1]

[1] University of Niš, Faculty of Electronic Engineering, Niš, Serbia
[2] The University Metropolitan; Belgrade, Serbia
[*] *Corresponding author:* Dragana Krstić (dragana.krstic@elfak.ni.ac.rs)

Abstract. *Since Global Navigation Satellite Systems (GNSS) are largely utilized in many applications ranging from commercial, military and industrial navigation (passenger aircrafts, helicopters, fighters), to unmanned aerial vehicles (UAVs), digital modelling, mapping, and cloud computing, they are vulnerable to advanced interference, signal jamming, and spoofing. Also, occurrences as multipath signals and fading should considered as distractions in these systems. Here, we analyze GNSS signal transmission disturbed by fading and co-channel interference (CCI), where both are described using the Beaulieu -Xie (BX) distribution. We pay special attention to the higher order moments of output signal-to-interference ratio (SIR). The moments play an important role in analysis of GNSS systems. Based on a few plotted figures of moments of different order, we analyse the impact of fading and CCI parameters on system behaviour. Afterwards, we show the methodology leveraging Vision Language Model (VLM) in order to make model-driven network design and experimentation more convenient, and evaluate the system using the previously derived expression as a case study.*

Keywords: *Beaulieu -Xie distribution; interference; fading; moments; Vision Language Model (VLM)*

University of Zadar

1. INTRODUCTION

Performance of Global Navigation Satellite Systems (GNSS) degrades under acting of broadband interference or rapid changes of the frequency of interference, or jamming signal. Many authors have analysed GNSS systems under these nuisances, but most often without taking into account the fading influence, as in [1]. There are several challenges to the GNSS signal reception in urban environment since GNSS Line-Of-Sight (LOS) signals can be blocked. This leads to a reduction of the number of satellites seeing each other. Such a situation can be fixed by using a multi-constellation receiver with more direct-LOS signals for the computation of a position solution [2]. That is the reason Norman Beaulieu and Xie Jiandong defined a new distribution taking into account a few direct (LOS) and NLOS signals [3]. In addition to fading, we also observe co-channel interference (CCI) with the same Beaulieu-Xie (BX) distribution, that disturbs GNSS signals. We derive expressions for key moments as very important performance of GNSS systems.

2. PERFORMANCE DERIVATION, PRESENTATION AND ANALYSIS

It is necessary to reduce the impact of disturbances on GNSS systems. Some mitigation techniques are presented in [4]. To mitigate the impact of fading and CCI we used diversity technique scheme with selection combining (SC).

The input signals to an SC diversity receiver having a BX PDF are [3]:

$$p_{x_i}(x_i) = 2\mathrm{e}^{-\frac{m_x}{\Omega_i}\left(x_i^2+\kappa_x\Omega_i\right)} \sum_{j_1=0}^{+\infty} \frac{\left(\kappa_x\Omega_i\right)^{j_1} x_i^{2j_1+2m_x-1}}{j_1!\Gamma\left(j_1+m_x\right)} \left(\frac{m_x}{\Omega_i}\right)^{2j_1+m_x} \tag{1}$$

The CCI appearing at antennas' inputs in SC receiver has also BX distribution:

$$p_{Y_i}(y_i) = 2\mathrm{e}^{-\frac{m_y}{s_i}\left(y_i^2+\kappa_y\gamma_i\right)} \sum_{j_2=0}^{+\infty} \frac{\left(\kappa_y\gamma_i\right)^{j_2} y_i^{2j_2+2m_y-1}}{j_2!\Gamma\left(j_2+m_y\right)} \left(\frac{m_y}{\gamma_i}\right)^{2j_2+m_y} \tag{2}$$

The definitions of quantities are, for fading with the prefix x, and for interference with the prefix y, as: m is severity parameter, κ is the K-factor of the Rician distribution representing the ratio of the LOS component power and the scatter

components' power, Ω_i are powers of signals at input antennas, i=1,2, …, L, and λ is non-centrality parameter equals to $\lambda_i = \sqrt{\kappa_x \Omega_i}$. From general BX distribution some other distributions can be obtained as is presented in **[5, Figure 1]**. Because of that this paper has general meaning.

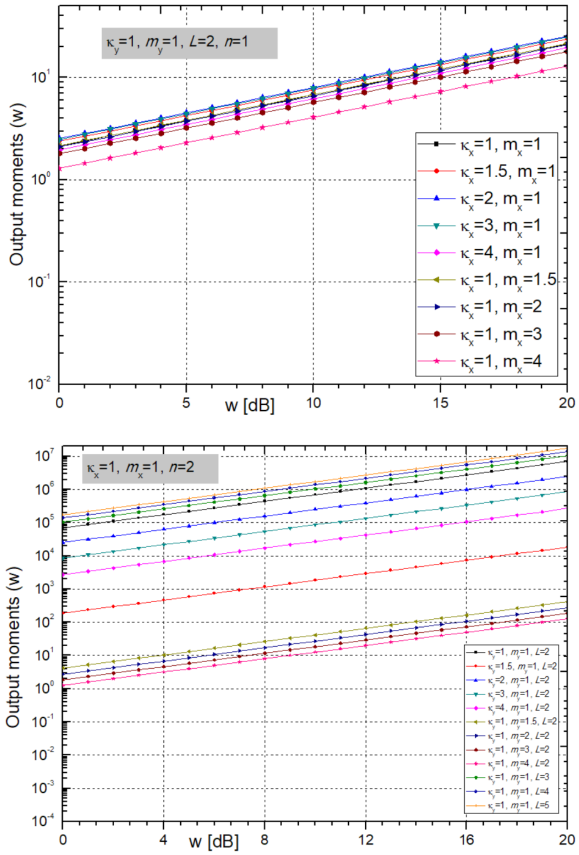

Figure 1. Output moments m_1 and m_2 for different values of fading and CCI parameters.

The instantaneous signal-to-interference ratio (SIR), z_i is x_i/y_i, and the average SIR, w, is $w=\Omega/s$. Starting from basic formula for PDF of SIR z_i **[6]**: $p_{z_i}(z_i) = \int_0^\infty p_{x_i}(z_i y_i)\, p_{y_i}(y_i)\, y_i \, \mathrm{d}y_i$, we obtained PDF of SIR z_i for our scenario as:

$$p_{z_i}(z_i) = \frac{2}{\mathrm{e}^{m_x\kappa_x + m_y\kappa_y}} \sum_{j_1=0}^{+\infty} \sum_{j_2=0}^{+\infty} \frac{(\kappa_x)^{j_1} (\kappa_y)^{j_2}\, {m_x}^{2j_1+m_x} {m_y}^{2j_2+m_y}\, {z_i}^{2j_1+2m_x-1} {\Omega_i}^{j_2+m_y} {\gamma_i}^{j_1+m_x} \Gamma(j_1+j_2+m_x+m_y)}{j_1!\, j_2!\, \Gamma(j_1+m_x)\Gamma(j_2+m_y)\left(\Omega_i m_y + m_x \gamma_i {z_i}^2\right)^{j_1+j_2+m_x+m_y}} \quad (3)$$

Further, the PDF of the output SIR z from SC receiver with L branches is calculated starting from formula [7]: $p_{z_i}(z) = Lp_{z_i}(z_i)\left(F_{z_i}(z_i)\right)^{L-1}$.

After many mathematical manipulations PDF is in the shape:

$$p_{z_i}(z) = \frac{2L}{e^{m_x\kappa_x + m_y\kappa_y}} \sum_{j_1=0}^{+\infty}\sum_{j_2=0}^{+\infty} \frac{(\kappa_x)^{j_1}(\kappa_y)^{j_2} m_x^{2j_1+m_x} m_y^{2j_2+m_y} z_i^{2j_1+2m_x-1} \Omega_i^{j_2+m_y} \gamma_i^{j_1+m_x} \Gamma(j_1+j_2+m_x+m_y)}{j_1!\, j_2!\, \Gamma(j_1+m_x)\Gamma(j_2+m_y)\left(\Omega_i m_y + m_x\gamma_i z_i^2\right)^{j_1+j_2+m_x+m_y}}$$

$$\left(\frac{1}{e^{m_x\kappa_x+m_y\kappa_y}} \sum_{j_3=0}^{+\infty}\sum_{j_4=0}^{+\infty}\sum_{j_5=0}^{+\infty} \frac{(\kappa_x m_x)^{j_3}(\kappa_y m_y)^{j_4}\Gamma(j_3+j_4+m_x+m_y)(j_3+m_x)_{j_5}(1-j_4-m_y)_{j_5}}{j_3!\, j_4!\, j_5!\, \Gamma(j_3+m_x)\Gamma(j_4+m_y)(j_3+m_x+1)_{j_5}(j_3+m_x)} \left(\frac{m_x\gamma_i z_i^2}{\Omega_i m_y + m_x\gamma_i z_i^2}\right)^{j_3+j_5+m_x}\right)^{L-1} \tag{4}$$

Let us now derive the moment of the n^{th} order of SIR z, starting from **[8, p. 98]**:

$$m_n = \overline{z^n} = \int_0^{+\infty} z^n p_{z_i}(z)dz \tag{5}$$

After we made serious mathematical process and changes, the n^{th} moment becomes:

$$m_n = \frac{L}{e^{m_x\kappa_x+m_y\kappa_y}} \sum_{j_1=0}^{+\infty}\sum_{j_2=0}^{+\infty} \frac{(\kappa_x)^{j_1}(\kappa_y)^{j_2}\Gamma(j_1+j_2+m_y+m_x) m_x^{\frac{2j_1-n}{2}} m_y^{\frac{2j_2+n}{2}}}{j_1!\, j_2!\, \Gamma(j_1+m_x)\Gamma(j_2+m_y)} \left(\frac{\Omega_i}{s_i}\right)^{\frac{n}{2}}$$

$$\left(\frac{1}{e^{m_x\kappa_x+m_y\kappa_y}} \sum_{j_3=0}^{+\infty}\sum_{j_4=0}^{+\infty}\sum_{j_5=0}^{+\infty} \frac{(\kappa_x m_x)^{j_3}(\kappa_y m_y)^{j_4}\Gamma(j_3+j_4+m_y+m_x)(j_3+m_x)_{j_5}(1-j_4-m_y)_{j_5}}{j_3!\, j_4!\, j_5!\, \Gamma(j_3+m_x)\Gamma(j_4+m_y)(j_3+m_x+1)_{j_5}(j_3+m_x)}\right)^{L-1} \tag{6}$$

$$B\left(\frac{n+2j_1+2Lj_3-2j_3+2Lj_5-2j_5+2Lm_x}{2}, \frac{2j_2+2m_y-n}{2}\right)$$

It can be shown that number of adders in sums is not too big for all parameters values, and the calculation time is reasonable.

The moments show quantitative measure of the shape of a function. When talking of probability distribution, then we should remember that zero-th moment of that function is total probability, the first moment is the mean value of the signal, the second is the variance, the third is skewness, and the fourth moment is kurtosis. To create a null sector toward the jamming source and strengthen the navigation signal, in algorithms used for detection of interference and jamming based on the shape of probability density function (PDF), fourth moment, kurtosis, is used **[9]**. This is a statistical parameter relating to the shape of random variable PDF.

The moments play an important role in analysis of GNSS systems, especially first few moments since one important system performance, Amount of Fading (AoF), measure of severity of fading, can be derived directly from moments:

$$AoF = m_2 / m_1^2 - 1 \tag{7}$$

Fig. 1 shows the 1st and 2nd output moments, m_1 and m_2, for different values of fading and CCI parameters and number of branches L. We can conclude from this figure that bigger L, m, and κ_x improve system performance.

3. VISION LANGUAGE MODEL (VLM) ADOPTION TO NETWORK EXPERIMENTATION

Building on our previous work in which we explored the potential of Large Language Models (LLMs) in network design and experimentation, LLMs excel at summarization, making them essential for extracting valuable insights from textual sources, leading to faster and more convenient experimentation **[10, 11]**. However, in this paper, we go a step further by adopting Vision Language Models (VLMs) in our work in order to extend this capability by interpreting concepts, their properties, and relationships through visual representations as well **[12]**. The reason why VLMs are considered beneficial in this area is the fact that significant portion of relevant information related to networks design and experimentation is conveyed through diagrams and graphs.

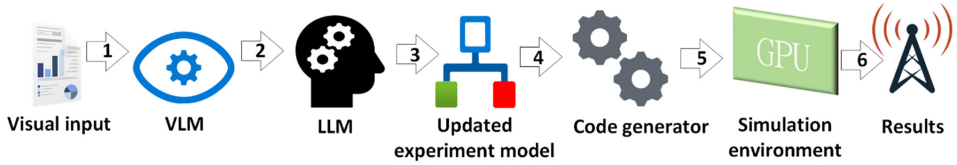

Figure 2. Workflow overview:
1 – Diagrams, graphs + prompts; 2 – New information; 3 – Model update; 4 – XMI model instance; 5 – Experiment configuration; 6 – Experiment execution.

However, while textual sources have been widely utilized in previous research **[10, 11]**, the potential of visual representations as inputs remains unexplored.

Our extensions to the experimental workflow form **[10, 11]** will be described and depicted in **Fig. 2**.

Within the initial step, the user must provide the details about the network experiment, including both visual and textual inputs. The visual input may consist of either a model instance diagram represented in Unified Modelling Language (UML) notation (aligned with the metamodel from **[10, 11]**) or graphs which aim to support performance analysis (as shown in **Fig. 1**). In case when an UML model instance diagram is provided, VLM can extract key aspects of the network experiment, including the receiver, fading environment, and desired performance metrics (e.g., output moments). Additionally, performance graphs can be also leveraged in order to identify performance trends, target performance values, and related parameters. This information is extracted through a series of VLM-driven prompts.

Furthermore, the underlying network experiment metamodel in textual form is considered as an input. Afterwards, the extracted information from visual input is then used to construct a network experiment model instance using an LLM. In scenarios where updatability aspects of particular network design are evaluated, the current state encapsulated within model instance, can be extended with new information generated through VLM-based image prompting.

Once the model instance integrates the new information based on both visual and textual inputs, it is further passed to a code generator. The role of code generator is to parse the model instance, extract relevant parameter values, and populate the experiment template accordingly. Finally, the generated experiment is then executed within a GPU-enabled simulation environment, following the approach outlined in our previous work **[13]**.

The proposed VLM-based workflow is implemented as Flask API web application in Python, relying on OpenGVLab's InternVL2-8B-MPO **[14]** as the underlying VLM. This model was selected for its promising output quality while maintaining a manageable size for local deployment. For execution, we use the Google Colab environment configured with an L4 GPU, as the VLM requires up to 22 GB of VRAM, necessitating activation of the lowest-tier paid plan. Regarding the evaluation, both the average execution times and the percentage of correct answers (within 10 attempts) were taken into account.

Table 1. VLM service evaluation for network experimentation.

Prompt/step	Input	Time [s]	Correctness [%]
What is the fading type?	Model	7.03	90
What is the receiver type?	Model	7.35	90
What is the target performance?	Graph	13.67	80
Updates identification	Current model, to-be model	18.41	70

Table 1 summarizes the results achieved for different steps in case of moment calculation within BX fading and CCI environment for SC receiver. As it can be noticed, simpler tasks exhibit shorter execution times and higher accuracy rates. However, identifying updates is more complex, requiring additional steps, resulting in longer execution times.

4. CONCLUSIONS

In this work we presented the derived expression for n^{th} moment of output SIR from L branch SC combiner used to mitigate the impact of BX fading and CCI that disturb GNSS signal. On the other side, the VLM-enabled approach gives the ability to leverage visual inputs to automate various steps within the network experimentation workflow. While execution times vary across different cases, they remained within the order of a second in our experiments.

Acknowledgments: This work is partially financed under the projects of the Ministry of Science, Technological Development and Innovation of the Republic of Serbia and partially supported by the project: "Enhancing IoT Systems Security", SPS Ref. No. G6259, NATO Science for Peace and Security (SPS) Programme.

REFERENCES

[1] Sharifi-Tehrani, O. (2022) Airborne GNSS-receiver threat detection in no-fading environments, *Journal of Beijing Institute of Technology*, 2022, Vol. 31, No. 6, pp. 613-620.

[2] Zhu, N., Marais, J., Bétaille, D., and Berbineau, M. (2018) GNSS position integrity in urban environments: a review of literature, *IEEE Transactions on Intelligent Transportation Systems*, Vol. 19, No. 9, pp. 2762-2778.

[3] Beaulieu, N. C. and Jiandong, X. (2015). A novel fading model for channels with multiple dominant specular components. *IEEE Wireless Communications Letters,* 4(1), 54–57. doi:10.1109/lwc.2014.2367501.

[4] Sharifi-Tehrani, O. and Ghasemi, M. H. (2022) A review on GNSS-threat detection and mitigation techniques, *Cloud Computing and Data Science*, Special Issue, pp. 1-25, doi:10.37256/ccds.4320231678.

[5] Olutayo A. (2021) *A Novel Fading Model for Emerging Wireless Communication Systems*. Doctoral dissertation. Okanagan: The University of British Columbia.

[6] Panic, S., Stefanovic, M., Anastasov, J., and Spalevic, P. (2014) *Fading and Interference Mitigation in Wireless Communications*; CRC Press, Taylor & Francis Group: Boca Raton, FL, USA.

[7] Mitrovic, Z., Nikolic, Z., B. Đordevic, G., and Stefanovic, M. (2009) Influence of imperfect carrier signal recovery on performance of SC receiver of BPSK signals transmitted over α-μ fading channel. *Electronics*, 13(1), pp. 58-62.

[8] Helstrom, C. V. (1991) *Probability and Stochastic Processes for Engineers*, McMillian, 2nd edition.

[9] Sharifi-Tehrani, O., Farzan Sabahi, M., and Danaee, M. R. (2020) Low-complexity framework for GNSS jamming and spoofing detection on moving platforms, *IET Radar, Sonar & Navigation*, Vol. 14, Iss. 12, pp. 2027-2038, doi: 10.1049/iet-rsn.2020.0285.

[10] Krstic, D., Suljovic, S., Petrovic, N., Djordjevic, G., Gurjar, D., and Yadav, S. (2024) Network experimental workflow leveraging MDE and LLM: Case study of wireless system performance in an α-μ fading environment with selection diversity receiver, *International Journal on Advances in Systems and Measurements*, Vol. 17, No. 1 & 2, pp. 56-66.

[11] Krstic, D., Suljovic, S., Djordjevic, G., Petrovic, N., and Milic, D. (2024) MDE and LLM synergy for network experimentation: case analysis of wireless system performance in Beaulieu-Xie fading and κ-μ cochannel interference environment with diversity combining, *Sensors*, 24(10), 3037; https://doi.org/10.3390/s24103037.

[12] F. Bordes et al., (2024) An introduction to vision-language modelling, preprint, arxiv, pp. 1-76, https://arxiv.org/abs/2405.17247.

[13] Petrović, N., Vasić, S., Milić, D., Suljović, S., and Koničanin, S. (2021) GPU-supported simulation for ABEP and QoS analysis of a combined macro diversity system in a Gamma-shadowed k-μ fading channel, *Facta Universitatis: Electronics and Energetics*, Vol. 34, No. 1, pp. 89-104. https://doi.org/10.2298/FUEE2101089P.

[14] OpenGVLab: InternVL Family: Closing the Gap to Commercial Multimodal Models with Open-Source Suites—A Pioneering Open-Source Alternative to GPT-4oOpen Release of Grok-1 [online], available on: https://github.com/OpenGVLab/InternVL, last accessed: 09/02/2025.

The 17th Baška Conference
GNSS
Global Navigation Satellite Systems
Green Navigation and Smart Systems

GNSS RTK MEASUREMENTS UNDER CONDITIONS OF INCREASED IONOSPHERIC ACTIVITY

Danijel Šugar*, Matija Matijević, Petar Jelić

University of Zagreb, Faculty of Geodesy, Zagreb, Croatia
* *Corresponding author:* Danijel Šugar (dsugar@geof.hr)

Abstract. *The Sun shows its activity in an approx. 11-year cycle. The ionosphere as a layer of the Earth's atmosphere is a dispersive medium for GNSS signals. Ionospheric refraction as the largest individual source of GNSS errors must be adequately treated or mitigated to ensure positioning and navigation with cm-level precision. Under increased ionospheric conditions, the ionospheric effect cannot always be eliminated only by a multi-frequency approach. This is why different GNSS receiver manufacturers have developed algorithms to mitigate the ionospheric effect of the RTK measurement. To test the Trimble's IonoGuard technology, three GNSS rover receivers performing RTK single-base measurements were simultaneously used at distances from the base receiver of approx. 8 km, 16 km, and 24 km, respectively. The observation schedule featuring 17 sessions was devised for 15th November 2024 with the IonoGuard option being simultaneously enabled or disabled at the base and rover receivers. The results were assessed and the session with the most pronounced ionospheric effects at the 24 km long baseline is presented. As expected, the effect is more pronounced as the distance from the base increases.*

Keywords: *GNSS; RTK; Ionospheric refraction; IonoGuard; Sun cycle*

University of Zadar

1. INTRODUCTION AND BACKGROUND

The Real-Time Kinematic (RTK) GNSS (Global Navigation Satellite System) surveying method relying on phase observations providing cm-level positioning has been used for surveying since the early 1990s [1]. The method includes at least two receivers: the base receiver collecting observations on the station with known coordinates, calculating the correction of observations, and broadcasting those corrections to the rover receiver observing the same satellites as the base receiver. The rover receiver then uses the received observation corrections to solve the double-difference (DD) phase ambiguities and subsequently obtain the coordinates with the cm-level in real-time [2]. Due to the spatial decorrelation of GNSS errors between the base and rover receivers, this method is limited to the distance of 10-20 km [3]. This holds for the times with regular ionospheric activity. In the presence of ionospheric disturbances, the maximum distance between the base and rover receiver can be just a few km [4]. Ionospheric delay is modelled and eliminated by dual-frequency observations enabling the Iono-free combinations of phase measurements. The effect of the ionosphere is almost removed (> 99.9%, at least to the first order) by the Iono-free linear combination, where the second order effect of the ionosphere (< 0.1%) is at mm-level and remains uncorrected [5], [6].

The ionosphere is a dispersive medium for the GNSS signals meaning that their propagation is frequency dependent. It extends from approx. 50 km above the surface of the Earth up to approx. 1000 km and it owes its existence primarily to the UV (UltraViolet) radiation from the Sun [7]. The ionosphere is electrically charged and characterized by the presence of ions and free electrons having spatially and temporally variable density. It is the density of electrons, or more specifically the Total Electron Content (TEC) between the station and the satellite broadcasting the signals that causes the ionospheric delay. The structure of the ionosphere is subject to continuous changes according to the changes in solar activity and Earth's magnetic field [8]. Coronal Mass Ejections (CME), solar flares, and extreme ultraviolet (EUV) radiation coming from the Sun are the causes of geomagnetic storms in the Earth's magnetic field, which in turn may lead to a loss of lock in satellite tracking and may cause signal acquisition problems. Generally, geomagnetic storms lead to increased spatial and temporal variation of the TEC and this can cause additional ionospheric scintillations defined as irregularities that can produce both diffraction and refraction effects causing short-term signal fading and adversely affecting the receiver's tracking

capabilities. Scintillation leads to rapid fluctuations in GNSS signal amplitude and phase as well as signal fading [9]. In such conditions, even the multi-frequency and multi-constellation RTK positioning solution can be negatively impacted [10]. We are currently in the 25th cycle of solar activity which is predicted to have its maximum in 2025 [11].

The I95 index is the value providing statistical information on the expected residual ionospheric biases. Indicators of the expected size of the residual ionospheric error are of great importance for the users of single-base RTK. I95 is based on the differential ionospheric residuals as computed in a network of GNSS reference stations. Hourly I95 index values derived from the CROPOS network are publicly available on the CROPOS GNSS Web [12]. I95 index is given in numbers with the following meaning: < 2 (very low activity, no impact), 2-4 (normal activity, very little impact), 4-8 (increased activity, the impact can be noticeable (possibly longer initialization times), > 8 (high activity, impact very likely noticeable (possibly no rover fixes at all)) [13].

Trimble has developed the IonoGuard technology for mitigation of the effect of solar activity on the precision positioning in Trimble ProPoint enabled receivers. The product was released in October of 2023 and was designed to mitigate ionospheric disruptions in positioning and navigation by minimizing performance impacts caused by scintillation or signal noise [14]. The increased solar activity may have the following negative effects on GNSS: moderate to severe tracking problems around equatorial anomaly and polar regions and occasional problems due to the Travelling Ionospheric Disturbances (TIDs) at mid-latitudes; degraded RTK initializations and positioning performance, degraded VRS network performance [15].

Since the appearance of commercial RTK receivers on the market in the early 1990s, the current solar cycle 25 is the fourth one posing issue to the users of phase GNSS positioning methods. Over the years, each solar cycle has resulted in development aimed at improving the receiver‘s tracking and processing algorithms. IonoGuard addressed the issue on two levels: in signal tracking and in RTK algorithms [13]. Optimum performance in RTK positioning is reached when the IonoGuard technology is enabled on the base and rover receivers. When IonoGuard is enabled at the base receiver, ionospheric information for each satellite is transmitted via Trimble‘s proprietary CMRx (Compact Measurement Record) or RTCM MSM protocol to the rover receiver.

2. METHODOLOGY

In order to test the performance of the single-base RTK method under increased ionospheric activity conditions, the three most recent Trimble receivers available on the market were used: R980, R12i, and R780. All those receivers are equipped with 672 channels, integrated antenna, capability of observation of all GNSS constellations, and featuring the ProPoint GNSS engine supporting the IonoGuard technology [16]. The GNSS receiver at the base station was Trimble Alloy with the Zephyr 3 Geodetic antenna. All rover receivers were accompanied by the appropriate field controller running Trimble Access 2024 software. Within the field software was chosen the survey style 'RTK & Data Logging' with the goal to record the raw GNSS observations along with the RTK survey. Within Trimble Access software, the measurement method 'Continuous Topo' was chosen to get the results with 1 second observation rate. The rover receivers Trimble R12i, R780, and R980 were collecting RTK observations at distances of approx. 8 km, 16 km, and 24 km respectively. The correction stream of RTK measurements was broadcast from the base and received by the rover receivers in CMRx format [17].

	Planned (GPST)					8 km: RANGE [m]		16 km: RANGE [m]		24 km:RANGE [m]	
Session	Start	Stop	BASE	ROVER	Duration	ΔE	ΔN	ΔE	ΔN	ΔE	ΔN
1	07:00	07:30	NO	NO	00:30			0.016	0.022	0.019	0.031
2	07:35	08:05	IONO	IONO	00:30			0.021	0.034	0.026	0.048
3	08:10	08:25	IONO	NO	00:15	0.009	0.015	0.012	0.021	0.117	0.101
4	08:25	08:40	NO	IONO	00:15	0.016	0.021	0.025	0.041	0.115	0.108
5	08:45	09:15	IONO	IONO	00:30	0.014	0.030	0.018	0.033	0.021	0.033
6	09:20	09:50	NO	NO	00:30	0.014	0.025	0.014	0.026	0.015	0.032
7	09:55	10:25	IONO	IONO	00:30	0.022	0.036	0.026	0.035	0.029	0.050
8	10:30	11:00	NO	NO	00:30	0.014	0.021	0.027	0.025	0.023	0.026
9	11:05	11:35	IONO	IONO	00:30	0.022	0.026	0.028	0.029	0.024	0.027
10	11:40	12:10	NO	NO	00:30	0.016	0.016	0.023	0.017	0.015	0.023
11	12:15	12:45	IONO	IONO	00:30	0.022	0.025	0.024	0.032	0.023	0.031
12	12:50	13:20	NO	NO	00:30	0.016	0.020	0.022	0.021	0.020	0.033
13	13:25	13:55	IONO	IONO	00:30	0.022	0.026	0.028	0.032	0.022	0.039
14	14:00	14:15	IONO	NO	00:15	0.012	0.016	0.018	0.016	0.012	0.019
15	14:15	14:30	NO	IONO	00:15	0.017	0.024	0.015	0.020	0.015	0.020
16	14:35	15:05	IONO	IONO	00:30	0.019	0.027	0.026	0.026	0.021	0.031
17	15:10	15:40	NO	NO	00:30	0.017	0.026	0.022	0.024	0.020	0.030

NO = IonoGuard **DISABLED**
IONO = IonoGuard **ENABLED**

Figure 1. RTK observation sessions (15th November 2024) with the IonoGuard option being enabled or disabled at the base and rover receivers. Range values (ΔE, ΔN) are given for the rovers with 8 km, 16 km, and 24 km long baselines. There is no observation data in session 1 and 2 at 8 km long baseline due to mobile internet connectivity problems.

At the beginning of each observation session, a mobile phone connected to the GNSS receiver via a Wi-Fi and running the WUI (Web User Interface) software was used to enable or disable the IonoGuard option according to the observation plan outlined in **Figure 1**. The communication link between the base and a rover receiver was realized via mobile Internet.

In order to collect 1-Hz RTK measurements under different time windows and ionospheric conditions on 15th November 2024, a special observation plan was designed. The observation day was divided into sessions with the IonoGuard option being enabled or disabled at the base and rover receivers. In that respect, there were four possible combinations with precedence being given to the combination including IonoGuard being enabled or disabled on both receivers. Such sessions were planned to last 30 minutes, other (hybrid) combinations with IonoGuard being enabled/disabled on the base receiver and being disabled/enabled at rover receivers lasted 15 minutes. Range values are given for each session obtained as MAX-MIN of coordinate components (ΔE, ΔN). The results in Sessions 3 and 4 (24 km long baseline) are marked in orange showing the largest range values. Other sessions showing increased range values are marked yellow. It is interesting to note that sessions 7 and 13 (with IonoGuard being enabled at all receivers) display increased ranges at all rover receivers, and those ranges increase as the baseline length increases.

3. RESULTS AND DISCUSSION

Each session was closed with observations being interrupted, the communication link to the base receiver terminated and the raw observation file saved internally for subsequent postprocessing. The activities at all three rover stations were carried out simultaneously according to the plan outlined in **Figure 1**. Before going deeper into the analysis of the results obtained by field measurements, the I95 index given by the CROPOS network (available at **[12]**) will be assessed. In the time-window 8-11 of local time (7-10 GPST) it was expected to have 'High activity' with possible ionospheric impact very likely noticeable. Sessions 3 and 4 showing by far the largest coordinate ranges fall within the period of the highest I95 values. Going to the end of the observation day, I95 values indicated medium to normal activity which is in line with the range values obtained in the Session 14 and later (**Figure 1**).

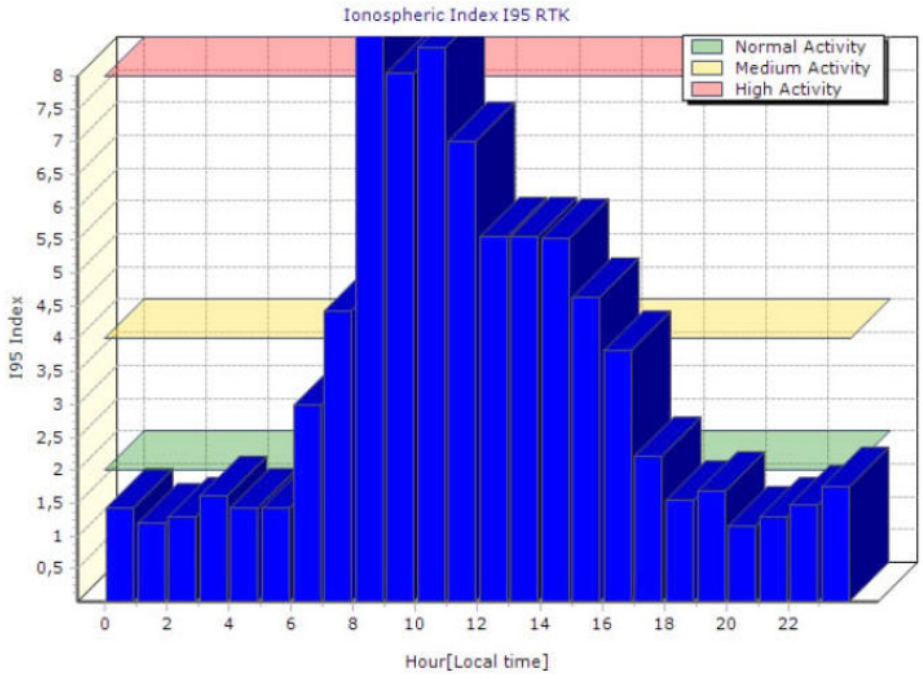

Figure 2. Hourly ionospheric index I95 RTK values (15th November 2024) from CROPOS network, time is given in local time (UTC+1).

Figure 3 shows all RTK results obtained in Session _3 (24 km long baseline). The first results determined in the session are displayed on the left side, and after approx. 150 epochs (2.5 minutes) of convergence, the remaining results are grouped around the red triangle representing the static processing value It should be pointed out that RTK positioning in Session_3 has been carried out with the IonoGuard enabled at the base station receiver, and disabled on the rover receiver. This is a combination that is not recommended by Trimble. It can be inferred that there was a systematic effect in the observation data which was not immediately handled. Most likely the rover receiver has encountered difficulties in resolving the phase ambiguities caused by the increased ionospheric activity.

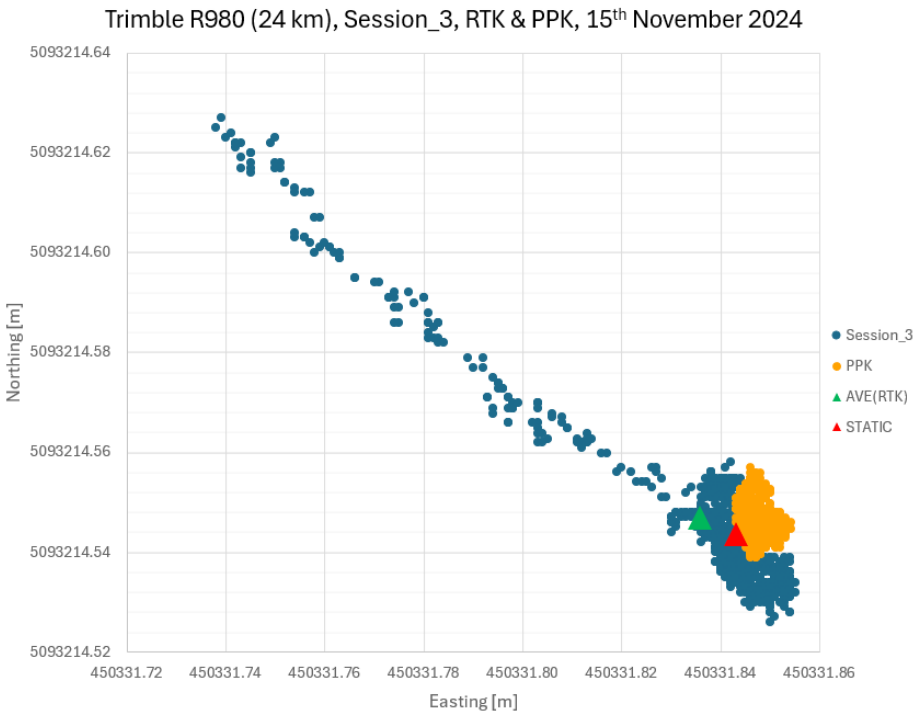

Figure 3. Session_3 (24 km long baseline) planar results (E, N). Along with RTK, the results obtained by PPK and static processing are displayed. The green triangle presents the Average value obtained from all RTK solutions in Session_3. The red triangle is the result of static processing.

To get a clear picture of the results obtained by IonoGuard option being enabled or disabled at both the base and rover receivers, the maximum range values (ΔE, ΔN) for the 8 km, 16 km, and 24 km long baselines are given in **Table 1**.

Table 1. Maximum range values (ΔE, ΔN) from the sessions 5-13 and 16-17 with IonoGuard enabled or disabled at the base and rover receivers.

BASE	ROVER	8 km: RANGE [m]		16 km: RANGE [m]		24 km: RANGE [m]	
		ΔE	ΔN	ΔE	ΔN	ΔE	ΔN
IONO	IONO	0.022	0.036	0.026	0.035	0.029	0.050
NO	NO	0.017	0.026	0,027	0,025	0.023	0.026

Contrary to the expected, larger maximum range values (ΔE, ΔN) are obtained with IonoGuard being enabled in comparison to the IonoGuard option being disabled at both base and rover receivers. This can lead to the conclusion that IonoGuard has not contributed to the performance of RTK positioning, but we have to be aware of the fact that the sessions having the IonoGuard enabled or disabled were not performed simultaneously. Nevertheless, the overall increase of the maximum range values (ΔE, ΔN) with the increase of the baseline length is clearly visible.

With static raw observations being stored at the base and the rover receivers, in Trimble Business Centre (TBC) 2024.00 software, the PPK (Post-Processed Kinematic) and static solutions were derived. PPK solutions show generally smaller range values in comparison to simultaneous RTK solutions. The coordinates obtained by static processing and the subsequent network adjustment are given with a sub-cm precision. Sessions carried out in the second half of the observation day (Session 8-17) generally show smaller range values (Figure 1) as a consequence of the smaller ionospheric activity and consequently smaller I95 index values (**Figure 2**).

4. CONCLUSIONS

The field testing of the single-base RTK method using three GNSS rover receivers featuring the ProPoint RTK processing engine was carried out at distances of 8 km, 16 km, and 24 km from the base receiver in conditions of increased ionospheric activity. Using the base and rover GNSS receivers, all of which support the IonoGuard technology, an observation schedule was created where the observation day was divided into 17 sessions with the IonoGuard option being enabled or disabled on the base or/and rover receivers. Along with the RTK measurements, the raw GNSS observations were stored for subsequent PPK and static processing. During field observations, the I95 index values ranged from 'High' to 'Medium' activity. The analysis of Sessions 3 (24 km long baseline) with the increased range RTK values (ΔE, ΔN) has shown that the initial results were under a sort of systematic influence (most likely caused by the ionospheric activity); the subsequent results have shown a convergence toward the average value of the session where the remaining results were grouped. The raw GNSS observations were processed against the base station observations resulting in PPK solutions with significantly smaller range values (ΔE, ΔN) compared to RTK results. The first half of the observation day (sessions 1-7) was under stronger

impact of ionospheric activity in comparison to the second half (sessions 8-17) of the observation day. This conclusion can be drawn from the range (ΔE, ΔN) as well as from the I95 index values. The main weakness of the field testing being carried out and presented here is that the sessions with the IonoGuard being enabled or disabled at the rover receiver were not carried out simultaneously. Generally, the results obtained with the IonoGuard being enabled at the base and rover receivers have shown larger maximum range values (ΔE, ΔN) compared to the results obtained with the IonoGuard being disabled at both receivers. Such results were not expected, meaning that the IonoGuard algorithm has room for the improvement. Nevertheless, to obtain simultaneous observations at the same location having the IonoGuard enabled and disabled under increased ionospheric activity, two receivers of the same model (e.g. two receivers Trimble R980) are needed, and observations should be taken over the baseline longer than 24 km under conditions of increased ionospheric activity.

REFERENCES

[1] Trimble (2024). Trimble ProPoint Engine, Next-Generation Centimeter Positioning and Orientation, White Paper, January 15, 2024. Available from: https://geospatial.trimble.com/en/resources/whitepaper/trimble-propoint-whitepaper-english, accessed 9 April 2025.

[2] European Space Agency (ESA). (2025). Navipedia - RTK Fundamentals. Available from: https://gssc.esa.int/navipedia/index.php?title=RTK_Fundamentals, accessed 9 April 2025.

[3] El-Mowafy, A. (2012). Precise Real-Time Positioning Using Network RTK, in Global Navigation Satellite Systems – Signal, Theory and Applications, edt. Shuanggen Jin, InTech, pp. 161-188, DOI: 10.5772/29502. Available from: https://www.intechopen.com/chapters/27714, accessed 9 April 2025.

[4] Wanninger, L. (2004). Ionospheric Disturbance Indices for RTK and Network RTK Positioning, Proc. ION GNSS 2004, Long Beach, CA, 2849-2854. Available from: https://www.wasoft.de/lit/ion04f64.pdf, accessed 9 April 2025.

[5] Ouassou, M. (2021) GNSS data analysis – Quality assessments and integrity design. Technical report of the Norwegian Mapping Authority, 19-04811-14. Available from: https://www.kartverket.no/globalassets/forskning-og-utvikling/rapporter/gnss-data-analysisquality-assesments-and-integrity-design.pdf, accessed 9 April 2025.

[6] European Space Agency (ESA). (2025). Navipedia – Ionospheric Delay. Available from: https://gssc.esa.int/navipedia/index.php?title=Ionospheric_Delay, accessed 9 April 2025.

[7] Klobuchar, J. A. (1991). Ionospheric Effect on GPS, GPS World, Vol. 2, No. 4, April 1991, pp. 48–51. Available from: http://gauss.gge.unb.ca/gpsworld/EarlyInnovation-Columns/Innov.1991.04.pdf, accessed 9 April 2025.

[8] Langley, R.B. (2000). GPS, the Ionosphere, and the Solar Maximum, GPS World, Vol. 11, No. 7, July 2000, pp. 44–49. Available from: http://chain.physics.unb.ca/docs/gpsworld-july2000.pdf, accessed 9 April 2025.

[9] U-Blox (2025). Why do solar storms affect GPS signals? Available from: https://www.u-blox.com/en/blogs/insights/solar-storm-gps-signals, accessed 9 April 2025.

[10] Riley, S. (2024). The Sun is Heating Up, But Stay Cool, Practical Advice as Solar Cycle 25 Peaks. The American Surveyor, Volume 21, Issue 3. Available from: https://amerisurv.com/2024/08/24/the-sun-is-heating-up-but-stay-cool/, accessed 9 April 2025.

[11] National Oceanic and Atmospheric Administration (NOAA). (2025). Solar Cycle Progression, Available from:https://www.swpc.noaa.gov/products/solar-cycle-progression, accessed 9 April 2025.

[12] Croatian Positioning System (CROPOS) (2025). I95 Ionosphere Index, Available from: https://gnss.cropos.hr/MemberPagesNetwork/Ionosphere.aspx, accessed 9 April 2025.

[13] Schrock. G. (2024). Preparing for the Effects of Solar Cycle 25 on GNSS Applications, XYHT Magazine. Available from: https://www.xyht.com/gnsslocation-tech/solar-cycle-25-and-gnss/, accessed 9 April 2025.

[14] Trimble (2023). Trimble Geospatial - Trimble IonoGuard, Available from: https://geospatial.trimble.com/en/resources/whitepaper/trimble-ionoguard-rtk-gnss-techpub, accessed 9 April 2025.

[15] Trimble (2025). Trimble GNSS Planning Online. Available from: https://www.gnssplanning.com/#/ionosphericeffects, accessed 9 April 2025.

[16] Trimble (2025). Trimble Geospatial – R780. Available from: https://geospatial.trimble.com/en/products/hardware/trimble-r780, accessed 9 April 2025.

[17] Trimble (2009). Trimble, White Paper (CMRx). Available from: https://trl.trimble.com/docushare/dsweb/Get/Document-469944/WhitePaper_HeavyHighway_CMRxrev1.pdf, accessed 9 April 2025.

The 17th Baška Conference
GNSS
Global Navigation Satellite Systems
Green Navigation and Smart Systems

A STUDY ON IONOSPHERIC AND GEOMAGNETIC DYNAMIC VARIATIONS IMPACT ON GPS L1 POSITIONING: EMERGENT STRUCTURAL SPECIFICITIES

Luka Matijašević[1*], Serdjo Kos[2], Mario Musulin[1], David Brčić[2]

[1] University of Defence and Security "Dr. Franjo Tuđman", Zagreb, Croatia

[2] University of Rijeka, Faculty of Maritime Studies, Rijeka, Croatia

[*] *Corresponding author:* Luka Matijašević (luka.matijasevic@morh.hr)

Abstract. *Satellite navigation signals are influenced by various atmospheric conditions that can alter their propagation and, in turn, impact positioning accuracy. Among these influences, ionospheric disturbances—particularly those driven by geomagnetic activity—play a crucial role, with the F2 layer being especially significant for Global Navigation Satellite System (GNSS) signal transmission. This study explores how ionospheric and geomagnetic variations affect single-frequency Global Positioning System (GPS) L1 positioning under a range of space weather conditions. Data from four mid-latitude International GNSS Service (IGS) stations was analysed over a two-year period. For each station, Total Electron Content (TEC) values were calculated, and three-day intervals per month were selected to represent different levels of geomagnetic activity, as defined by Kp index thresholds. Positioning solutions were generated for two scenarios: one incorporating the standard ionospheric correction model, and the other without ionospheric correction. The differences between these approaches (positioning residuals)*

were used to evaluate the model's performance under varying geomagnetic conditions. The results were further examined through statistical correlation with TEC and Kp values, offering additional insights into the nature of space weather dynamics and its influence on positioning reliability. During quiet conditions, TEC displayed a regular diurnal pattern consistent with model expectations. However, under severe geomagnetic storms, TEC values were significantly reduced and the expected diurnal trend nearly disappeared, suggesting ionospheric depletion effects. These findings highlight the limitations of the standard model during disturbed periods and point to the need for improved correction strategies in single-frequency GPS applications.

Keywords: *satellite navigation; total electron content; ionospheric delay; space weather; statistical analysis*

1. INTRODUCTION

Satellite navigation signals are subject to ionospheric delays, which represent the most significant source of error in single-frequency satellite positioning [1-3]. A variety of satellite data and products in standardized formats are provided by global and regional GNSS reference networks [4]. These datasets can be employed to compute positioning solutions [5], which, when combined with ionospheric and geomagnetic indices, enable comprehensive analyses of the effects of the propagation medium on satellite positioning accuracy. The aim of this study was to investigate GPS L1 positioning deviations under varying levels of geomagnetic and ionospheric activity and to evaluate the effectiveness of the standard ionospheric correction model under both quiet and disturbed space weather conditions. In this context, positioning deviations are interpreted as indicators of the satellite navigation environment and of the dispersive characteristics of the ionosphere.

2. METHODOLOGY

Ground truth data was collected from four globally distributed IGS stations located in the mid-latitude zone, over a two-year observation campaign. Based on the Kp index values that characterize geomagnetic activity levels [6] representative three-day periods within each month were selected for further analysis.

Table 1. Locations of the elaborated IGS stations; source: [7].

Station	Position		
	Latitude	Longitude	Elevation (m)
Halifax, Canada	44.68 N	63.61 W	3
Morpeth, United Kingdom	55.21 N	1.68 W	144
Chumysh, Kazakhstan	42.99 N	74.75 E	716
Usuda, Japan	36.13 N	138.36 E	1508

Positioning solutions were computed for two scenarios: (i) including, and (ii) excluding the application of the standard ionospheric correction model. Navigation and observation data in Receiver Independent Exchange Format (RINEX) [4] was processed using the RTKLIB software package [5]. TEC values for each station during the selected periods were calculated by applying ionospheric dual-frequency combinations, incorporating Differential Code Bias (DCB) corrections, and utilizing data from standard IONosphere map EXchange (IONEX) formats [8-10]. Further analyses were conducted within the R programming environment [11], including descriptive statistics, time series investigations and correlation between observables.

3. RESULTS

Correlation matrices (**Figure 1**), obtained using the Pearson metric, show a correlation between space weather parameters and positioning observables.

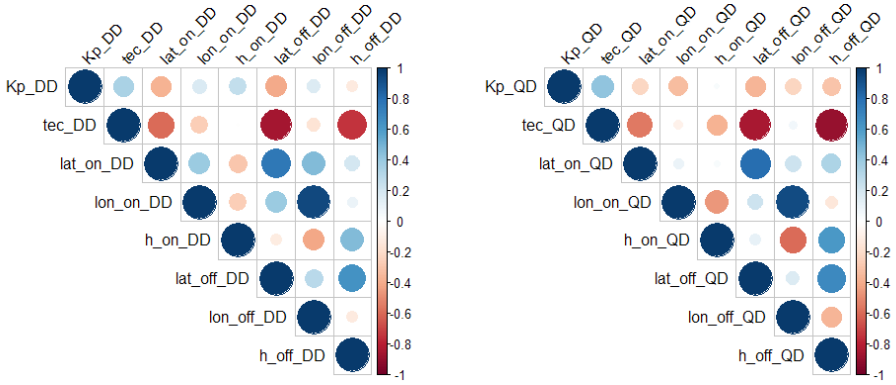

Figure 1. The overall correlation between geomagnetic and ionospheric indices, and positioning deviations for selected quiet (QD) and disturbed (DD) periods at all locations.

While the differences between modelled and unmodelled solutions in the horizontal components (latitude and longitude) are minimal, noticeable discrepancies are observed in the vertical (height) component. This indicates a stronger sensitivity of height estimation to ionospheric dynamics under varying geomagnetic conditions.

This is confirmed by the residual values—calculated as the differences between modelled and unmodelled solutions in latitude, longitude, and height (**Figure 2**). These residuals illustrate that while horizontal discrepancies remain minor, the vertical component shows a more pronounced deviation, reinforcing the sensitivity of height estimation to ionospheric effects.

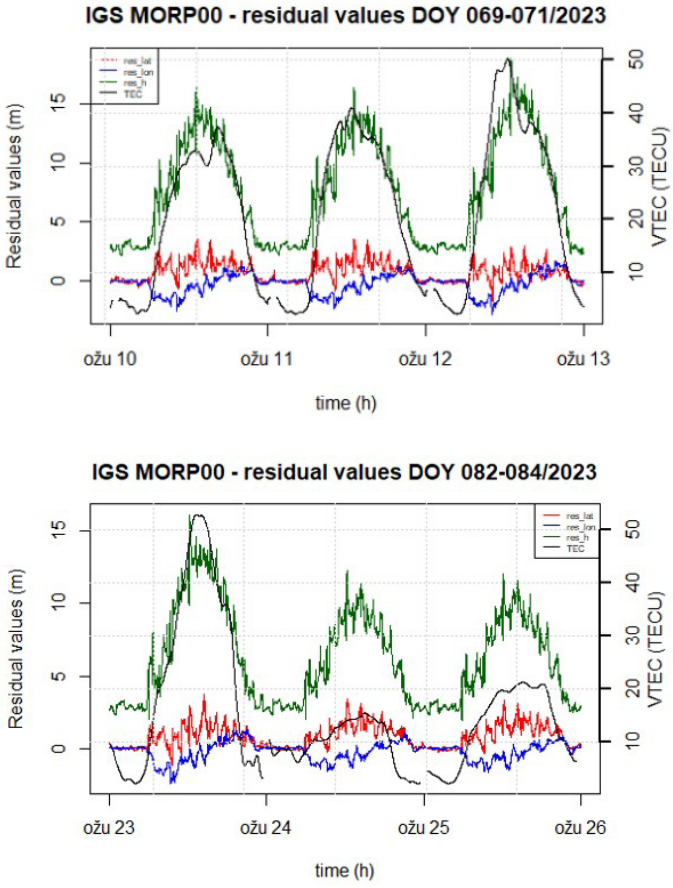

Figure 2. Time series of TEC patterns and positioning deviations as calculated for March 2023 quiet (above) and disturbed (below) three-days period at Morpeth IGS.

As for the TEC behaviour, a stable and regular diurnal pattern was observed during one representative three-day interval characterized by low geomagnetic activity (low Kp values). In this period, TEC values followed the expected trend—rising during the daytime and decreasing during the night, which is in line with the predictions of the Klobuchar model. However, during a severe geomagnetic storm (Kp = 8), this typical pattern was significantly disrupted. TEC values were markedly reduced, and the diurnal variability nearly disappeared. This behaviour reflects a known but peculiar classic negative storm effect, where intense geomagnetic activity leads to ionospheric depletion in mid-latitudes, likely driven by storm-induced changes in thermosphere circulation and electric fields [12]. These dynamics suppress the ionosphere's ability to accumulate and sustain electron density, resulting in lower TEC values even during daytime hours.

4. DISCUSSION AND CONCLUSION

The correlation analysis revealed a relationship between geomagnetic indices (Kp) and Total Electron Content (TEC) variability, and their influence on the performance of the standard ionospheric correction model. The standard model proves generally effective under quiet space weather conditions but shows limitations during geomagnetic disturbances, particularly in accurately modelling the height component. The results confirm that ionospheric and geomagnetic dynamics, particularly during periods of elevated space weather activity, have a measurable impact on single-frequency GPS positioning accuracy. These findings underscore the importance of accounting for space weather variability in GNSS applications which rely on single-frequency positioning. Future work will incorporate multi-frequency and multi-GNSS datasets, consider regional ionospheric models, and explore real-time correction strategies to enhance the robustness and accuracy of satellite positioning systems in dynamic space weather environments.

REFERENCES

[1] Klobuchar, J. A. (1987). Ionospheric time-delay algorithm for single-frequency GPS users. IEEE Transactions on Aerospace and Electronic Systems.

[2] Misra, P. and Enge, P. (2006). Global Positioning System: Signals, Measurements, and Performance. 2nd Edition, Ganga-Jamuna Press, Lincoln.

[3] Kaplan, E. D., & Hegarty, C. (2017). Understanding GPS/GNSS: Principles and Applications. Artech House.

[4] Gurtner, W. i Estey, L. (2009). RINEX: The Receiver Independent Exchange Format. V3.01. Pasadena: IGS Central Bureau.

[5] RTKLIB. (2013). An Open Source Program Package for GNSS Positioning. Tokyo. Takasu, T. Available at: http://www.rtklib.com, accessed 4 October 2021.

[6] SpaceWeatherLive (SWL) (2025). Available at: https://www.spaceweatherlive.com/en.html, accessed 11 June 2023.

[7] International GNSS Service (IGS) (2025). Available at: https://www.igs.org/, accessed 28 July 2023.

[8] Gopi K. Seemala. GPS-TEC analysis application (2020). Available at: https://seemala.blogspot.com/2020/12/gps-tec-program-version-3-for-rinex-3.html, accessed 4 October 2021.

[9] Manucci, A. J. et al. (1998). A global mapping technique for GPS-derived ionospheric total electron content measurements. Radio Science, 33 (3).

[10] The Astronomical Institute, University of Bern (AUIB). Available at: ftp://ftp.unibe.ch/aiub/CODE/, accessed 16 August 2023.

[11] RStudio Team (2020). RStudio: Integrated Development for R. RStudio, PBC, Boston, MA URL. Available at: http://www.rstudio.com/, accessed 4 October 2021.

[12] Mendillo, M. (2006), Storms in the ionosphere: Patterns and processes for total electron content, Rev. Geophys., 44, RG4001, doi:10.1029/2005RG000193.

The 17th Baška Conference
GNSS
Global Navigation Satellite Systems
Green Navigation and Smart Systems

POSITION NAVIGATION AND TIMING AS A SERVICE (PNTaaS) DEPLOYMENT FOR EUROPEAN OPERATIONS

Alison Brown*, Calvin Reese, Dien Nguyen, Zach Ruble

NAVSYS Corporation, 14960 Woodcarver Road, Colorado Springs, Colorado 80921 USA

* *Corresponding author:* Dr Alison Brown (abrown@navsys.com)

Abstract. *In this paper, we describe the operation of the open architecture Position, Navigation, and Timing (PNT) as a Service (PNTaaS) solution and the status of deploying this capability to provide a backup PNT capability in Europe for operation under Global Navigation Satellite Systems (GNSS) denial. PNTaaS provides data services that publish content which allows existing broadband satellite communications (SATCOM) signals to be used as Signals of Opportunity (SoOP) for PNT. Users can then subscribe to the PNTaaS services to receive data content snapshots of the broadband SoOP along with the timing and satellite location data needed to use these signals for PNT using a simple Software Defined Radio (SDR).*

Keywords: *GPS denial; PNT as a Service (PNTaaS); SATCOM; Signals of Opportunity (SoOP)*

University of Zadar

1. INTRODUCTION AND BACKGROUND

This study will include the details of the PNTaaS implementation and a description of the status of PNTaaS ground infrastructure installations in Europe. Initial test results showing the timing accuracy provided by the initial deployment will be included with plans for the full PNTaaS infrastructure to deliver precision PNT service.

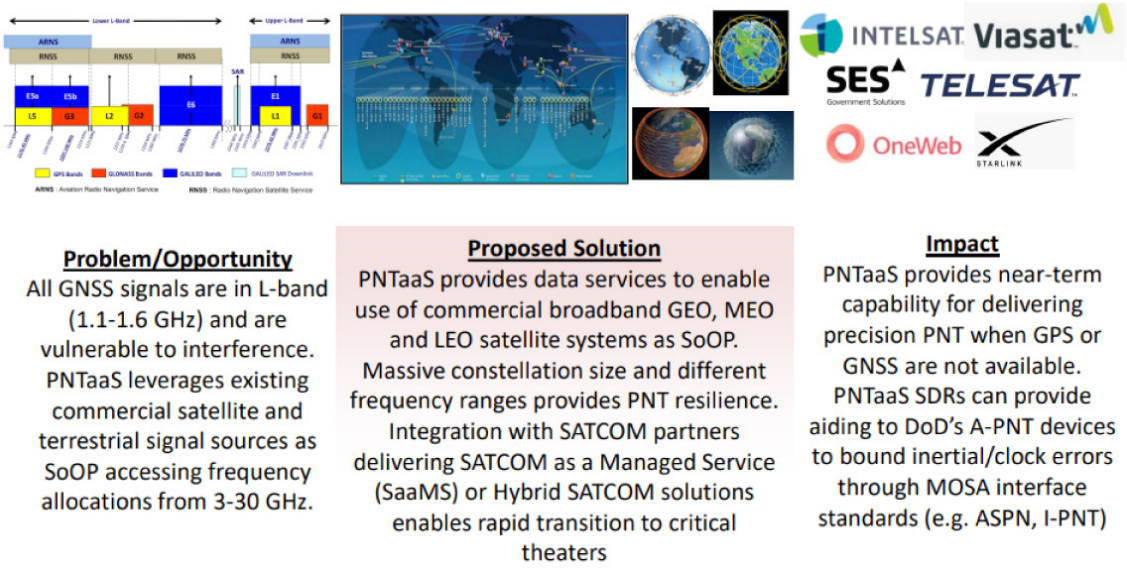

Figure 1. PNTaaS Solution Benefits.

2. METHODOLOGY

The PNTaaS Cloud Platform published SoOP data collected from ground infrastructure that monitors the selected SATCOM SoOP. The published data includes snapshots of the SoOP signal content that are used by PNTaaS subscribers to correlate with snapshots collected at the same time and frequency from the user's SDR. With a knowledge of the Time of Arrival (TOA) of the PNTaaS published snapshot and the frequency and bandwidth of the selected SoOP, as well as the precise location of the broadcasting satellite, a pseudo-range is provided that can be applied to update an embedded clock for timing, or an inertial unit for full PNT.

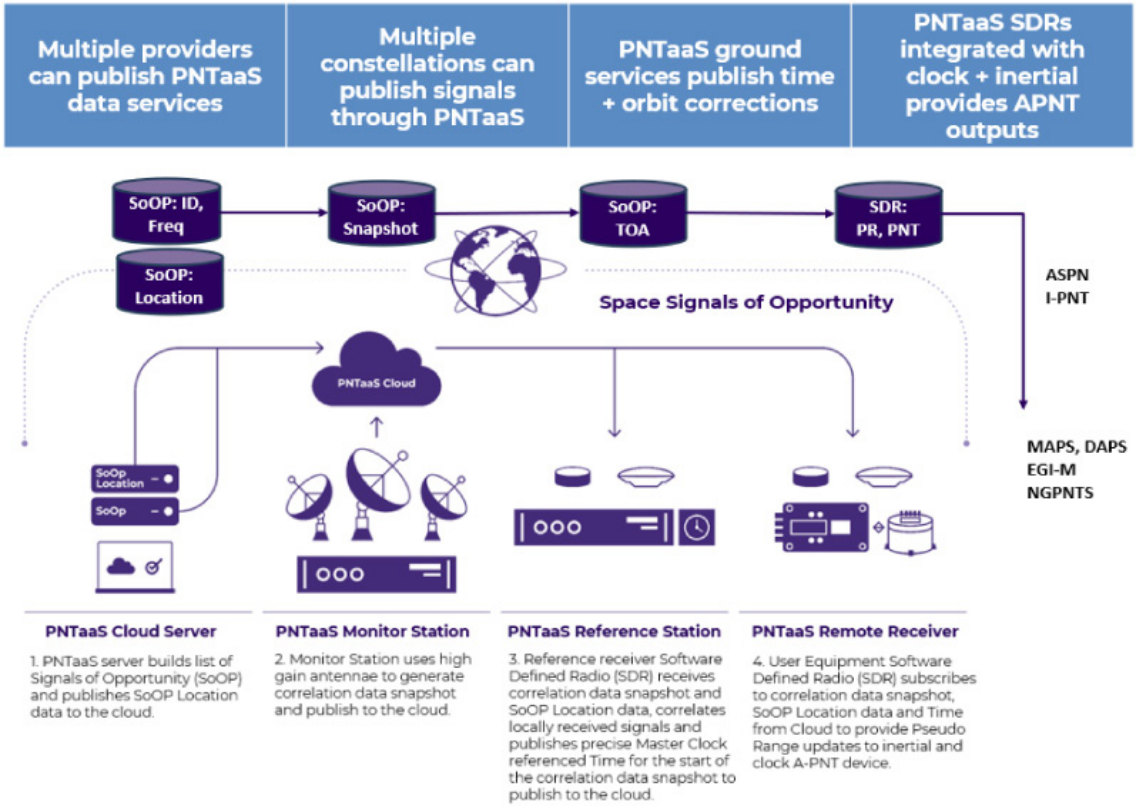

Figure 2. PNTaaS Open Architecture leverages existing space industrial base.

3. RESULTS AND DISCUSSION

The results presented will include timing accuracy from deployed PNTaaS SDR user equipment as compared with GNSS receivers to show the expected performance. We shall include test results using a variety of different SATCOM signals operating at Ku-band for PNT. Link budgets will be presented for the satellites used for the PNTaaS trials and also actual results comparing the received signal/noise ratio against the predicted Signal to Noise Ratio (SNR) results for selected satellites.

Table 1. Link Margin Examples at L, C, Ku and Ka for PNTaaS.

Downlink Performance	L-Band GNSS	C-Band SES-3	Ku-Band SES-2
Downlink EIRP per Carrier (dBW)	28.5	39	46.4
Power in Snapshot Bandwidth	27.5	32.5	40.8
Antenna pointing error	-0.5	-0.5	-0.5
Downlink Path Loss, ClearSky (dB)	-184.1	-197.0	-206.1
Downlink Rain Attentuation	-0.5	-0.5	-0.5
Earth Station G/T (dB/K)	-24.8	-24.8	-24.8
Boltzman Constant (dBW/K·Hz)	228.6	228.6	228.6
Downlink C/NO dB-Hz at SOR	**46.2**	**38.3**	**37.5**
Snapshot length (msec)	11	85	85
Processing Loss (dB)	-3	-5	-5
SoOP SORS/N (dB)	**23.7**	**22.6**	**21.8**
Antenna Gain (dBi)	0	0	0
Antenna Temperature (deg K)	303	303	303
Carrier Bandwidth (MHz)	20	36	36
PNTaaS SDR Bandwidth (MHz)	20	10	10
Broadcast Frequency (MHz)	1575	4200	12020
Satellite Altitude (km)	20,200	35,800	35,800
Max Range to satellite (km)	24,200	40,000	40,000
Min Elevation (rad)	0.261	0.279	0.279

4. CONCLUSIONS

The PNTaaS solution has been shown to provide a cost-effective augmentation alternative to provide precision PNT in the absence of GPS. SATCOM at C-band and Ku-band has been tested and the open architecture facilitates integration of new satellite constellations (GEO, MEO and LEO) as they become available.

NAVSYS is working with our commercial partners to integrate PNTaaS capability into their satellite infrastructure and to offer commercial SATCOM and Assured Positioning, Navigation, and Timing (A-PNT) products to their customers. We are actively seeking additional partners interested in offering PNTaaS services and integrating A-PNT capability into their products.

REFERENCES

[1] Brown, A., Nguyen, D., Silva, T., Redd, J., and Linan, A. (2023). PNT as a Service (PNTaaS): Providing a Resilient Back-up to GPS by Leveraging Broadband Satellite Constellations and Ground. In: Proceedings of *Institute of Electrical and Electronics Engineers (IEEE)/Institute of Navigation (ION) Position, Location and Navigation Symposium (PLANS) 2023 Conference*, April 2023, Monterey, California USA. Available from: https://static1.squarespace.com/static/570a836659827e091de14a8a/t/6453e555f6ce8378f12ddeb5/1683219798831/23-04-001+PNTaaS+Providing+a+resilient+Back-Up+to+GPS+by+Leveraging+Broadband+Satellite+Constellations+and+Ground+Infrastructure.pdf, accessed 24 January 2025.

[2] Brown, A., Nguyen, D., and Huerta, S. (2024). Leveraging commercial SATCOM services as Signals of Opportunity to provide PNT as a Service (PNTaaS). In: Proceedings of *National Defense Industrial Association's (NDIA) Emerging Technologies for Defense Conference and Exhibition,* August 2024, Washington, DC USA. Available from https://static1.squarespace.com/static/570a836659827e091de14a8a/t/66de092a6660ed040cb966f0/1725827373201/24-02-001_Leveraging+commercial+SATCOM+services+as+Signals+of+Opportunity+to+provide+PNT+as+a+Service+%28PNTaaS%29.pdf, accessed 24 January 2025.

[3] Brown, A. (2023). PNT as a Service (PNTaaS): Leveraging SATCOM for PNT. In: Proceedings of Position Navigation and Timing Advisory Board, May 2023. Washington, DC USA. Available from https://www.gps.gov/governance/advisory/meetings/2023-05/brown.pdf, accessed 24 January 2025.

[4] Brown, A. (2023). PNT as a Service (PNTaaS) Leveraging Commercial SATCOM. In: Proceedings of *Stanford University's Center for Position, Navigation and Time (SCPNT) 17th annual Position, Navigation and Time (PNT) Symposium*, November 2023. Stanford, California USA. Available from https://drive.google.com/file/d/1_bzo8qHmbRjKkmb9r3dB7O0HSAnsc82m/view, accessed 24 January 2025.

The 17th Baška Conference
GNSS
Global Navigation Satellite Systems
Green Navigation and Smart Systems

EVALUATION OF EDA SENSORS PERFORMANCE IN SIMULATED PORT APPROACH NAVIGATION

Dejan Žagar*, Franc Dimc

University of Ljubljana, Faculty of Maritime Studies and Transport, Slovenia

* *Corresponding author:* Dejan Žagar (dejan.zagar@fpp.edu)

Abstract. *This study compares wired wet-electrode and wireless dry-electrode wearable systems for monitoring physiological responses of* Officers of the Watch *(OOW) during port approaching scenarios in a nautical simulator. The wired system offers high precision but lacks practicality due to its complexity and grid-power supply. In contrast, the wireless system, while less precise, is portable, user-friendly, and capable of collecting data in real-time.*

Keywords: *Electro-Dermal Activity; EDA Sensors; Stress response; Nautical Simulator; OOW*

University of Zadar

1. INTRODUCTION AND BACKGROUND

This research focuses on the viability of wireless wearable devices for physiological data collection in maritime scenarios where wired systems are impractical, such as in dynamic environments on ship's bridge. *Electro-Dermal Activity* (EDA), which tracks changes in skin conductivity, serves as an indirect measure of autonomic nervous system arousal and is commonly linked to psychological stress and cognitive strain [1, 2]. By monitoring EDA data in real-time, particularly during simulated port approach tasks, including alarms which act as stressors, we aim to identify the weaknesses of both sensors, evaluating their accuracy and reliability in a simulated stress-induced environment. The findings are important for advancing remote monitoring in the maritime sector, where stress and human error have been key contributors to accidents [3]. By analysing results, we highlight the limitations and potential for further development of using wearable EDA devices in practical applications, such as remote monitoring, particularly in environments where mobility and ease of use are essential.

2. METHODOLOGY

The study included 15 participants, averaging 33.6 years old (SD = 8). All were students or are alumni of the Faculty of Maritime Studies. They are well-trained in simulator navigation, but lack real-world navigation experience. All had completed simulated maritime assessments, including *Automatic Radar Plotting Aids* (ARPA) navigation and the *Electronic Chart Display and Information System* (ECDIS) course, in accordance with *Standards of Training, Certification, and Watchkeeping* (STCW), ensuring proficiency in vessel handling, narrow waterway and traffic separation zone navigation, and collision avoidance. Research took place in *Wartsila's Navi Trainer 5000* simulator with a modern console, standard navigation tools, multifunctional displays, a conning station, radar, and an overhead monitor.

Participants were equipped with two EDA sensors. The experimental data were recorded using the *EmbracePlus* wristband [4], a wireless, dry-electrode EDA system with a 4 Hz sampling rate, connected via Bluetooth to a mobile app for real-time data transfer (**Figure 1**). The app uploads data to a cloud platform via Wi-Fi for secure storage, visualization, and preliminary analysis.

Control data were recorded using the *Biopac MP 150* [5], a wired medical-grade system with high-precision EDA acquisition via Ag-AgCl wet electrodes on the

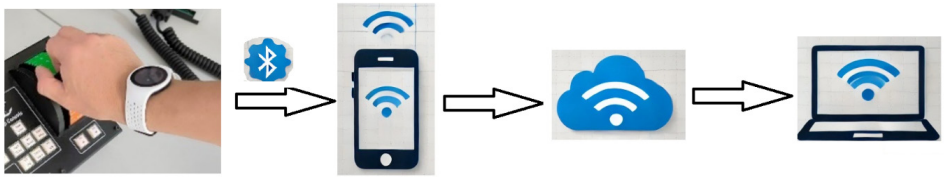

Figure 1. A wireless EDA sensor collects data via a wristband, transmitting it to a mobile phone via Bluetooth. The data was then stored in the cloud via Wi-Fi, allowing secure internet access from a computer.

distal phalange (**Figure 2**). It supports sampling rates up to 200,000 Hz and real-time analysis but requires extensive setup, technical expertise, and a lab environment due to its reliance on grid power.

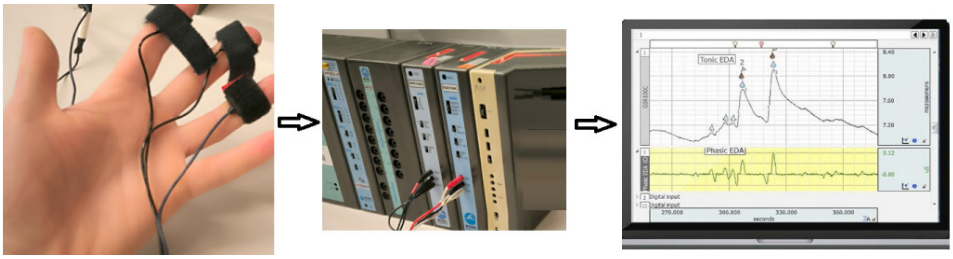

Figure 2. A wired EDA sensor transmits readings to a data acquisition (DAQ) system, which then processes it using specialized software for analysis. This setup ensures high accuracy and real-time monitoring but it relies on a power grid supply.

The exercise involved a 20-minute manoeuvring session focused on standard collision avoidance with a large vessel. Traffic and environmental parameters were modelled after typical North Adriatic conditions, incorporating typical vessel traffic, meteorological settings, navigational aids, traffic density, and challenges such as shallow-water navigation. As participants navigated the assigned route, they executed a standard port entry procedure including response to an auditory fire alarm, which served as the trigger for EDA data collection.

Recorded EDA data was analysed for skin conductance response in micro siemens (μS) and peak values at stressor onset. Readings were compared for accuracy, consistency, and sensitivity to auditory-alarm responses, evaluating the wireless system's potential for future real-world applications. Sensor similarity was quantified by comparing detected peaks, with Python libraries used to pre-

process signals and identify local maxima, as well as identifying peak height and distance parameters. The similarity ratio is calculated to assess alignment with the medical-grade sensor. A Bland-Altman analysis is conducted to evaluate sensor agreement, ensuring statistical reliability [6].

3. RESULTS AND DISCUSSION

Both the wired and wireless sensors accurately captured changes in skin conductance, reflecting physiological arousal in response to the alarm. As shown in **Figure 3a**, both systems successfully detected the increase in skin conductance following the alarm activation. The wired system (**Figure 3a** – green trend), utilizing wet electrodes and a high sampling rate, consistently produced stronger conductance signals, making it more reliable for capturing fine physiological changes. Its stable electrode contacts resulted in smooth and high-resolution data, minimizing artefacts and ensuring precise readings.

In contrast, the wireless sensor (**Figure 3a** – purple trend), equipped with dry electrodes and a lower sampling rate, generated signals with about one-tenth the amplitude of the wired system. While it still captured the general trend of physiological arousal, its lower signal strength limits its ability to detect subtle variations in skin conductance. The limitation of the wireless system was also sensitivity to motion artefacts. Due to the less stable contact of dry electrodes with the skin, wrist-movement introduced false peaks in the recorded data. As illustrated in **Figure 3b**, the artefacts resulted in sudden spikes that did not correspond to actual physiological responses but were rather caused by weak electrode-skin contact. The mentioned motion-induced disturbances occurred more frequently when participants moved their hands, adjusted their posture, or had very dry or very hairy skin.

To further evaluate the agreement between the two sensors, a similarity test was performed, revealing variation in the wireless sensor's performance under specific conditions, such as dry, hairy, or cold skin, affecting the signal consistency and occasionally causing a reduction in data reliability. To quantify the agreement between the wired and wireless sensors, the Bland-Altman method was applied, offering a statistical approach to assess the systematic differences and variability between the two measurement systems. The method defines the Limits of Agreement (LOA), representing the range in which 95% of the measurement differences between the sensors are expected to fall (red lines).

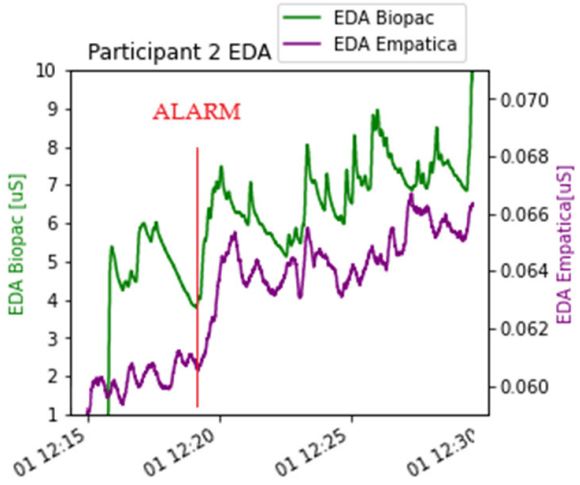

(a)

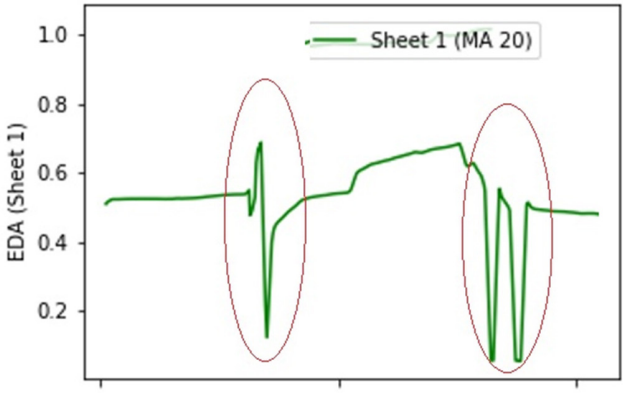

(b)

Figure 3. The wired and wireless sensors accurately recorded changes in skin conductance, reflecting heightened arousal in response to the alarm (a); Sensitivity to motion artefacts caused by the less stable contact of dry electrodes, resulting in false peaks in the data (b).

A narrower range in **Figure 4a** suggests a closer alignment between the wired and wireless sensors, while the wider range in **Figure 4b** demonstrates increased discrepancies, particularly in scenarios where the wireless sensor was affected by motion artefacts or varying skin conditions.

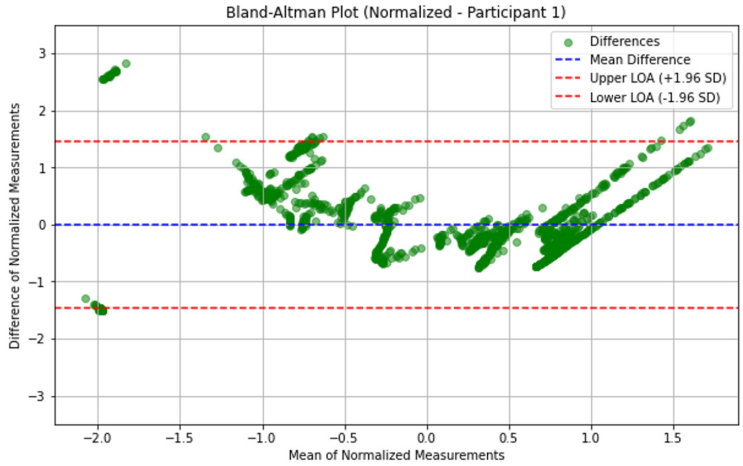

(a)

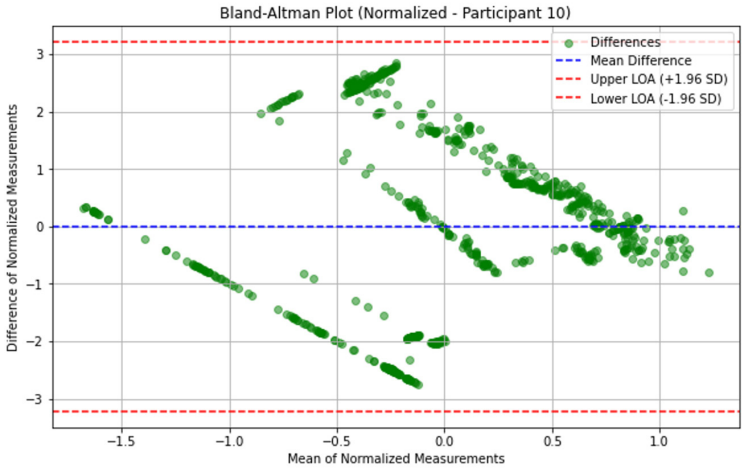

(b)

Figure 4. Bland-Altman method: Narrower ranges, as shown in figure (a), indicate stronger agreement between sensors, whereas wider ranges in figure (b) reflect greater variability in measurements. LOA defines the limits of agreement.

4. CONCLUSIONS

In conclusion, both wired and wireless sensors successfully detected changes in skin conductance, capturing arousal responses to the alarm. The wired system provided stronger signals due to its wet electrodes and higher sampling rate, while the wireless sensor exhibited lower signal amplitude and increased sensitivity to motion artefacts. Despite its limitations, the wireless sensor remains a viable option for mobile environments. Given that movement across the bridge is necessary in real-world ship operations, a wired system is impractical. Therefore, our next experiment on an actual ship bridge will utilize the wireless sensor to assess its performance in dynamic maritime conditions. Future research should address challenges like battery life, mechanical vibrations, and environmental interferences, including long-term effects of wearing such devices.

REFERENCES

[1] Boucsein, W. (2012). Electrodermal Activity. *Second Edition*. *Springer.*

[2] Geršak G. (2020). Electrodermal activity – a beginner's guide. *Electrotechnical Review* 87(4): 175-182, 2020.

[3] Žagar, D.; Svetina, M.; Brcko, T.; Perkovič, M.; Dimc, F.; Košir, A.(2022). Analysis of Marine-Pilot Biometric Data Recordings during Port-Approach Using a Full-Mission Simulator. *Sensors* 2022, 22, 2701. https://doi.org/10.3390/s22072701.

[4] Empatica EmbracePlus (2023). Available on: https://www.empatica.com/embraceplus/, accessed 12 April 2024.

[5] Biopac MP150 system (2021). Available: https://www.biopac.com/wp-content/uploads/MP150-Systems.pdf accessed 04 March 2024.

[6] Giavarina D.: Understanding Bland Altman analysis (2015). *Biochem Med (Zagreb).* 2015;25:141–151. DOI: https://doi.org/10.11613/BM.2015.015.

The 17th Baška Conference
GNSS
Global Navigation Satellite Systems
Green Navigation and Smart Systems

SEAFARERS' PERSPECTIVES ON ECDIS USAGE: BENEFITS, CHALLENGES, AND BEST NAVIGATIONAL PRACTICES

Maro Car[1*], David Brčić[2], Nermin Hasanspahić[1], Mario Bakota[3]

[1] University of Dubrovnik, Faculty of Maritime Studies, Dubrovnik, Croatia
[2] University of Rijeka, Faculty of Maritime Studies, Rijeka, Croatia
[3] University of Split, Faculty of Maritime Studies, Split, Croatia
[*] *Corresponding author:* Maro Car (mcar1@unidu.hr)

Abstract. *The Electronic Chart Display and Information System (ECDIS) was introduced to improve the safety of navigation and facilitate navigation tasks carried out by Officers of the Navigational Watch (OOW). However, despite its advantages, maritime accident reports indicate that inadequate use, insufficient training, and overreliance on ECDIS have led to navigational errors. This paper examines seafarers' views on ECDIS usage, focusing on their satisfaction with various models, its influence on the safety of navigation, and the benefits and drawbacks of Electronic Navigational Charts (ENC) compared to Paper Navigational Charts (PNC). A questionnaire was distributed to maritime industry stakeholders, and in this paper, responses from 154 active seafarers are discussed. Results show that while most respondents acknowledge ECDIS as an important tool for improving situational awareness and facilitating voyage planning, there are ongoing concerns about overreliance on electronic systems and the possible decline of traditional navigation skills. Findings indicate a necessity for improved*

training and standardised enhancements to ensure effective ECDIS utilisation while preserving the safety of navigation.

Keywords: *ECDIS; situational awareness; safety of navigation; electronic navigation chart (ENC)*

1. INTRODUCTION

Electronic Chart Display and Information System (ECDIS) was introduced on board ships to improve the safety of navigation and increase situational awareness. However, although it has facilitated the process of voyage planning and navigation, according to some studies and maritime accident investigation reports, it has contributed to maritime accidents [1-3]. Among the identified ECDIS-related key factors that have led to maritime accidents are inadequate usage and insufficient knowledge of the system, among others [3]. Furthermore, another problem identified is an overreliance on the system and the lack of use of other available means that improve the safety of navigation. Overreliance on the system has been recognised as one of the human factors that has caused several maritime accidents since officers of the navigational watch (OOWs), especially after the introduction of ECDIS, often rely solely on it as a navigational and collision avoidance means at sea [2,4,5]. Traditional navigation methods have fallen into the background, and it has even been observed that officers often fully trust the data displayed by ECDIS and fail to verify the ship's position using other methods and means, which should be mandatory [6]. In addition, research has shown that many OOWs prefer paper navigational charts (PNC) to electronic navigational charts (ENC) [7]. Accordingly, there is a need for further research into seafarers' professional opinions on the use of ECDIS. Therefore, this paper aims to examine the use of ECDIS from the seafarers' perspective, focusing on its impact on navigational safety, user satisfaction, and the advantages and limitations of ECDIS compared to PNCs. To achieve the aim described in this paper it is necessary to (a) identify the most frequently used ECDIS models on board ships and assess seafarers' satisfaction with them; (b) evaluate seafarers' perceptions of whether ECDIS has improved navigational safety or introduced new risks; (c) analyse the comparative advantages of ECDIS and PNCs, identifying key features that contribute to safe navigation; and (d) investigate concerns related to overreliance on ECDIS, insufficient training, and potential situational awareness challenges. By addressing these objectives, the paper aims to provide insights into the effective-

ness of ECDIS, highlight existing challenges, and offer recommendations for improving its implementation and training within the maritime industry.

2. METHODOLOGY

As this paper is a part of more extensive research that was carried out to investigate the safety of navigation in restricted waters using ECDIS and other navigational information systems, only part of the research results are presented. The authors used a questionnaire already developed for maritime industry stakeholders related to ECDIS to answer the research questions posed. For the purpose of more extensive research, a questionnaire titled "Navigation with ECDIS and beyond" was created and distributed internationally to maritime stakeholders related to ECDIS, including ECDIS makers, navigational charts producers, instructors at Maritime Education and Training (MET) institutions, ECDIS maintenance providers, Port State Control (PSC) Officers, ship owner representatives, and seafarers. It consisted of several interrelated sections, with questions referring to navigational information systems and data usage, features of voyage planning and monitoring processes, manoeuvring in restricted waters and related safety parameters. There was a total of 51 questions, where the first part dealt with personal data (7 demographic questions), and the following five parts contained 44 questions related to navigational information systems and their usage on board ships from the perspective of the mentioned stakeholders. A total of 203 respondents participated in the survey; however, for this study, the authors singled up active seafarers (154 respondents) since the aim of the study is to identify the advantages and shortcomings of ENC over PNC, the most frequent models of ECDIS in use on board ships, satisfaction with the usage of different models and opinions on how ECDIS usage affects navigational safety from the perspective of seafarers. Furthermore, in this paper, the responses to only ten questions were analysed because they are aligned with this study's aim. The survey was distributed online via Google Forms, and for those respondents who were unable to access the Internet, paper questionnaires were made available.

3. RESULTS AND DISCUSSION

This paper included two survey demographic questions about respondents' navigational ranks and sea-going experience. Most of the respondents were Masters (30%) and Chief Officers (26%), followed by 2nd Officers (20%) and other navi-

gational ranks. Regarding sea-going experience, 36% of respondents have been sailing up to nine years, 39% between ten and 19 years, and 25% had more than 20 years of sea-going experience. From the answers, it could be concluded that seafarers involved in the survey were experts and had the highest navigational ranks.

When asked what ECDIS models they use on their ships, the most frequent model was Furuno FMD 3200 – 3300 (22.7% of responses), followed by SAM Electronics ECDIS pilot platinum (20.8%) and TRANSAS NAVI—Sailor 4000 (12.3%). Hence, more than half of the respondents use these three ECDIS models on board their ships. According to the results obtained in [7], TRANSAS was the most frequently used system for obtaining the ECDIS generic certificate. In contrast, for the type-specific certificate, the most frequent system was SAM Electronics. Therefore, an interesting finding is that most seafarers use ECDIS Furuno models, while most of the training is conducted on other models.

The respondents (79%) are mostly or completely satisfied with the model used, 13% are neutral, while 8% are mostly or completely dissatisfied (**Figure 1**).

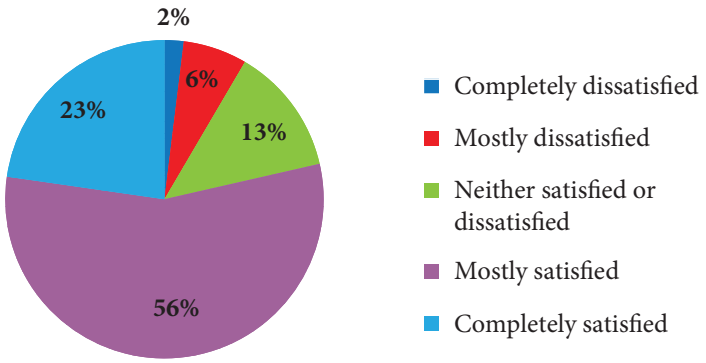

Figure 1. User satisfaction with ECDIS model used on board their ships.

The majority of respondents (46% agree and 38% strongly agree) believe that ECDIS implementation has improved the safety of navigation. Only 3% have a negative opinion on the ECDIS's effect on safety, while 13% remain neutral.

The most significant advantage of the ECDIS and ENC over the PNC, as recognised by the respondents, was that the ship's position is continuously displayed

(86 responses), followed by easier chart corrections (78 responses), reduced time required for voyage planning (73 responses), and improved situational awareness (69 responses). As expected, the continuous display of ship's position is the highest advantage of ECDIS, significantly improving situational awareness and facilitating navigational tasks. However, OOWs must not become over-reliant on the system and hence rely solely on the position obtained by the Global Navigation Satellite System (GNSS). The position should be regularly cross-checked and compared with the position obtained by other means to ensure it is correct [5].

In the context of ENC, the most desirable features that ECDIS could potentially provide, as per respondents' opinions, are additional environmental layers related to weather data (45 responses), improved standardisation (39 responses) followed by additional navigational and non-navigational layers (33 responses). Furthermore, 32 respondents would like to have ENC updates that are not dependent on satellite communication systems and the Internet. Some of the features, such as the weather overlay,that respondents would like to have on their ECDIS will be available through S-100x standards that are being developed, which will integrate meteorological and oceanographic information into ECDIS.

Although the findings indicate that most respondents are satisfied with the ECDIS models they use on board their ships, maritime accidents related to inadequate usage and insufficient knowledge of ECDIS suggest gaps in training [8]. Although mandated under the International Convention on Standards of Training, Certification and Watchkeeping for Seafarers (STCW), variations in training quality and seafarers' prior usage of different ECDIS models can affect competency levels. The lack of a standardised interface across different ECDIS types has also been identified as a challenge, requiring officers to adapt quickly to other ECDIS types when changing vessels [2]. Improved standardisation in ECDIS design and functionality is of the utmost importance since it would facilitate ECDIS-related training and reduce the familiarisation period with onboard navigational equipment for new joining officers and masters.

An interesting finding was obtained while analysing responses to whether PNCs have advantages over ENCs. The respondents could be divided into three almost equally numbered groups: 39% are against the statement (13% strongly disagree, 26% disagree), 31% remain neutral, and 30% are in favour (27% agree, and 3% strongly agree). Findings indicate that even though the system is a mandatory navigational aid, all users still do not fully accept it. Although ECDIS is mandatory for SOLAS ships, the results revealed that a notable portion of seafarers still

recognise the advantages of PNCs, particularly their independence from power sources and immunity to system failures. In addition, as reported by [7], a minimum required set of PNCs should be kept on board a ship as a backup measure. This emphasises the importance of maintaining basic paper chartwork skills among navigational officers to ensure resilience during power outages (blackouts).

Regarding the advantages of the PNC, the largest proportion of responses (59) refers to the fact that they are autonomous, power-independent, and not susceptible to malfunctions and technical issues (53 responses). Another recognised advantage, according to the respondents, is that there is no risk of information overload, which is the case with ECDIS.

When asked about their opinions regarding the impact of over-reliance on electronic aids to navigation and whether it contributes to decreased situational awareness, most participants (62%) expressed concern, agreeing or strongly agreeing that electronic navigational aids may reduce situational awareness. Only 15% disagreed with this statement, while the 23% remained neutral. While ECDIS provides real-time positioning and automated alerts, excessive dependence on it leads to complacency, where officers of the watch may neglect to cross-check ship position using other means such as radar or visual bearings [4,5]. The responses suggest that many seafarers acknowledge this issue, yet it persists as a contributing factor to navigational incidents.

4. CONCLUSIONS

This study examined seafarers' perspectives on ECDIS usage, focusing on its impact on navigational safety, user satisfaction, and the comparative advantages and limitations of ECDIS and PNCs. The results show that the majority of respondents are satisfied with the ECDIS models they use, with Furuno, SAM Electronics, and Transas being the most widely used on ships. However, concerns remain regarding overreliance on ECDIS, inconsistent training quality, and differing system interfaces among various manufacturers.

While ECDIS has significantly facilitated voyage planning, real-time positioning, and navigational efficiency, reliance on electronic systems without cross-checking by other navigational methods introduces significant navigational risks. This paper emphasises the need for standardised training, enhanced system usability, and additional ECDIS features, including weather overlays and offline ENC up-

dates. Despite PNCs being valued for their autonomy and reliability, the transition to digital navigation is unavoidable. Therefore, a hybrid approach that combines ECDIS with traditional methods is essential to ensure the safety of navigation.

Although this study provides valuable insights, it has limitations. The dependence on self-reported data introduces potential bias, as personal experiences and reluctance to acknowledge overreliance on ECDIS may influence responses. Additionally, only ten survey questions were analysed, which may not adequately represent all aspects of ECDIS usage, inadequate training, and safety issues. Future research should consider a more extensive questionnaire to gain more insight into ECDIS training effectiveness and its impact on the safety of navigation.

REFERENCES

[1] Asyali, E. (2012). The Role of ECDIS on Improving Situation Awareness. 13th Annual General Assembly of the IAMU, St. John's, Newfoundland and Labrador Canada, ISBN: 978-088901-439-9.

[2] Barić, M., Grbić, L., Peričin, J. and Jelić, R. (2023). The Role of the ECDIS on the Development of Situational Awareness – a Study on Grounding Accidents. The International Journal on Marine Navigation and Safety of Sea Transportation, 17 (1), pp. 219-225, https://doi.org/10.12716/1001.17.01.24.

[3] Vojković, L., Bakota, M. and Kuzmanić Skelin, A. (2024). Using the Bayes Probability Model to Evaluate the Risk of Accidents Caused by the Electronic Chart Display and Information System. Journal of Marine Science and Engineering, 12(8), 1391. https://doi.org/10.3390/jmse12081391.

[4] Bielić, T., Hasanspahić, N. and Čulin J. (2017). Preventing marine accidents caused by technology-induced human error. Scientific Journal of Maritime Research 31, pp. 33-37.

[5] Kristić, M., Žuškin, S., Brčić, D. and Car, M. (2021). Overreliance on ECDIS Technology: A Challenge for Safe Navigation. The International Journal on Marine Navigation and Safety of Sea Transportation, 15 (2), pp. 277-287, https://doi.org/10.12716/1001.15.02.02.

[6] The Standard Club (2016). Web Alert: Over reliance on technology a regular feature of navigation claims. Available at: https://www.standard-club.com/risk-management/knowledge-centre/news-and-commentary/2016/04/web-alert-over-reliance-on-technology-a-regular-feature-of-navigation-claims.aspx, accessed on 15 February 2025.

[7] Car, M., Brčić, D., Žuškin, S. and Sviličić, B. (2020). The Navigator's Aspect of PNC before and after ECDIS Implementation: Facts and Potential Implications towards Navigation Safety Improvement. Journal of Marine Science and Engineering, 8(11), 842; https://doi.org/10.3390/jmse8110842.

[8] Turna, I. and Öztürk, O. B. (2019). A causative analysis on ECDIS-related grounding accidents. Ships and Offshore Structures, 15(8), pp. 792–803. https://doi.org/10.1080/17445302.2019.1682919.

The 17th Baška Conference
GNSS
Global Navigation Satellite Systems
Green Navigation and Smart Systems

ENHANCING MARITIME SECURITY THROUGH MULTI-SATELLITE SHIP DETECTION

Marko Delić[1*], Nina Lenkić[1], Luka Tolić[1], Miro Petković[2]

[1] University of Split, Faculty of Maritime Studies, Split, Croatia (students)
[2] University of Split, Faculty of Maritime Studies, Split, Croatia (mentor)
[*] *Corresponding author:* Miro Petković (mpetkovic@pfst.hr)

Abstract. *This article examines the application of remote sensing technologies for ship detection in the Split Channel, Croatia, using Sentinel-1 Synthetic Aperture Radar (SAR) and Sentinel-2 multispectral imagery. The Sentinel-2 images were processed using the Normalised Difference Water Index (NDWI) to isolate sea areas, and then converted into vector masks. These masks were applied to the Sentinel-1 SAR data within the SNAP platform to minimise noise from land. Ship detection was performed using an adaptive threshold algorithm (CFAR detector), with results analysed at different Probability of False Alarm (PFA) levels. A lower PFA value (e.g., 12.5) increased the detection rate but resulted in false positives, while a higher value (e.g., 17) improved accuracy at the expense of failing to detect smaller vessels. Validation against AIS data revealed discrepancies, such as undetected vessels, highlighting the need to integrate data from multiple sources. The main results show that the combination of SAR and optical data is effective for maritime surveillance, although challenges remain in balancing detection sensitivity and false alarms.*

Keywords: *remote sensing; ship detection; adaptive thresholding; maritime surveillance*

University of Zadar

1. INTRODUCTION

Remote sensing is a scientific data collection method without direct physical contact with the observed objects or phenomena. It is used to obtain information over large areas quickly and accurately, allowing the monitoring of changes on Earth, such as daily, seasonal or annual variations [1]. This article deals with the detection of ships using remote sensing, specifically satellite images from Sentinel-1 and Sentinel-2. The satellite images cover the area of the Split Channel, including the islands of Čiovo, Brač and Šolta. The focus of the investigation is on the detection of ships based on a satellite image taken on 2 November 2024 at 05:03 over the above-mentioned area.

Sentinel-1 and Sentinel-2 are key satellites in the European Copernicus programme, providing valuable data for maritime research and the monitoring of marine areas [2]. The Sentinel-1 mission comprises two satellites, Sentinel-1A and Sentinel-1B, which are in polar orbit and use Synthetic Aperture Radar (SAR) to capture images of the Earth's surface [2]. Sentinel-2 is a satellite consisting of Sentinel-2A and Sentinel-2B with 13 multispectral channels that enable detailed imaging of the sea surface in different areas of the electromagnetic spectrum. The spatial resolution ranges from 10 metres to 60 metres.

This research aims to analyse how ships are detected using satellite technology, as it enables ships to be monitored and tracked regardless of whether they have activated their AIS device or deliberately switched it off. In addition, this kind of ship detection can provide data on ships that are beyond the range of radar surveillance. This improves navigation monitoring and safety at sea, prevents illegal activities and protects the environment [3].

2. METHODOLOGY

The project began with two satellite images (Sentinel-1 and Sentinel-2). The satellite images were obtained through the "Copernicus Browser". The image from Sentinel-1 was taken on 02 November 2024 at 05:03 and the image from Sentinel-2 on 28 October 2024 at 09:51.

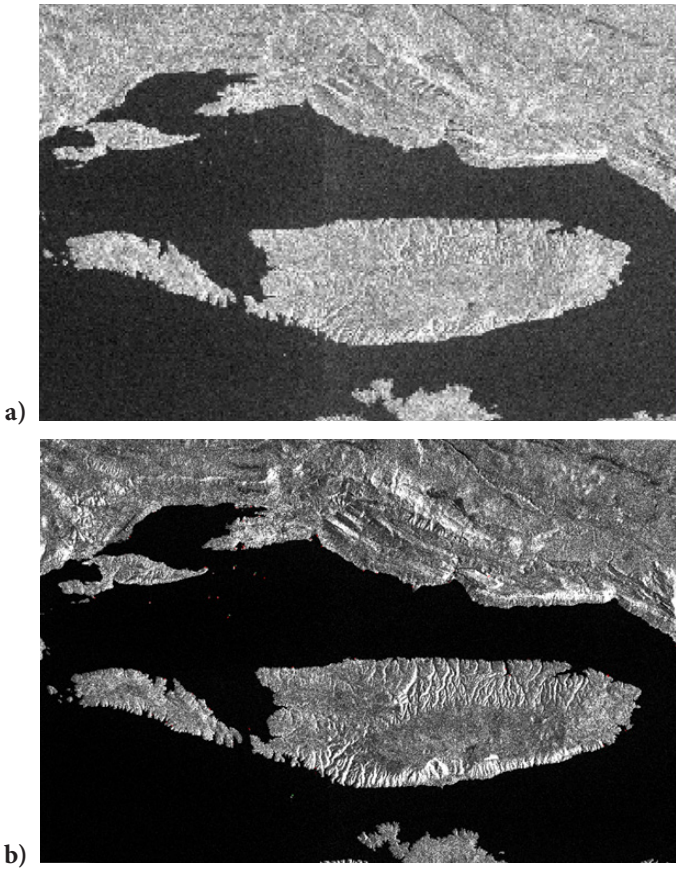

Figure 1. a) Sentinel-1 satellite image; b) Sentinel-2 satellite image.

To avoid the detection of "false targets" (ships) on land, a custom vector mask is first created using the QGIS software and the Sentinel-2 image. A geographic information system (GIS) is a tool that enables spatial information to be processed and analysed. GIS makes it possible to work with geographical data such as maps, images and other information relating to geographical locations [4]. GIS consists of three main components: digital data (geographic data), computer hardware (computers for data storage and processing) and software applications that enable data manipulation.

To create a mask that separates the sea from land areas, the Normalised Difference Water Index (NDWI) is used. This index highlights water features in satellite imagery and is calculated using a combination of the visible green part of the

spectrum and the near-infrared part of the spectrum. The NDWI values range from -1 to +1, with values greater than 0 indicating water surfaces and negative values indicating non-water surfaces. **Figure 2 a)** shows the Sentinel-2 image after applying the NDWI index, while **Figure 2 b)** shows the extracted vector mask of the sea area where the ship detection is to be performed.

After creating the mask and before the actual detection of ships at sea, the Sentinel-1 images must be pre-processed within SNAP (Sentinel Applications Platform). This is a free application developed by the European Space Agency (ESA) for processing satellite data, primarily from the Sentinel programme, but also for third-party missions [5].

a) **b)**

Figure 2. a) Sentinel-2 satellite image with NDWI index; b) Extracted vector mask.

Pre-processing began by removing thermal noise. This corrects the backscatter interference caused by thermal noise. The correction or removal of thermal noise is necessary to normalise the backscattered signal over the entire SAR image. Thermal noise is particularly noticeable in SAR images with cross-polarisation, such as VH or HV, and in SAR images with low backscatter. The S-1 Remove GRD Border Noise tool (in SNAP) is then used to remove the noise at the edges of the image. When generating Sentinel-1 GRD data, noise or artefacts may appear at the edges of the image. These artefacts can be caused by various factors, e.g., differences in antenna sensitivity or signal processing. Finally, the Range-Doppler terrain correction is applied as distances in SAR images can be distorted due to topographical variations in the scene and sensor tilt. **Figure 3 a)** shows a pre-processed Sentinel-1 image with vector mask applied.

a)

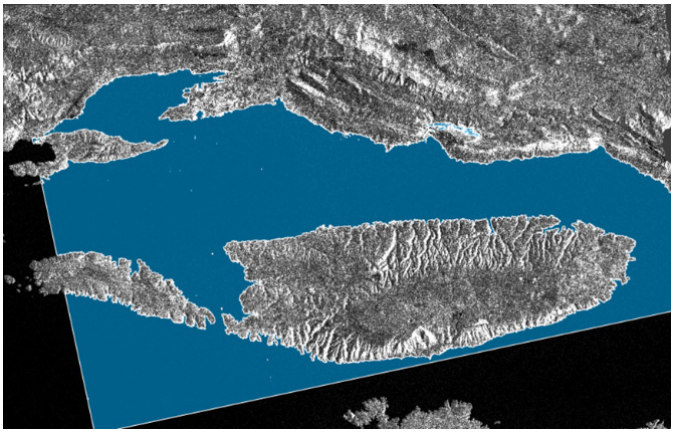

b)

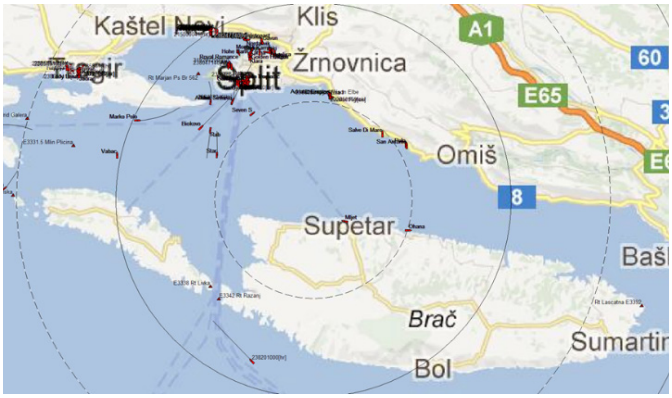

Figure 3. a) Pre-processed Sentinel-1 satellite image with vector mask applied; b) AIS data.

In order to obtain an overview of ship traffic, the AIS (Automatic Identification System) data is recorded and displayed in **Figure 3b**). In order to perform ship detection, in SNAP a CFAR detection is carried out in SNAP [6]. The CFAR detector compares the brightness of the pixels with that of the surroundings in order to detect unusually bright pixels as objects. The detection is adaptive, as the threshold value depends on the local background noise statistics. PFA (Probability of False Alarm) represents the probability of a false alarm. The adaptive threshold method dynamically adjusts the threshold for each pixel based on local statistics, reducing the number of false alarms and improving detection accuracy under different conditions. Based on preliminary experiments aimed at balancing detection sensitivity and false alarm rates, the PFA values of 12.5 and 17 are empirically chosen.

3. RESULTS AND DISCUSSION

The ship detection results are shown in **Figure 4**, where green pins represent detections for PFA = 17 (4 in total), while red circles represent detections for PFA = 12.5 (59 in total). It can be seen that a higher number of ships are detected when the PFA is set to 12.5 compared to 17. However, it is important to note that most of the detections are not necessarily ships, but false detections. When comparing the ship detection results with the AIS data (**Figure 3b**), most of the ships were detected at a lower PFA setting, while at a higher setting some ships were not detected even though they were relatively large, such as the 'Marko Polo' and the 'Bokova'. The fishing boat 'Vabac', on the other hand, was not detected at any PFA setting due to the low resolution of the satellite images, which hindered the identification of smaller or less reflective targets.

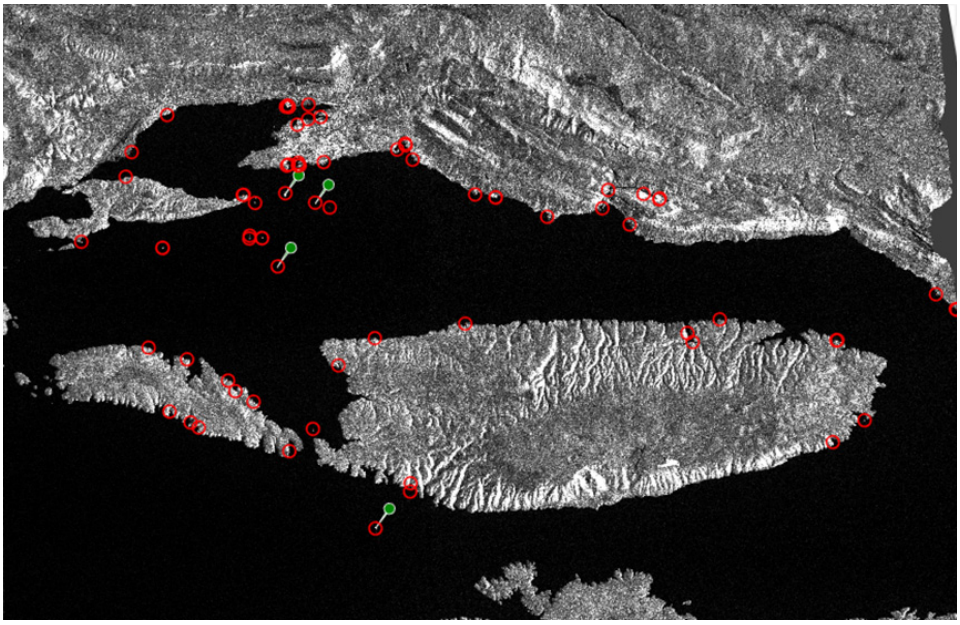

Figure 4. Ship detection results using two PFA thresholds.

4. CONCLUSION

This paper demonstrates the effectiveness of the combination of Sentinel-1 SAR and Sentinel-2 optical data for ship detection in the Croatian Split Channel. Adaptive thresholding (CFAR) with different PFA parameters (12.5 vs. 17)

showed trade-offs: A lower PFA value increased the detection rate but led to false positives, while a higher PFA value improved specificity but at the expense of failing to detect vessels such as the "Marko Polo". Validation using AIS data revealed gaps, emphasizing the need to utilize higher-resolution satellite data and combine it with ground-based systems to ensure reliable maritime traffic monitoring.

The results highlight the potential of multi-sensor remote sensing to improve maritime safety and environmental protection, although challenges remain in balancing sensitivity and accuracy. Future advances in machine learning and higher-resolution satellites could improve the reliability of detection, providing important tools for combating illegal activities and protecting coastal ecosystems.

Acknowledgment: This paper was written by students as part of the European Space Agency project "Remote Sensing in Function of Sustainable Development of the Maritime Sector".

REFERENCES

[1] Lin, L. and Zhao, Z. (2024). ShipDC: A New Baseline for Optical Remote Sensing Ship Detection and Classification. In Wang, Y. and Chen, T., (eds) Proceedings of the Fourth International Conference on Geology, Mapping, and Remote Sensing, p. 73. SPIE, January 23 2024.

[2] Fefilatyev, S., Goldgof, D., Shreve, M. and Lembke, C. (2012). Detection and Tracking of Ships in Open Sea with Rapidly Moving Buoy-Mounted Camera System. Ocean Engineering, 54, 1–12, doi:10.1016/j.oceaneng.2012.06.028.

[3] Demir, M. (2024). Ship Detection from Optical Remote Sensing Images. In Proceedings of the 2024 IEEE International Conference on Big Data, pp. 7302–7307, IEEE, December 15 2024.

[4] QGIS (2024). Introducing GIS — QGIS Documentation. Available from: https://docs.qgis.org/3.34/en/docs/gentle_gis_introduction/introducing_gis.html, accessed on 18 December 2024.

[5] Sentinels Copernicus (2022). ESA Releases New and Improved Version of SNAP - Sentinel Online. Available from: https://sentinels.copernicus.eu/web/sentinel/-/esa-releases-new-and-improved-version-of-snap, accessed on 18 December 2024.

[6] ESA. (2024). SNAP Online Help. Available from: https://step.esa.int/main/wp-content/help/?version=11.0.0&helpid=ObjectDetection. accessed on 18 December 2024.

The 17th Baška Conference
GNSS
Global Navigation Satellite Systems
Green Navigation and Smart Systems

OIL SPILL DETECTION USING SATELLITE RADAR IMAGE CLASSIFICATION

Ivan Budimir[1], Domagoj Žarković[1], Bartul Domazet[1], Anita Gudelj[2], Merica Slišković[2*]

[1] University of Split, Faculty of Maritime Studies, Split, Croatia (students)
[2] University of Split, Faculty of Maritime Studies, Split, Croatia (mentors)
[*] *Corresponding author:* prof Merica Slišković (merica@pfst.hr)

Abstract. *Oil spills represent a serious environmental problem that threatens marine ecosystems, fishing, the economy and human health. The timely development of oil spill detection and monitoring method is crucial to reduce consequences of such incidents. Modern remote sensing methods, especially those which use satellite images, provide an efficient and economical way of detecting and monitoring oil spills.*
This paper explores the potential of applying Sentinel-1 Synthetic Aperture Radar (SAR) data in combination with machine learning methods for the accurate identification and classification of oil spill-affected areas. A convolutional neural network (CNN) based on a pre-trained VGG16 architecture was implemented. The model was validated using real oil spill cases obtained through the Google Earth Engine. To further confirm the accuracy of the prediction, the oil spill areas detected using the trained model were extracted in the form of binary masks and compared with the masks generated by the analysis of the histogram of the reflection of SAR data. The results show that the proposed model can distinguish oil spills from other phenomena on the sea surface with high accuracy, which confirms its applicability in oil incident monitoring and response systems.

Keywords: *deep learning; image classification; machine learning; oil spill; Sentinel-1; SAR*

University of Zadar

1. INTRODUCTION

Due to the severity of the environmental and economic consequences of oil spills, it is crucial to develop effective methods for timely detection and monitoring of spills. Traditional detection methods, such as visual inspections, aerial and ship-based surveillance, have proven unreliable due to high cost, limited coverage, and weather conditions that can make observation difficult. SAR systems enable continuous sea monitoring regardless of light and weather conditions [2]. They detect oil spills by recognizing dampened waves and reduced radar reflection, which appear as black spots in SAR images (**Figure 1**). As part of the European Copernicus program, Sentinel-1 satellites provide high-resolution SAR images for machine learning applications [4]. Previous oil spill detection studies have been based on radar signal reflection analysis, but have been subject to false positive detections due to the presence of natural phenomena [1]. To increase the accuracy of recognition, this paper proposes a combined approach of the a CNN model and a reflection histogram based on the signal intensity threshold enabling initial detection of potential oil spills.

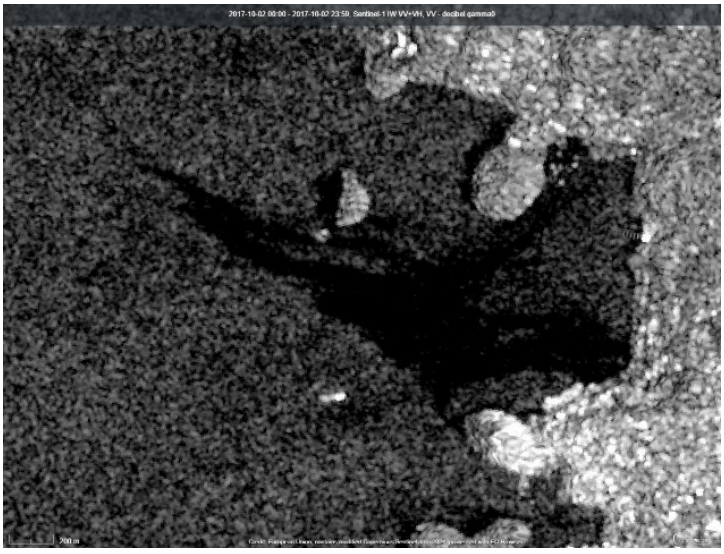

Figure 1. The SAR-C image captured by Sentinel-1 showing an oil spill near Rovinj, Croatia, on October 2, 2017.

2. METHODOLOGY

This work uses a deep learning model based on a convolutional neural network (CNN) to classify SAR images and detect oil spills. The approach combines transfer learning with a pre-trained VGG16 model, which achieves high recognition accuracy. The model was trained on a dataset containing labelled images of oil spills and clean sea surfaces, divided into a training (80%) and a test (20%) set. The model was evaluated using standard metrics such as accuracy (percentage of correctly classified images), precision (the proportion of correctly detected spills in relation to the total number of detections), and confusion matrix (analysis of the relationship between correctly and incorrectly classified samples).

The dataset used was downloaded from the Kaggle platform [5], which contains pre-processed images categorized as "oil spill" and "no oil spill". This dataset allows the model to learn from known examples of oil spills. Out of the total 5,643 satellite images, 60% are labelled as "0" (no oil spill), while 40% are labelled as "1" (oil spill present).

To ensure consistency and improve the quality of data for deep learning processing, the following pre-processing techniques have been implemented:

- Speckle Noise Filtering: Since SAR images often contain speckle noise, a Lee Sigma filter was applied, reduces noise while preserving key image features.
- Normalization: Pixel values are scaled to a range of [0,1] to ensure consistency of input data and to improve the stability and learning speed of the model.
- Data augmentation: Rotation, zooming, and horizontal mapping techniques were applied, improving the model's ability to generalize.
- Image resizing: All images are resized to 240×240 pixels, ensuring compatibility with convolutional neural networks.

To test the practical applicability of the model, validation was carried out on three real-world oil spill cases identified through the Google Earth Engine (**Figure 2**). The following incidents were analysed:

- **Case 1:** Sentinel-1 SAR imagery north of Corsica, acquired on October 9, 2018.
- **Case 2**: SAR imagery from September 10, 2017, showcasing oil spills in Greek waters near industrial zones and shipping lanes.

- **Case 3:** Sentinel-1 SAR imagery of the Crimean coast, acquired on December 15, 2024, featuring small but distinct oil spills in open waters.

The model analysed SAR images and generated binary masks of the oil spill, which were then compared with a histogram of reflection to assess the accuracy of detection. This analysis is crucial to validate the applicability of the model in marine ecosystem monitoring and environmental incident management systems.

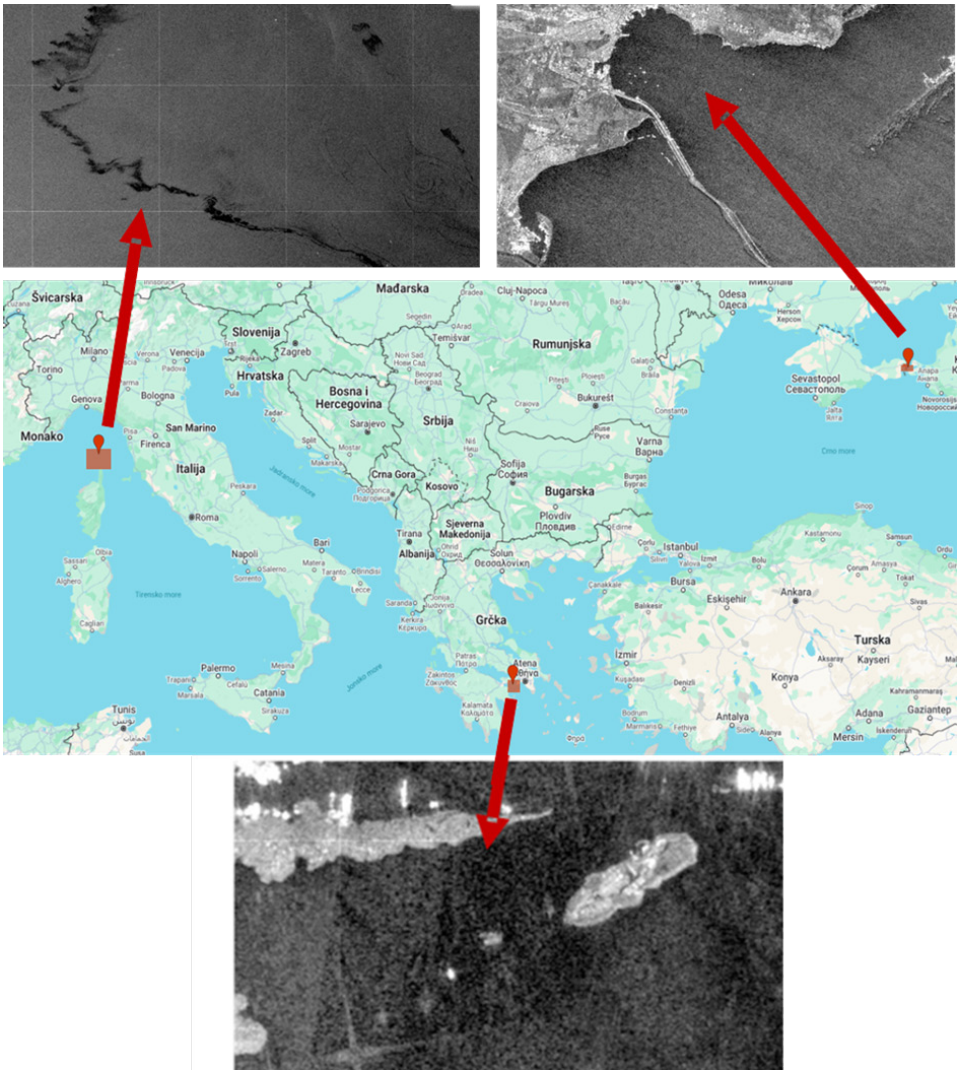

Figure 2. Real oil spill incidents used for validation.

3. RESULTS

After training the model, its accuracy was evaluated on a test dataset. The model achieved a validation accuracy of **90.0%**, indicating high reliability in distinguishing between areas with oil spills and clean sea surfaces. The results from **Table 1** show that the model better recognizes clean sea areas (92% accuracy) compared to areas with oil spills (87% accuracy). The higher classification accuracy of oil-free areas can be explained by their higher representation in the training set and visual homogeneity. In contrast, regions with oil spills show greater variability in shape and reflectance, which makes their detection more difficult and leads to slightly lower results for that class. However, despite a slightly lower response rate in oil spill detection, the model achieves a high overall F1 ratio of 0.90, which confirms its stability and reliability.

Table 1. Evaluation of the model using precision, response, and F1-measure metrics.

Class	Precision	Recall	F1-measure	Number of samples
Oil-free	0.92	0.93	0.93	749
Oil spill	0.87	0.83	0.85	380
Altogether	0.90	0.90	0.90	1129

The confusion matrix shows that the model:

- Correctly classified 700 non-petroleum samples.
- Misclassified 49 non-oil samples as oil spills.
- Correctly detected 317 oil spills.
- Misclassified 63 oil spills as pure sea surface.

Two segmentation methods were used to isolate oil spills, each with a different approach.

- CNN-based mask – uses a pre-trained convolutional neural model (CNN) to predict the likelihood of an oil spill based on Sentinel-1 SAR data.
- Mask based on filtered SAR data and reflection histogram – is based on the analysis of the intensity of the reflected radar signal. In the example Case 1 – Corsica, an empirically determined reflectance threshold of –18.7 dB (**Figure 3**) was applied, with all pixels below this threshold being classified as potentially contaminated. As SAR reflectance depends on the shooting angle, wavelength, sea surface morphology and atmospheric conditions, the threshold needs to be adjusted for each new case.

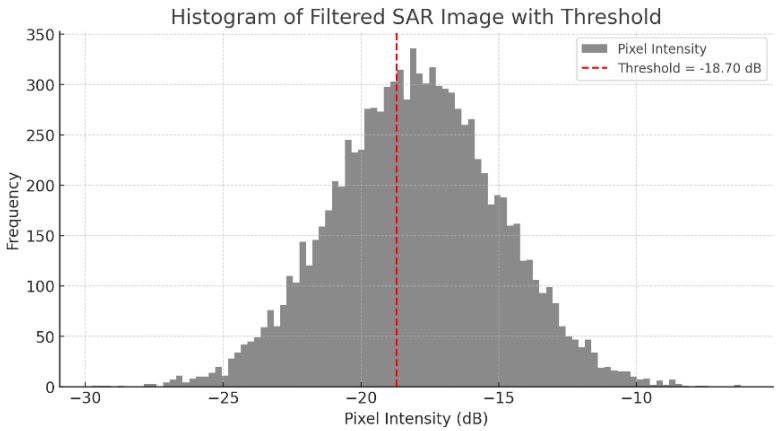

Figure 3. Histogram of the SAR signal reflectance after filtering (Lee Sigma), with the threshold for oil slick extraction (-18.7 dB) marked.

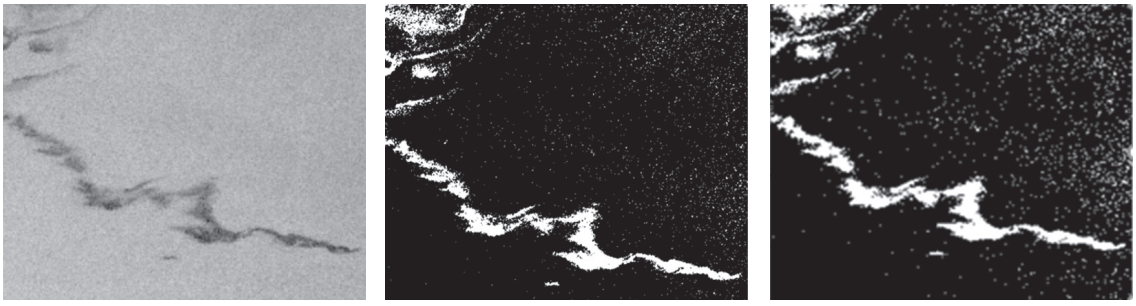

Figure 4. Comparison of the original SAR image (left), the CNN mask (centre), and the histogram-based mask (right).

4. CONCLUSIONS

This research makes a significant contribution to the field of automatic oil spill detection by combining deep learning methods with physical analysis of SAR data. A CNN model was developed not only to classify images, but also to generate binary masks that accurately isolate contaminated areas. To enhance the robustness of the results, additional validation was carried out by comparing the model-generated masks with the ones derived from the intensity histogram of SAR backscatter, using an empirically determined threshold. Future research could include the integration of multi-sensor data and advanced segmentation techniques to further improve detection reliability.

Acknowledgments: This paper was written by a student as part of the European Space Agency project "Remote Sensing in Function of Sustainable Development of the Maritime Sector".

REFERENCES

[1] Krestenitis, M., Orfanidis, G., Ioannidis, K., Avgerinakis, K., Vrochidis, S. & Kompatsiaris, I. (2019). Oil Spill Identification from Satellite Images Using Deep Neural Networks. *Remote Sensing*. Available from: https://www.mdpi.com/2072-4292/11/15/1762, accessed 20 February 2025.

[2] Chen, G., Li, Y., Sun, G. & Zhang, Y. (2017). Application of Deep Networks to Oil Spill Detection Using Polarimetric Synthetic Aperture Radar Images. *Applied Sciences*, 7, 968. Available from: https://doi.org/10.3390/app7100968, accessed 26 February 2025.

[3] Yang, Y.-J. & Singha, S. (2021). Fully Automated SAR-Based Oil Spill Detection Using YOLOv4. In: IGARSS – *IEEE International Geoscience and Remote Sensing Symposium*. pp. 5303-5306. Available from: https://api.semanticscholar.org/CorpusID:238752666, accessed 30 January 2025.

[4] European Space Agency (ESA). (2023). Copernicus Sentinel Data Access Annual Report 2022. Available from: https://sentinels.copernicus.eu/-/copernicus-sentinel-data-access-annual-report-2022?utm_source=chatgpt.com, accessed 10 January 2025.

[5] Kaggle. (n.d.). Oil Spill Detection Dataset. Available from: https://www.kaggle.com/datasets/nabilsherif/oil-spill, accessed 15 January 2025.

The 17th Baška Conference
GNSS
Global Navigation Satellite Systems
Green Navigation and Smart Systems

COMPUTER VISION-BASED REAL-TIME VESSEL DETECTION AND TRACKING IN MARINAS

Nikola Lopac[1,2*], Karlo Severinski[1,2], Tomislav Krljan[1], Jonatan Lerga[2,3]

[1] University of Rijeka, Faculty of Maritime Studies, Rijeka, Croatia
[2] University of Rijeka, Centre for Artificial Intelligence and Cybersecurity, Rijeka, Croatia
[3] University of Rijeka, Faculty of Engineering, Rijeka, Croatia
[*] *Corresponding author:* Nikola Lopac (nikola.lopac@pfri.uniri.hr)

Abstract. *This study presents a computer vision-based system for real-time vessel detection and tracking in marinas. The approach integrates YOLOv8 for object detection and the Kalman filter for continuous tracking, ensuring accurate and stable performance in dynamic marina environments. The model was trained on a real-world dataset collected from Marina Punat, Croatia, achieving 95.02% precision, 94.17% recall, and a 94.59% F1-score, confirming its effectiveness in vessel monitoring. The results demonstrate the system's capability to automate vessel detection and tracking, providing a reliable and efficient solution for monitoring marina traffic and improving operational oversight.*

Keywords: *Computer vision; Kalman filter; machine learning; vessel detection; YOLO*

University of Zadar

1. INTRODUCTION

Vessel monitoring is crucial for marina efficiency and safety, yet traditional manual surveillance is labour-intensive, time-consuming, and prone to human error. As marina traffic increases, real-time automation becomes essential for effective management. Advances in artificial intelligence (AI), machine learning and computer vision, particularly object detection and tracking, enable automated traffic monitoring [1, 2]. This study explores their feasibility for vessel detection in marinas by implementing a YOLOv8-based model with the Kalman filter for real-time tracking. Trained on real-world marina data from Croatia, the system demonstrates the feasibility of AI-driven maritime surveillance, improving accuracy and efficiency.

2. METHODOLOGY

This study employs YOLOv8 for real-time vessel detection and the Kalman filter for object tracking. YOLO (You Only Look Once) is a state-of-the-art object detection model known for its speed and accuracy. It operates on a one-stage detection principle, performing object localization and classification in a single pass through the neural network [3]. Convolutional neural networks (CNNs) have demonstrated outstanding and reliable performance in computer vision tasks, including image classification and object detection, across a wide range of fields [4]. Since its introduction in 2016, YOLO has undergone multiple iterations, with YOLOv8 offering significant improvements in real-time performance, model efficiency, and detection accuracy [5]. Given these advantages, YOLOv8 was selected for vessel detection, ensuring precise and timely identification in real-world marina conditions.

To ensure continuous vessel tracking, this study integrates the Kalman filter, a widely used predictive algorithm in surveillance, robotics, and autonomous systems. The Kalman filter enhances tracking accuracy by estimating an object's state based on past observations, refining predictions with incoming data, and reducing uncertainties [6]. The tracking process consists of two primary steps: first, the prediction step, where the object's current state and uncertainty are estimated based on a motion model and prior information. This is followed by the update step, where new measurements refine the prediction, reducing uncertainty and improving state estimation accuracy. By integrating YOLOv8 detections as measurement inputs into the Kalman filter, the system achieves stable and consistent vessel tracking, even when detections momentarily fail due to occlusion or environmental conditions.

The system was developed using Python, with key libraries including Ultralytics for training the YOLOv8 model, OpenCV for video processing, and Tkinter for the visualization interface. The vessel detection model was trained using a dataset compiled from approximately 30 hours of video footage, recorded under varying lighting conditions in Marina Punat, Island of Krk, Croatia. From this footage, 1,427 images were extracted, with 1,135 used for training, 134 for validation, and 158 for testing. Image annotation was conducted using the VGG Image Annotator (VIA) [7], an open-source, browser-based tool requiring no installation. Each annotated object was assigned the "vessel" class, with bounding box coordinates normalized between 0 and 1 for compatibility with YOLO's format.

For efficient training, the YOLOv8-nano model was selected, leveraging transfer learning to optimize performance with a limited dataset and reduced computational resources. Input images were resized to 800×800 pixels to match the model architecture. Training was performed for 30 epochs using the AdamW optimizer, with an initial learning rate of 0.002 and a momentum of 0.9, both automatically optimized by Ultralytics. The model parameters were organized into three groups: 57 weight parameters with no decay, 64 weight parameters with a decay of 0.0005, and 63 bias parameters with no decay.

3. RESULTS AND DISCUSSION

The model was evaluated on a separate test dataset to objectively assess detection and tracking performance. The evaluation classified detections as true positives (TP), false positives (FP), and false negatives (FN) based on an Intersection over Union (IoU) threshold of 50%. The model achieved a precision of 95.02%, recall of 94.17%, and an F1-score of 94.59%, indicating high detection accuracy and practical applicability for real-time vessel monitoring. **Figure 1** illustrates sample detections from the validation dataset, showcasing the effectiveness of the model in identifying vessels under various conditions.

Following validation, the trained model was integrated into a real-time demonstration framework, where pretrained weights were loaded to ensure consistency with training conditions. Video frames, captured and processed using OpenCV, were converted from BGR to RGB format before being fed into YOLOv8 for object detection. The model returned confidence scores for each detection, with detections below a 60% confidence threshold filtered out to minimize false positives. Duplicate detections were removed, and high-confidence detections were subsequently proc-

essed by the Kalman filter-based tracking algorithm. The YOLOv8 outputs served as measurement inputs for the Kalman filter, which refined object state predictions by reducing detection inconsistencies and improving tracking stability.

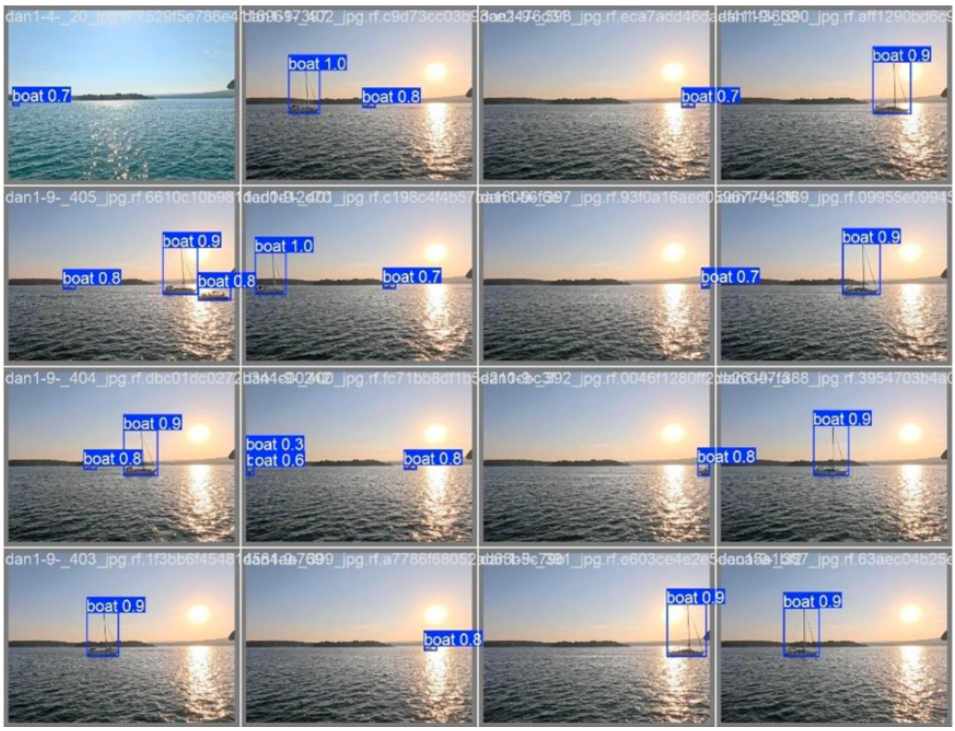

Figure 1. Detection examples on validation set.

The Kalman filter played a crucial role in maintaining tracking continuity, particularly in cases where vessels were temporarily occluded or detection confidence fluctuated. Each vessel detected by YOLOv8 was linked to a KalmanTracker instance, which managed state prediction and updates. The tracker initialized each detected object with its centre coordinates and an initial velocity of zero. A state transition matrix was used to estimate movement, while covariance matrices accounted for uncertainties in motion and detection. During the prediction step, the vessel's new position and velocity were estimated based on its previous state and process noise. When a new measurement was available, the Kalman gain refined the prediction, minimizing uncertainty. To prevent premature deletion of vessels due to temporary occlusion, objects that were undetected for up to 20 con-

secutive frames were retained unless confirmed lost. This approach ensured smooth tracking while maintaining logical consistency in vessel movements.

For visualization purposes, a demonstration window was developed, featuring an integrated boat counter to track vessel entries and exits. The marina's entry and exit boundaries were marked with blue lines positioned at 20% and 80% of the frame width, respectively. Vessel movement was tracked across frames, with objects crossing from left to right counted as entries and those moving in the opposite direction counted as exits. **Figure 2** presents an example of the visualization from the demonstration interface, illustrating the real-time tracking capabilities of the system.

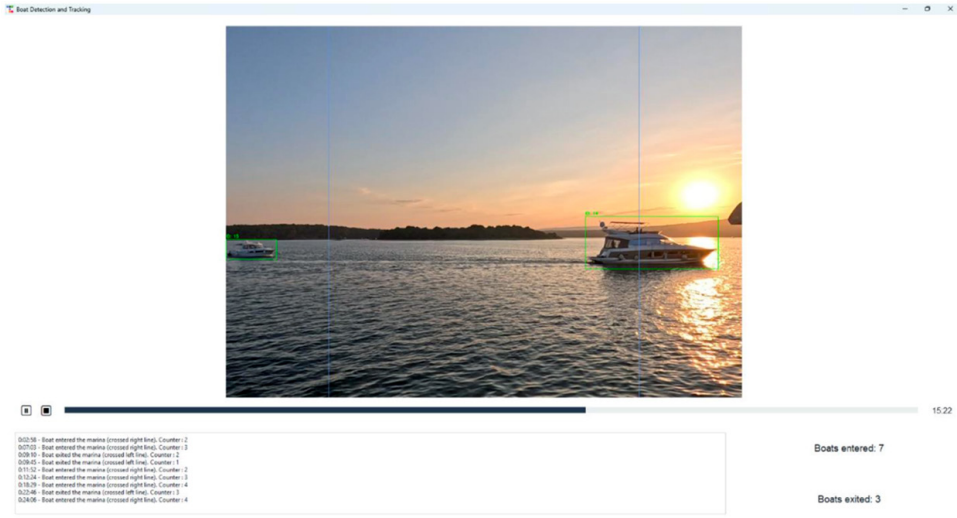

Figure 2. Demonstration window example.

4. CONCLUSIONS

This study presented an automated vessel detection and tracking computer vision system using YOLOv8 for real-time object detection and the Kalman filter for continuous tracking. The trained machine learning model achieved a precision of 95.02%, recall of 94.17%, and an F1-score of 94.59%, demonstrating high reliability for real-time marina vessel monitoring. Further improvements could enhance the model's performance in specific conditions, such as poor lighting conditions and object occlusion. Future work will focus on expanding the dataset, refining tracking algorithms, and integrating advanced deep learning techniques like Deep-

SORT to improve robustness in dense maritime environments. These findings confirm the feasibility of AI-driven maritime surveillance for real-world applications in marina traffic management and security.

Acknowledgments: This research was supported by the Operational Program NPOO under the project NPOO.C3.2.R3-I1.01.0124 funded by the European Union - NextGenerationEU. The researchers also acknowledge the support of their work by the University of Rijeka project uniri-mladi-tehnic-23-15, the project line ZIP UNIRI of the University of Rijeka for the project UNIRI-ZIP-2103-4-22, and the bilateral Croatian-Slovenian project "Predicting Anomalous Trajectories Using Machine Learning" funded by the Ministry of Science, Education and Youth of the Republic of Croatia. Special thanks are extended to Marina Punat, Island of Krk, Croatia, for their valuable cooperation and support during data collection.

REFERENCES

[1] Nguyen, H., Kieu, L.-M., Wen, T., and Cai, C. (2018). Deep learning methods in transportation domain: a review. IET Intelligent Transport Systems, 12(9), 998–1004. doi:10.1049/iet-its.2018.0064.

[2] Lopac, N., Jurdana, I., Brnelić, A., and Krljan, T. (2022). Application of laser systems for detection and ranging in the modern road transportation and maritime sector. *Sensors*, 22(16), 5946. doi: 10.3390/s22165946.

[3] Redmon, J., Divvala, S., Girshick, R., and Farhadi, A. (2016). You only look once: Unified, real-time object detection. In *2016 IEEE Conference on Computer Vision and Pattern Recognition (CVPR)*, pp. 779–788. doi: 10.1109/CVPR.2016.91.

[4] Li, Z., Liu, F., Yang, W., Peng, S., and Zhou, J. (2022). A survey of convolutional neural networks: Analysis, applications, and prospects. *IEEE Transactions on Neural Networks and Learning Systems*, 33(12), pp. 6999–7019. doi: 10.1109/TNNLS.2021.3084827.

[5] Varghese, R. and Sambath, M. (2024). YOLOv8: A Novel Object Detection Algorithm with Enhanced Performance and Robustness. *Proceedings of the 2024 International Conference on Advances in Data Engineering and Intelligent Computing Systems (ADICS)*, Chennai, India, pp. 1–6. doi: 10.1109/ADICS58448.2024.10533619.

[6] Welch, G., and Bishop, G. (1995). An Introduction to the Kalman Filter. *University of North Carolina at Chapel Hill*.

[7] Dutta, A. and Zisserman, A. (2019). The VIA Annotation Software for Images, Audio and Video. *Proceedings of the 27th ACM International Conference on Multimedia (MM '19)*, October 21–25, 2019, Nice, France. New York: ACM, pp. 2276–2279. doi: 10.1145/3343031.3350535.

The 17th Baška Conference
GNSS
Global Navigation Satellite Systems
Green Navigation and Smart Systems

ESTIMATION OF SHIP'S WIND ADDED RESISTANCE BY ANALYZING WIND DATA FROM COPERNICUS SERVICES

Iru Haddad Marrero*, Giuseppe Rosa Falcón, Zdeslav Jurić, Ante Čalić

University of Split, Faculty of Maritime Studies, Split, Croatia
* *Corresponding author:* Iru Haddad Marrero (iruhmarrero@gmail.com)

Abstract. *This study investigates the impact of wind conditions on ship resistance along a predefined route using Copernicus satellite data. By analysing wind and sea current data, the research estimates the aerodynamic force exerted on a vessel and its influence on propulsion power, a factor known to significantly affect ship performance. The methodology involves data acquisition from Copernicus, waypoint-specific wind extraction, and a simplified aerodynamic force model. Results reveal variable wind forces and a significant increase in required propulsion power compared to calm water conditions, particularly at specific waypoints. The analysis highlights the critical role of incorporating wind effects in maritime route planning to optimize fuel efficiency and reduce operational costs. These findings underscore the importance of integrating readily available satellite wind data for enhanced maritime operations and sustainable practices.*

Keywords: *Aerodynamic Force; Fuel Consumption; Head Winds; Maritime Route; Operational Efficiency; Route Analysis*

University of Zadar

1. INTRODUCTION

The maritime sector is continuously driven to enhance operational efficiency and reduce its environmental footprint. For seagoing vessels, achieving optimal performance is a complex undertaking, influenced by a multitude of factors, particularly prevailing weather conditions. Wind, in particular, produces a significant force on ships, especially vessels characterized by large superstructures and exposed deck areas, such as LNG carriers. This aerodynamic interaction directly contributes to ship resistance, demanding increased propulsion power and leading to higher fuel consumption, as detailed in studies on wind resistance of merchant ships [1][3].

This paper addresses this challenge by presenting a simplified analysis of wind conditions along a specific ship route, utilizing remote sensing data from the Copernicus program. The primary objective is to estimate the influence of wind on ship resistance. To systematically explore this, the paper is organized into the following sections: Methodology, detailing the data and methods employed; Results, presenting the findings of the analysis; and Conclusion, summarizing the key outcomes and implications of the study.

2. METHODOLOGY

For this study historical hourly sea surface wind data was acquired from the Copernicus Marine Data Store. The ship was a 300-meter LNG vessel estimated from Vessel Finder [4] images, utilizing a readily available online resource. Waypoint-specific wind data extraction involved temporal filtering (±30 minutes of planned passage time) and spatial filtering (closest geographical point). Aerodynamic force was estimated using a simplified drag force equation:

$$Ra = 1/2 \times Cd \times \rho \times A \times V^2 \quad (1)$$

with Cd = 0.7 [1] and variable wind-exposed area (lateral or bow area depending on wind angle). Total ship resistance was calculated by summing calm water resistance (based on baseline propulsion power, data provided by ship owner) and the estimated aerodynamic force. Propulsion power was then calculated as the product of total resistance and ship speed. Python libraries (pandas, xarray, numpy, matplotlib, windrose) were used for data processing and visualization. In this calculation, we simplified the impact of the wind, reducing it only to head and stern winds (winds 45 degrees south and north from the stern and bow) since

these are the most predominant winds influencing the ship, and using all winds would complicate the calculations much more.

3. RESULTS AND DISCUSSION

The results of this analysis, visualized through maps, diagrams, and graphs, reveal several key findings regarding wind conditions and their impact on ship's resistance. Full map visualizations (**Figure 1** and **Figure 2**) effectively contextualize wind data spatially and illustrate the data filtering process.

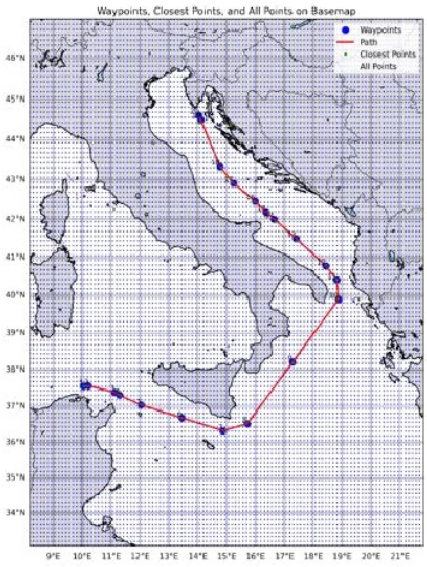

Figure 1. All data information and route.

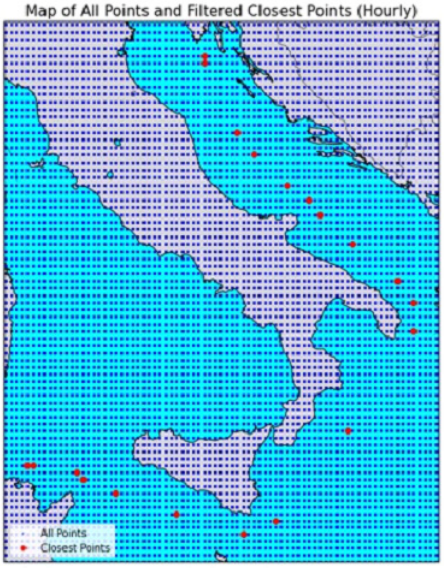

Figure 2. Closest points of wind to the waypoint of the route.

The wind rose diagram (**Figure 3**) indicated a prevailing trend of higher wind frequencies and speeds in the North-South hemisphere, with light winds being most frequent overall, yet stronger winds present from the North and South, as further contextualized by F**igure 6**, showing waypoints and route.

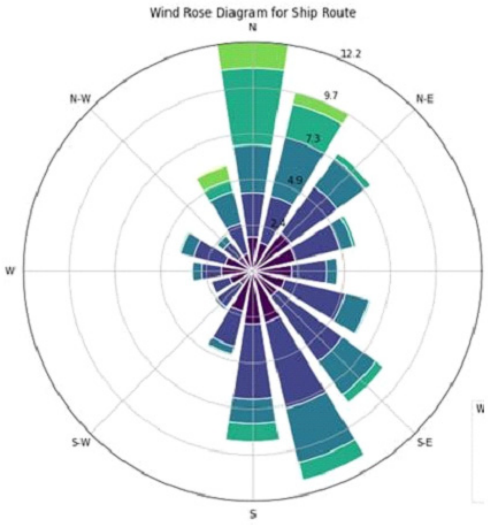

Figure 3. Windrose diagram, units measured in m/s.

Wind vector maps (**Figure 5** and **Figure 6**) further clarified wind conditions by showing both true and relative wind, demonstrably illustrating how ship motion influences perceived wind direction to be generally opposite the vessel's course.

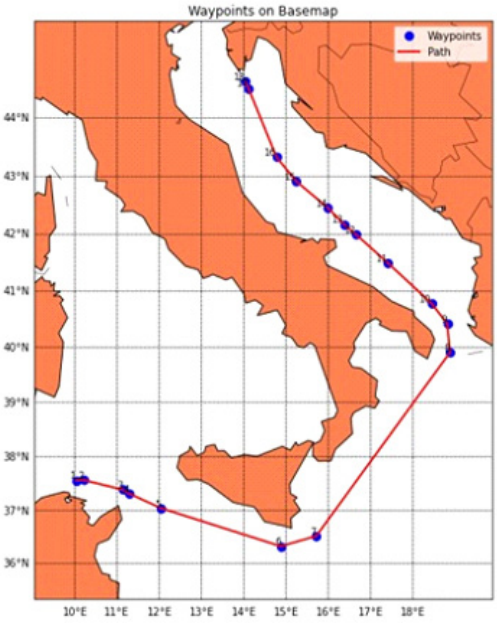

Figure 4. Waypoints and route.

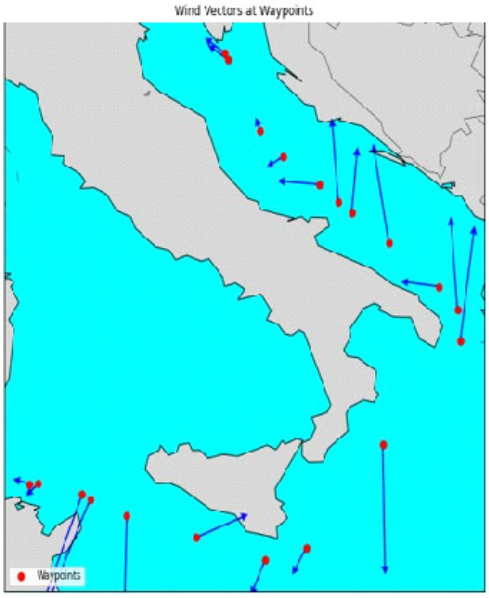

Figure 5. The true wind at the time of the ship's passage through the waypoint.

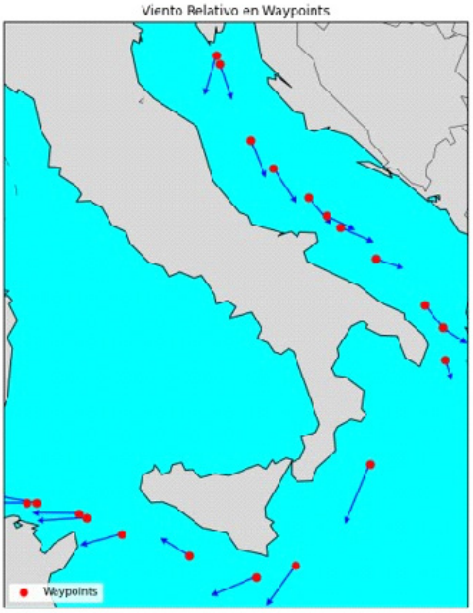

Figure 6. Apparent wind at the time of the ship's passage through the WP.

Estimates of aerodynamic force along the route, presented in **Figure 7**, showed significant variability and a notable peak mid-journey, indicating a fluctuating aerodynamic resistance. Finally, the propulsion power analysis, graphically summarized in **Figure 8**, consistently revealed an increased power demand at waypoints due to wind influence, with variability across the route and a peak demand observed, ultimately highlighting wind's contribution to elevated fuel consumption during maritime voyages.

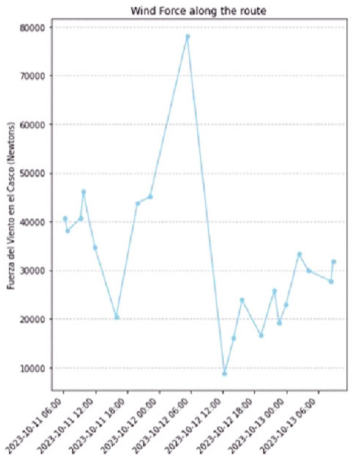

Figure 7. Wind force along the route.

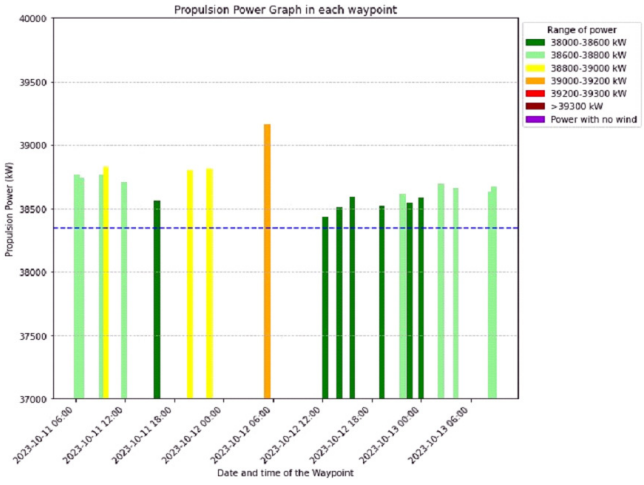

Figure 8. Propulsion power graph.

4. CONCLUSIONS

In conclusion, this study provides a comprehensive analysis of wind conditions and their aerodynamic impact on a vessel along a predefined route. Using Copernicus satellite data, wind distribution patterns are identified, and variations in wind characteristics are highlighted at specific waypoints. The analysis reveals significant directional trends, with higher wind frequencies and speeds predominantly from the North and South.

Additionally, the study emphasizes the difference between true and apparent wind vectors, demonstrating the influence of the ship's movement on wind perception. The aerodynamic resistance estimations, although based on simplified models, show variable wind forces, with notable peaks at certain waypoints. This resistance has direct implications for the vessel's propulsion power, leading to increased fuel consumption along the route. The analysis underscores the importance of considering wind forces in maritime planning to optimize operational efficiency.

Acknowledgments: The weather data used in this paper were obtained from Copernicus Marine Services and processed with support from the project 'Remote sensing in a function of sustainable development of maritime sector' (HR-08 4000143488, ESARS).

REFERENCES

[1] Blendermann, W. (1994). Parameter identification of wind loads on ships. J. Wind Eng. Ind. Aerodyn., 51, 339-351.

[2] Islam, H., et al. (n.d.). Comparison between empirical and CFD based methods for ship resistanceand power prediction. Originally published for written discussion.

[3] Isherwood, R. M. (n.d.). Wind Resistance of Mercant Ships. Originally published for written discussion.

[4] Vessel Finder. (n.d.). Available from: https://www.vesselfinder.com.

[5] Wikipedia contributors. (2024, October 7). Viento. In Wikipedia, La Enciclopedia Libre. Available from: https://es.wikipedia.org/wiki/Viento?

[6] Wnęk, A. D., et al. (n.d.). Experimental study of aerodynamic loads on an LNG carrier and floating platform. Centre for Marine Technology and Engineering (CENTEC), Lisbon, Portugal.

[7] Wnęk, A. D.*, et al. (n.d.). Numerical and experimental analysis of the wind forces acting on LNG carrier. Centre for Marine Technology and Engineering (CENTEC), Lisbon, Portugal.

The 17th Baška Conference
GNSS
Global Navigation Satellite Systems
Green Navigation and Smart Systems

PRELIMINARY INSIGHTS INTO PERMEABILITY EFFECT ON PROGRESSIVE FLOODING SIMULATION

Enrico Del Piero[1], Luca Braidotti[1*], Jasna Prpić-Oršić[2]

[1] Department of Engineering and Architecture, University of Trieste, Trieste, Italy

[2] University of Rijeka, Faculty of Engineering, Rijeka, Croatia

[*] *Corresponding author:* Luca Braidotti (lbraidotti@units.it)

Abstract. *Recent research on ship survivability after damage has focused on large cruise ships using progressive flooding simulation algorithms. However, compartment permeability, a key factor, remains largely overlooked. This study examines how permeability modelling affects progressive flooding simulations for a cruise ship, considering damages from grounding or side contact. Results indicate that different modelling approaches alter flooding progression, highlighting that the permeability effect on ship survivability assessment is not negligible. A more accurate representation of permeability could improve flooding predictions, thus enhancing safety standards and ship design.*

Keywords: *permeability; progressive flooding simulation; safety; cruise ship*

University of Zadar

1. INTRODUCTION

Current research and regulations overlook permeability [1]. While various tools assess flooding dynamics [2], permeability's effect on progressive flooding remains underexplored. This study evaluates its impact on progressive flooding simulations for a large cruise ship. Simulations are performed on two ship models—one with and one without the main machinery modeled—using the algorithm from [3]. The used breaches result from grounding or side contact damage, as they can lead to disastrous events, particularly for passenger ships [4][5].

2. METHODOLOGY

Permeability, μ, is defined as the percentage of a compartment's submerged volume that can be occupied by water:

$$\mu = \frac{\Delta_{water}}{\Delta_{room}} \tag{1}$$

The SOLAS (International Convention for the Safety of Life at Sea) provides permeability values based on compartment usage, without accounting for internal details [6]. Usually, these values are employed in progressive flooding simulations. In addition to these reference values, here, permeability is modelled using a hybrid approach: main machinery is integrated into the cruise ship's 3D model (**Figures 1** and **2**), with a volume correction applied to account for structures, ducts, pipelines, and various equipment. For compartments without significant machinery, permeability is assigned based on usage. The adopted correction factors and permeability values are derived from the FLARE (FLooding Accident REsponse) project [7]. For the structures, a correction factor of 1% is adopted, while for ducts, pipelines, and various equipment it ranges from 0% to 3.5% depending on the machinery contained in the room. In the absence of modelled machinery, a permeability of 0.9 is applied if the room is intended for cargo, accommodation or contains machinery, while for empty spaces or intended for liquids it is equal to 0.98.

Grounding/contact side damages were chosen for analysis because they are not considered by SOLAS even though they pose a significant risk to cruise ships. The breach is generated based on the probability distributions of the damage's geometric characteristics. The damage is box-shaped and classified as potential, meaning it can extend beyond the hull, either partially or entirely above or below the ship's bottom [4].

The adopted simulation algorithm models flooding as a quasi-static process, assuming all liquid surfaces are flat and parallel to the sea surface. The governing equations include mass and momentum conservation for floodwater, with a water level correction to account for potential air pockets forming during the process. Openings are considered deeply submerged, with a correction factor applied for free overflow in partially submerged cases. At each integration step—whose duration varies to capture different flooding rates—water levels are computed by solving a system of Linearised Differential Algebraic Equations (LDAE) [3].

3. APPLICATION

Two ship models were created: the first, referred to as the reference model (**Figure 1** and **Figure 2a**), applies the permeability values prescribed by SOLAS; the second, referred to as the hybrid model (**Figure 2b**), uses the hybrid modelling approach described above. Two models were chosen to compare the regulatory approach with the one developed here.

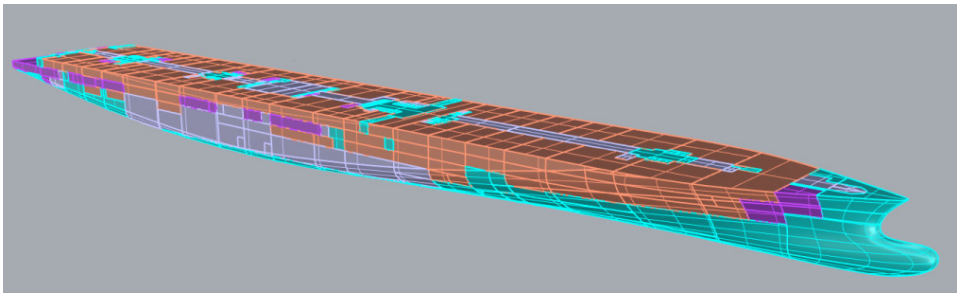

Figure 1. Ship 3D model.

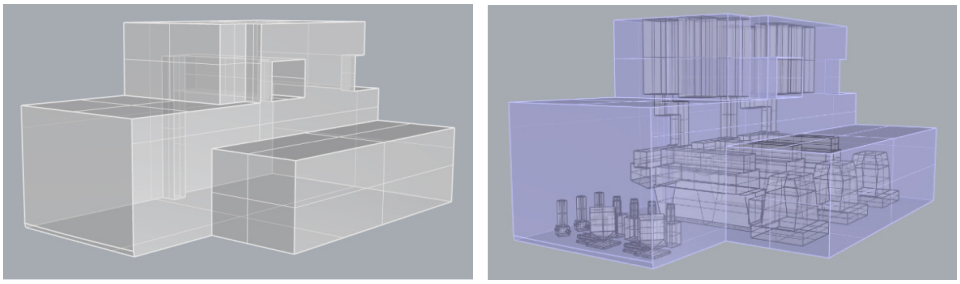

a. **b.**

Figure 2. Diesel-Generator room a: reference model, b: hybrid model.

To carry out an initial analysis, 750 simulations were conducted. Each simulation corresponds to a different side grounding/contact breach, generated with a Monte Carlo method. Each damage was applied to both the reference and hybrid model, to be able to compare the results.

4. RESULTS AND DISCUSSION

The analysis of the simulation results provides the following statistics: in 19% of cases, the flooding duration for the reference model is longer than for the hybrid model; in 16.90% of cases, the outcomes of the two models differ. Specifically for the latter, in 4.93% of cases, the reference model results in the loss of the ship (2.82% due to capsizing and 2.11% due to the ship failing to reach a stable equilibrium), whereas the hybrid model does not. The opposite occurs in only 0.70% of cases. Comparing the flooding duration between the two models for each scenario, the difference is defined as:

$$\Delta t_{stop} = t_{stop,ref} - t_{stop,hyb} \tag{2}$$

where $t_{stop,ref}$ and $t_{stop,hyb}$ represent the flooding duration of the reference and hybrid models, respectively. Since damage cases are generated randomly, the corresponding Empirical Cumulative Distribution Function (ECDF) was constructed (**Figure 3**).

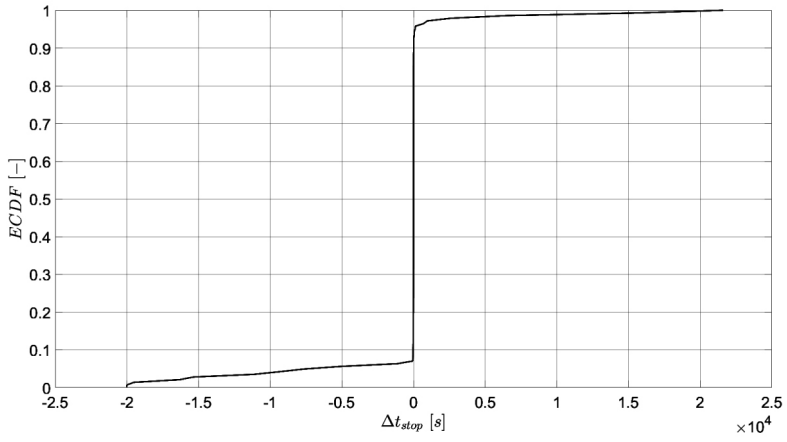

Figure 3. Empirical Cumulative Distribution Function: Δt_{stop}.

The function indicates an 81% probability that $t_{stop,hyb} < t_{stop,ref}$. Additionally, a comparison of the ECDF of flooding duration for both models was performed in cases where the ship is lost (**Figure 4**), showing that a longer flooding duration is more likely for the hybrid model.

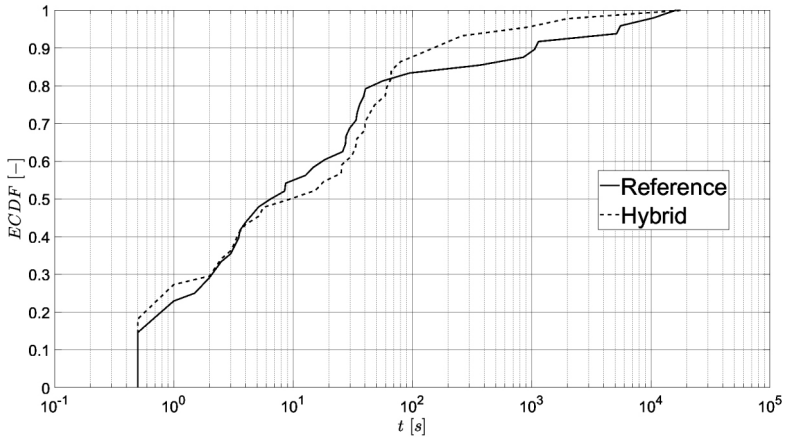

Figure 4. Empirical Cumulative Distribution Function: t_{stop} in the event of loss of the ship.

5. CONCLUSIONS

The simulation results show that different permeability modelling strategy significantly affects progressive flooding. Comparing the more realistic hybrid model with SOLAS permeability, there are differences in time to flood reaching the order of hours and, sometimes, different survivability outcomes have been observed. Applying SOLAS permeabilities to the specific test ship appears to be a conservative approach regarding casualty outcomes but causes significant fluctuations in flooding duration and dynamics. For the development of a DSS (Decision Support System) for flooding, reliability is crucial. This study highlights that choosing one permeability model over another leads to different results, introducing potential risks.

Acknowledgments: This work was supported by the Croatian Science Foundation under the project HRZZ-IP-2022-10-2821.

REFERENCES

[1] Vassalos, D., Atzampos, G., Paterson, D. and Mauro, F. (2022). PERMEABLE VOLUME - THE FORGOTTEN "GALAXY" IN SHIP DESIGN. In: *SNAME 14th International Marine Design Conference, IMDC 2022*. 26 June 2022 through 30 June 2022, Vancouver, Canada. Society of Naval Architects and Marine Engineers.

[2] Rodrigues, J.M. (2024). A Review of Methods for Modelling Flooding, Its Progression and Outcome in Damaged Ships. *Journal of Marine Science and Engineering*, 12, 251. doi: 10.3390/jmse12020251.

[3] Braidotti, L., Prpić-Oršić, J., Bertagna, S. and Bucci, V. (2024). A Consolidated Linearised Progressive Flooding Simulation Method for Onboard Decision Support. *Journal of Marine Science and Engineering*, 12, 1367. doi: 10.3390/jmse12081367.

[4] Bulian, G., Cardinale, M., Dafermos, G., Lindrith, D., Ruponen, P. and Zaraphonitis, G. (2020). Probabilistic assessment of damaged survivability of passenger ships in case of grounding or contact. *Ocean Engineering*, Volume 218. doi: 10.1016/j.oceaneng.2020.107396.

[5] Eliopoulou, E., Alissafaki, A. and Papanikolaou, A. (2023). Statistical Analysis of Accidents and Review of Safety Level of Passenger Ships. *Journal of Marine Science and Engineering*, 11, 410. doi: 10.3390/jmse11020410.

[6] International Maritime Organization. (2020). *International Convention for the Safety of Life at Sea (SOLAS)*. Convention. London: IMO.

[7] Luhmann H., Cardinale M., Wettstein N., Routi A.-L., Bertin R. (2019). Project "FLooding Accident REsponse (FLARE), *Deliverable 2.3 -Analysis of Permeabilities*, 30-11-2019 (V04).

The 17th Baška Conference
GNSS
Global Navigation Satellite Systems
Green Navigation and Smart Systems

UNCERTAINTY IN ESTIMATING SHIP VOLUNTARY SPEED REDUCTION

Jasna Prpić-Oršić*, Ivan Sulovsky, Marijana Marjanović

University Rijeka, Faculty of Engineering, Rijeka, Croatia
* *Corresponding author:* Jasna Prpić-Oršić (jasnapo@riteh.hr)

Abstract. *One of the key aspects of speed reduction in real weather conditions is the voluntary speed reduction of the ship. This situation occurs in heavy seas when the Master believes that maintaining the current speed could endanger the ship, cargo or people on board and decides to deliberately reduce the speed of the ship. The reasons and criteria that influence the Master's decision to reduce speed are highly subjective and depend on Master's experience and personality. This paper sheds light on the uncertainty in estimating ship voluntary speed reduction.*

Keywords: *voluntary speed reduction; seakeeping; fuel consumption; CO_2 emissions*

University of Zadar

1. INTRODUCTION

The reduction of ship's speed at sea can generally be attributed to two main factors: natural causes and technical or design-related reasons. Natural causes include added resistance from wind, waves and sea currents, changes in the wake field and loss of thrust. Technical factors, on the other hand, which are controlled by the Master, involve excessive motion amplitudes, high velocities and accelerations, slamming, green water on deck and overloading of the main engine. Natural causes usually have an effect on the ship's speed even at relatively low significant wave heights.

2. UNCERTAINTY OF SHIP SPEED ESTIMATION

Assessing the reliability of attainable ship speed requires a thorough understanding and quantification of the associated uncertainties. In ship design, ensuring safety also involves assessing the reliability of seakeeping analysis, wave loading and expected operating conditions. These uncertainties also apply to the prediction of attainable speed, which is closely linked to the performance of the engine and propulsion system, as illustrated in **Figure 1**.

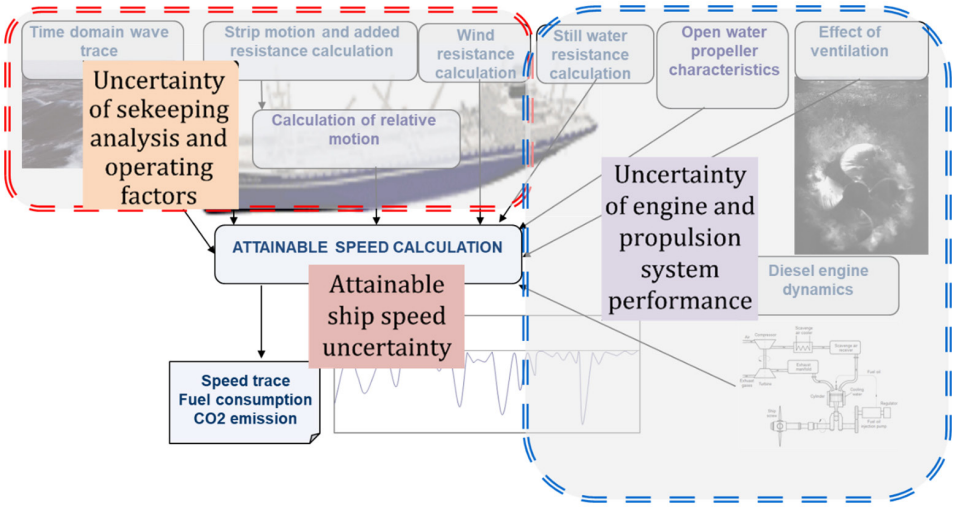

Figure 1. Diagram illustrating ship speed computation in a given sea state.

Among the most significant uncertainties is the voluntary reduction of ship's speed. In heavy seas, the Master has two primary options to avoid excessive ship motion and potential hull damage: changing the course or intentionally reducing speed. However, there is no universal rule prescribing when a Master should reduce speed, leading to a range of criteria proposed by different authors.

Prpić-Oršić et al. **[1, 2]** investigated the effects of variations in the limits for certain criteria that influence a Master's decision to voluntarily reduce speed. For the container ship S175, which has a length between perpendiculars of 175 metres, the study analysed the thresholds for slamming, deck wetness, excessive acceleration, propeller emergence, and rolling at different significant wave heights in head and following seas (Prpić-Oršić et al., **[3, 4]**).

3. CONCLUSIONS

The accurate estimation of voluntary speed reduction is crucial for predicting overall speed loss, fuel consumption and greenhouse gas emissions. However, this estimate is subject to numerous uncertainties. To effectively support Masters in decision-making, guidance systems should assist in the assessment of ship behaviour in difficult weather conditions. Such a system should distinguish between acceptable and unacceptable ship motions and dynamic effects and integrate probability-based assessments to help ship Masters decide whether to reduce speed, change course or both.

Acknowledgments: This work was supported by the Croatian Science Foundation under the project HRZZ-IP-2022-10-2821.

REFERENCES

[1] Prpić-Oršić, J., Faltinsen, O. M., Parunov, J. (2015). The effect of voluntary speed reduction criteria on attainable ship speed. 16th Congress IMAM 2015, Pula, pp. 143-149.

[2] Prpić-Oršić, J., Parunov, J., Šikić, I., (2014). Operation of ULCS - real life. International Journal of Naval Architecture and Ocean Engineering 6. pp. 1014-1023.

[3] Prpić-Oršić, J., Sasa, K., Valčić, M., Faltinsen, O. M. (2020). Uncertainties of Ship Speed Loss Evaluation Under Real Weather Conditions. Journal of Offshore Mechanics and Arctic Engineering, Vol. 142 (June 2020), ISSN 08927219, pp. 031106-1-031106-5, ASME, USA, (for the Book, printed) Norris, A. (2001). ECDIS and Positioning. London: The Nautical Institute.

[4] Prpić-Oršić, J., Faltinsen, O. M., Valčić M., Sulovsky I. (2024). Uncertainties of the decision support system for green ships, Croatian Academy of Sciences and Arts CASA, Book 561 (invited paper for Glasnik HAZU – Journal of CASA, ISSN 1330-0822, HAZU, Zagreb.

The 17th Baška Conference
GNSS
Global Navigation Satellite Systems
Green Navigation and Smart Systems

DECISION SUPPORT FOR SHIP ROUTING CONSIDERING WEATHER FORECAST UNCERTAINTIES

Marijana Marjanović[1*], Jasna Prpić-Oršić[1], Marko Valčić[1,2]

[1] University of Rijeka, Faculty of Engineering, Rijeka, Croatia
[2] University of Zadar, Maritime Department, Zadar, Croatia
[*] *Corresponding author:* Marijana Marjanović (marijana.marjanovic@riteh.uniri.hr)

Abstract. *This research presents possibilities for incorporating weather forecast uncertainty into maritime decision support systems (DSS) for more efficient ship weather routing. Traditional approaches to ship routing rely on deterministic models that overlook inherent variability in meteorological predictions, potentially leading to suboptimal or high-risk routing decisions. The proposed framework leverages probabilistic weather forecasting methods to enhance ship routing decisions, while also addressing limitations of current algorithms in operational contexts. Results demonstrate improved fuel efficiency, enhanced safety, and more reliable estimated time of arrival (ETA) predictions compared to conventional routing methods.*

Keywords: *decision support systems; probabilistic forecasting; ship routing; uncertainty propagation; weather forecast; weather routing*

University of Zadar

1. INTRODUCTION

Ship weather routing is primarily dependent on weather forecasts, which significantly influence routing decisions that impact safety, efficiency, and environmental sustainability of ships [4]. Prpić-Oršić et al. [6] highlighted that despite advances in ensemble prediction systems, underlying uncertainty remains an inherent aspect of weather prediction. Previous research has also addressed this particularly for wave forecasts in the North Atlantic region [3]. As demonstrated by Vettor and Guedes Soares [2], these uncertainties directly affect fuel consumption predictions and routing decisions. Despite the availability of probabilistic weather data, current decision support systems for maritime applications still mostly rely on deterministic approaches that fail to account for forecast variability [5]. This research integrates probabilistic weather forecasting and decision support systems by developing methodologies that effectively incorporate uncertainty into ship routing frameworks. Such approaches have the potential implications for reducing CO2 emissions, as outlined in IMO's recent strategy [7].

2. DECISION SUPPORT AND UNCERTAINTIES

The research was conducted in three parts: (1) forecast uncertainty analysis, (2) uncertainty propagation in ship routing algorithms and (3) investigation of possible uncertainty integrations in decision-making processes.

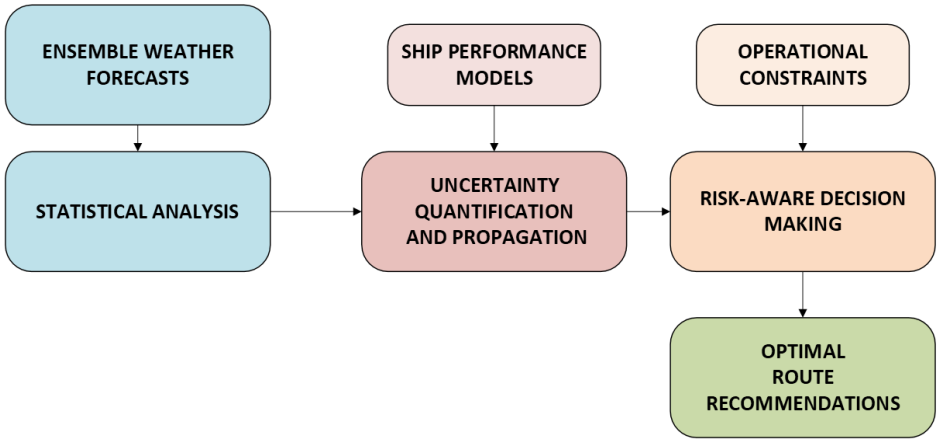

Figure 1. Decision support system structure.

Ensemble weather forecasts were used to analyse meteorological data for the North Atlantic region. In uncertainty propagation, probabilistic distributions of weather variables were embedded into routing algorithms to evaluate how forecast variability influences the decision variables. The basic decision support system structure (**Fig. 1**) connects these research elements to ensure informed, practical, uncertainty-aware routing recommendations.

3. CONCLUSION

This research demonstrates that incorporating weather forecast uncertainty into maritime decision support systems significantly enhances ship routing reliability, efficiency, and safety. The need for a robust methodology for uncertainty handling maritime operations is apparent. By systematically quantifying and propagating forecast uncertainty through routing algorithms, more informed operational decisions can be made, that balance multiple objectives under variable conditions.

Acknowledgments: This work was supported by the Croatian Science Foundation under the project HRZZ-IP-2022-10-2821.

REFERENCES

[1] Prpić-Oršić, J., Faltinsen, O. M. (2012). Estimation of ship speed loss and associated CO2 emissions in a seaway. Ocean Engineering, 44(1), 1-10.

[2] Vettor, R., Guedes Soares, C. (2022). Reflecting the uncertainties of ensemble weather forecasts on the predictions of ship fuel consumption. Ocean Engineering, 250, 110866.

[3] Kodaira, T., Sasmal, K., Miratsu, R., Fukui, T., Zhu, T., Waseda, T. (2023). Uncertainty in wave hindcasts in the North Atlantic Ocean. Marine Structures, 89, 103383.

[4] Zis, T.P.V., Psaraftis, H.N., Ding, L. (2020). Ship weather routing: A taxonomy and survey. Ocean Engineering, 213, 107697.

[5] Vettor, R., Bergamini, G., Guedes Soares, C. (2021). A comprehensive approach to account for weather uncertainties in ship route optimization. Journal of Maritime Science and Engineering, 9(12), 1434.

[6] Prpić-Oršić, J., Sasa, K., Valčić, M., Faltinsen, O. M. (2020). Uncertainties of ship speed loss evaluation under real weather conditions. Journal of Offshore Mechanics and Arctic Engineering, 142(3), 031602.

[7] International Maritime Organization. (2023). Strategy on Reduction of GHG Emissions from Ships. Resolution MEPC.377(80).

The 17th Baška Conference
GNSS
Global Navigation Satellite Systems
Green Navigation and Smart Systems

POSSIBILITIES OF GNSS AUGMENTATION USING UWB TRANSCEIVERS

Luka Kramarić*, Mario Muštra, Tomislav Radišić

University of Zagreb, Faculty of Transport and Traffic Sciences, Zagreb, Croatia

* *Corresponding author:* Luka Kramarić (lkramaric@fpz.unizg.hr)

Abstract. *Unmanned Aerial Vehicles (UAVs) primarily rely on GNSS for navigation due to its global availability and ease of use. However, GNSS alone lacks the precision required for many UAV applications, particularly in GNSS-denied environments or scenarios demanding centimetre-level accuracy. Ultra-Wideband (UWB) communication enables relative localization of UAVs but depends on additional sensor data to achieve reliable results. This paper examines recent studies on alternative localization methods, with a focus on radio frequency (RF)-based augmentation of GNSS, particularly through the UWB localization. While GNSS provides global coverage, its accuracy limitations in certain environments emphasize the need for hybrid localization systems. By analysing the existing research, we explore the integration of GNSS and UWB and its potential benefits for UAV applications, including swarm coordination, precision landings, and urban navigation.*

Keywords: *GNSS; localization; UAV; UWB*

University of Zadar

1. INTRODUCTION AND BACKGROUND

Positioning using Global Navigation Satellite Systems is the most widely used localization method for UAVs due to its global coverage, real-time capability, and ease of implementation. However, GNSS alone does not provide sufficient accuracy for certain UAV applications, particularly those requiring centimetre-level precision, such as swarm formations and precision landings. Additionally, GNSS signals can degrade significantly in urban environments, indoors, or other GNSS-denied areas, leading to unreliable positioning.

Ultra-Wideband (UWB) is a short-range, high-bandwidth radio technology that enables high-precision localization through the Time Difference of Arrival (TDoA) and the Time of Flight (ToF) techniques. UWB localization systems rely on optimal anchor placement and outlier rejection algorithms for precise localization. Unlike GNSS, UWB provides centimetre-level accuracy but has a limited operational range, making it unsuitable as a standalone global localization system.

By integrating GNSS-based localization with UWB-based localization technology, it is possible to leverage the global coverage of GNSS and the high accuracy of UWB, creating a hybrid localization system that improves UAV positioning accuracy. This study explores the possibility and potential benefits of GNSS-UWB integration, analysing existing research to highlight its applications in urban navigation, UAV swarms, and precision landing scenarios.

2. METHODOLOGY

Beyond its established use in indoor applications and GNSS-denied environments, UWB localization technology has also been explored as a complementary technology to GNSS. Studies by Gao et al. [2] and Zabalegui et al. [8] have been at the forefront of integrating GNSS with UWB, emphasizing their complementary nature. GNSS provides global coverage with relatively low accuracy, while UWB offers localization with higher accuracy within a limited range. Although their research primarily focused on ground vehicles, as experiments are easier to conduct compared to UAVs, their findings are relevant for UAVs as well. Gao et al. [2] utilised a Thales UWB system, whereas Zabalegui et al. [8] employed DWM1000 transceivers from DecaWave. Both studies concluded that UWB localization technology is a reliable solution for mitigating the primary limitations of GNSS in urban environments, low-visibility conditions, and indoor-outdoor

transitions, achieving sub-meter accuracy. Given their recent publication in 2023, these studies lay a foundation for further GNSS/UWB integration, which could be particularly valuable for UAV applications. **Table 1** presents the data obtained from Gao et al. [2] which contains the statistical details of the positioning performance comparison between standalone GPS and GPS/UWB integration. The authors improved the positioning accuracy by 63.4% for 2D positioning and by 54.6% for 3D positioning. The GPS data were obtained by driving on a road segment within the coverage of a GPS reference station and enough GPS satellite coverage. The UWB ranging was done by the TDoA technique, because it requires synchronization only among the reference nodes.

Table 1. Comparison of the positioning performance between the GPS-alone and the integration of GPS/UWB, (Gao, Jing, Dianati, *et al.*, 2023).

Case		2D	3D
GPS	RMS, [m]	0.68	1.19
	STD, [m]	0.22	0.35
	Max, [m]	1.07	1.79
GPS/UWB	RMS, [m]	0.25	0.54
	STD, [m]	0.11	0.14
	Max, [m]	0.94	0.97

Figure 1 shows the comparison of localization accuracy when GPS is used as a standalone system and when it is used with UWB.

Huang et al. [4] demonstrated that integrating multi-GNSS with UWB significantly improves positioning accuracy and reduces convergence time. Their results achieved an accuracy of under 10 cm, highlighting the effectiveness of hybrid localization approaches. Similarly, Wang et al. [7] proposed a fusion system combining GNSS Real-Time Kinematic (RTK), UWB, and a Differential Barometric Altimeter (DBA), achieving sub-5 cm accuracy in northing, easting, and altitude. Liu et al. [5] proposed a tightly coupled integration algorithm of GNSS RTK, UWB, and visual inertial odometry (VIO) to enhance the accuracy and reliability for autonomous vehicles seamless localization.

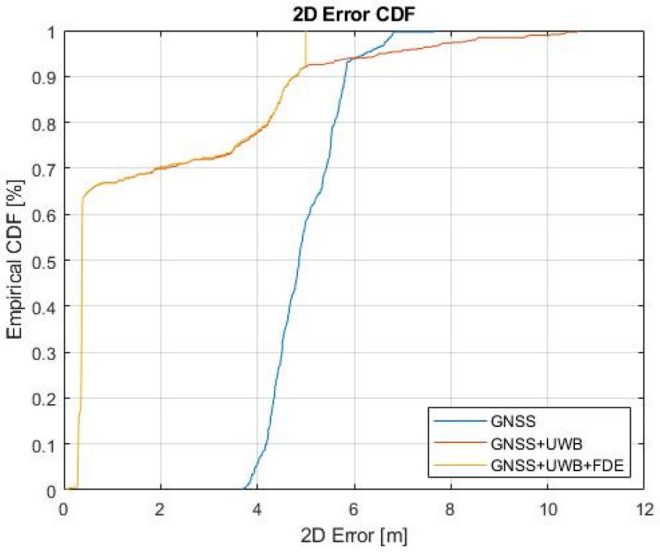

Figure 1. Accuracy comparison of GNSS and GNSS+UWB, [8].

This paper greatly emphasizes UWB's usability as a replacement for GNSS while highlighting its downsides in non-line-of-sight conditions which are covered by VIO system to some degree. Tommingas et al. [6] used machine learning models for estimating UWB and GNSS positioning uncertainties. The authors used real-life data for training and tested the model with UWB and GNSS nodes moving from indoor space to outdoor and vice versa. They obtained better results than contemporary dilution of precision-based approaches. The authors also believe that the model can provide even better results when trained with more relevant data or when fused with complementary sensors such as IMU and cameras. Di Pietra et al. [1] used the GNSS/UWB integration with an Inertial Navigation System (INS) to track pedestrians. The authors used extended Kalman filter (EKF) for data fusion and the UWB ranging was obtained with the ToF technique. The authors used Pozyx UWB transceivers, but mention that DWM1000 is probably superior due to its support for double-sided two-way ranging. Guo et al. [3] focused on solving inconsistent data fusion caused by clock drifts and different sampling rates. Time synchronization plays a critical role in GNSS/UWB tight integration using centralized EKF, and this study analyses the negative impact of uncalibrated time-offsets on localization accuracy. To address this, a double-update EKF framework that models time-offsets within the state space and adaptively adjusts UWB covariance was proposed, achieving up to 57.58% improvement in horizontal

positioning accuracy in real-world scenarios. These findings suggest that GNSS/UWB integration has a strong potential to enhance UAV navigation in scenarios requiring high precision, such as swarm coordination, precision landings, and urban operations.

3. RESULTS AND DISCUSSION

The combined usage of GNSS and UWB localization technology in localization of UAVs presents a significant advantage in improving positioning accuracy and robustness, particularly in environments where GNSS alone is unreliable. By equipping UAVs with both GNSS receivers and UWB transceivers, it is possible to leverage the global availability of GNSS alongside the high precision of UWB. This enables UAVs to operate efficiently in a wide range of environments, from outdoor spaces to congested urban areas.

Mathematical models and (non-Linear) filtering algorithms, such as Kalman Filter, are needed to estimate and compensate for errors from different sources. The primary goal is to fuse GNSS and UWB data in a way that reduces overall positioning error. For instance, in outdoor environments with strong GNSS signals, GNSS provides a baseline position, while UWB refines the position in the final phase of a landing sequence. In GNSS-denied or weak-signal environments, UWB serves as the primary localization system. Fusion of GNSS and UWB data requires robust filtering to ensure accurate and consistent position estimation due to the different update rates and noise characteristics.

One of the key applications of GNSS/UWB integration is in UAV swarm coordination. In multi-UAV systems, precise localization is crucial to ensure the formation control. GNSS allows global navigation, but its accuracy alone is not sufficient for maintaining safe inter-UAV distances in tight formations. By introducing UWB-based localization, UAVs can measure relative distances with high precision, enabling efficient swarm movement and obstacle avoidance. This technology can also provide redundancy in GNSS-degraded scenarios. For example, if a UAV temporarily loses its GNSS signal due to urban interference, it can rely on relative positioning data from neighbouring UAVs equipped with UWB transceivers to maintain formation until GNSS connection is restored.

Autonomous landing is another scenario where GNSS/UWB integration offers significant benefits. While GNSS-based localization can guide a UAV to a general landing zone, its accuracy limitations can cause deviations that make precise

landings difficult, especially in constrained environments. UWB anchors placed near the landing site can enhance positioning accuracy, ensuring a UAV can land safely within a precise area. This is particularly valuable for applications such as drone delivery, where UAVs must land on designated pads, and for military or emergency scenarios where accurate landings are critical. By utilizing UWB in the final landing phase, UAVs can achieve consistent and highly precise landings, even in environments with GNSS disruptions.

4. CONCLUSIONS

This study highlights the potential benefits of GNSS/UWB integration, demonstrating how it enhances UAV positioning accuracy in both open and constrained environments. Through swarm coordination, UAVs can maintain precise relative distances, improving formation control and collision avoidance. Additionally, in precision landing applications, UWB anchors can refine positioning in the final descent phase, ensuring safe and accurate landings even in GNSS-degraded conditions. However, much of the existing research is simulation-based and creates the need for comprehensive field testing. Due to UWBs' short range, it is important to place UWB nodes in optimal positions to reduce system costs. Future work should focus on obtaining experimental results for UAV swarm flights and explore sensor fusion techniques aside from Kalman filters. With the advancements in sensor fusion and localization techniques, GNSS/UWB integration has the potential to become a standard approach for enhancing UAV navigation in complex environments.

Acknowledgments: This research was conducted within a Horizon Europe CSA project, "Strengthening Research and Innovation Excellence in Autonomous Aerial Systems-AeroSTREAM", call HORIZON-WIDERA-2021-ACCESS-05, grant agreement number 101071270.

REFERENCES

[1] Di Pietra, V., Dabove, P. & Piras, M. (2020). Loosely Coupled GNSS and UWB with INS Integration for Indoor/Outdoor Pedestrian Navigation. *Sensors*. [Online] 20 (21), 6292. Available from: doi:10.3390/s20216292.

[2] Gao, Y., Jing, H., Dianati, M., Hancock, C.M., et al. (2023). Performance Analysis of Robust Cooperative Positioning Based on GPS/UWB Integration for Connected Autonomous Vehicles. *IEEE Transactions on Intelligent Vehicles*. [Online] 8 (1), 790–802. Available from: doi:10.1109/TIV.2022.3144341.

[3] Guo, Y., Vouch, O., Zocca, S., Minetto, A., et al. (2023). Enhanced EKF-Based Time Calibration for GNSS/UWB Tight Integration. *IEEE Sensors Journal*. [Online] 23 (1), 552–566. Available from: doi:10.1109/JSEN.2022.3223974.

[4] Huang, Z., Jin, S., Su, K. & Tang, X. (2022). Multi-GNSS precise point positioning with UWB tightly coupled integration. *Sensors*. 22 (6), 2232.

[5] Liu, T., Li, B., Chen, G., Yang, L., et al. (2024). Tightly Coupled Integration of GNSS/UWB/VIO for Reliable and Seamless Positioning. *IEEE Transactions on Intelligent Transportation Systems*. [Online] 25 (2), 2116–2128. Available from: doi:10.1109/TITS.2023.3314836.

[6] Tommingas, M., Laadung, T., Varbla, S., Müürsepp, I., et al. (2025). UWB and GNSS Sensor Fusion Using ML-Based Positioning Uncertainty Estimation. *IEEE Open Journal of the Communications Society*. [Online] 1–1. Available from: doi:10.1109/OJCOMS.2025.3554352.

[7] Wang, S., Dong, X., Liu, G., Gao, M., et al. (2022). GNSS RTK/UWB/DBA Fusion Positioning Method and Its Performance Evaluation. *Remote Sensing*. [Online] 14 (23), 5928. Available from: doi:10.3390/rs14235928.

[8] Zabalegui, P., De Miguel, G., Mendizabal, J. & Adin, I. (2023). Innovation-Based Fault Detection and Exclusion Applied to Ultra-WideBand Augmented Urban GNSS Navigation. *Remote Sensing*. [Online] 15 (1), 99. Available from: doi:10.3390/rs15010099.

The 17th Baška Conference
GNSS
Global Navigation Satellite Systems
Green Navigation and Smart Systems

INTEGRATING LARGE LANGUAGE MODELS INTO MARITIME OPERATIONS: ENHANCING AUTOMATION AND DECISION-MAKING

Karlo Severinski[1*], Nikola Lopac[1,2], Jonatan Lerga[2,3]

[1] University of Rijeka, Faculty of Maritime Studies, Rijeka, Croatia
[2] University of Rijeka, Centre for Artificial Intelligence and Cybersecurity, Rijeka, Croatia
[3] University of Rijeka, Faculty of Engineering, Rijeka, Croatia
[*] *Corresponding author:* Karlo Severinski (karlo.severinski@pfri.uniri.hr)

Abstract. *The rapid advancement of Large Language Models (LLMs) is transforming various industries, including maritime operations. This paper explores the application of LLMs in autonomous navigation, risk management, and maritime communication, emphasizing their role in decision-making, situational awareness, and regulatory compliance. Techniques such as fine-tuning, Retrieval-Augmented Generation (RAG), and Knowledge-Augmented Generation (KAG) enhance LLM performance in maritime applications. Despite their potential, significant challenges remain, including regulatory adaptation, real-time updates, and reliability concerns. This study highlights the transformative role of LLMs in maritime operations and outlines key research directions to address existing limitations and enhance automation and digitalization in the sector.*

Keywords: *large language models (LLMs); maritime automation; risk management; maritime digitalization*

University of Zadar

1. INTRODUCTION

The development of Large Language Models (LLMs) has revolutionized multiple industries, assisting in software development, medical diagnostics, financial analysis, and legal text interpretation [1]. As digitalization and automation advance, the potential applications of LLMs are expanding into new domains, including maritime operations. Given the increasing complexity of maritime navigation and decision-making [2], the integration of LLMs presents a significant opportunity for improving efficiency and safety. This paper examines recent advancements in LLM applications in the maritime industry and discusses their future potential.

2. LARGE LANGUAGE MODELS: PRINCIPLES AND DEVELOPMENT

LLMs encompass a broad category of machine learning (ML) and artificial intelligence (AI) models designed for natural language processing (NLP) tasks. Modern LLMs are primarily based on transformer architectures, first introduced by Google researchers [3]. The transformer model employs a multi-head attention mechanism that allows the model to process multiple parts of an input sequence simultaneously, improving contextual understanding and response accuracy. This breakthrough has led to the development of widely used LLMs, including OpenAI's GPT models (e.g., ChatGPT) and Meta's LLaMA family [1]. These models are trained on vast datasets and demonstrate remarkable capabilities in text generation and contextual reasoning, making them valuable across various domains.

Before evaluating LLM applications in maritime operations, it is essential to understand their training process, information processing, and text generation capabilities. The LLM training pipeline comprises four key stages: data collection and pre-processing, model configuration, model pretraining, and fine-tuning, as shown in **Figure 1**. Data collection forms the foundation of model training, where high-quality structured and unstructured text from sources such as books, academic papers, and online sources is collected and refined to ensure data quality and relevance. Following this, the model is configured by defining its architectural parameters, including the number of layers, attention heads, and token embeddings, with initial weights randomly assigned before training begins. During pretraining, the model learns linguistic patterns by processing vast amounts of text, allowing it to generate coherent responses, although these may

initially lack specificity. Fine-tuning is a crucial step in adapting the model for specialized applications, where additional domain-specific data is used to refine responses, making them more relevant and accurate for targeted industries such as medicine, finance, or maritime operations [4].

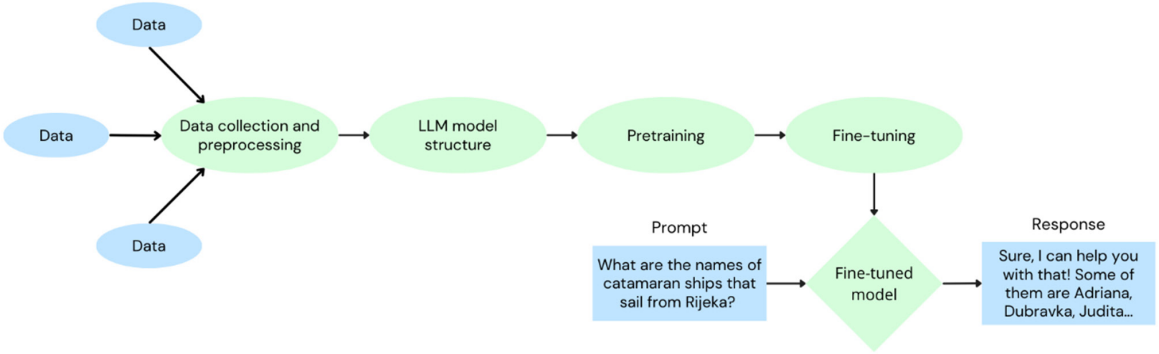

Figure 1. Graphical representation of LLM training and information processing

Fine-tuning significantly improves LLM adaptability across various industries. For instance, a model trained on medical records can assist in healthcare decision-making, while an LLM fine-tuned with maritime navigation data and safety regulations can enhance ship operations. Additionally, approaches such as Retrieval-Augmented Generation (RAG) [5] and Knowledge-Augmented Generation (KAG) [6] further optimize LLM performance for industry-specific applications, enabling real-time updates to knowledge databases.

3. APPLICATIONS OF LARGE LANGUAGE MODELS IN MARITIME OPERATIONS

Despite their widespread adoption in various industries, the application of LLMs in maritime operations remains relatively underexplored. However, recent studies indicate their potential in key areas, including autonomous navigation, risk assessment, communication, and decision support systems.

Pei et al. [7] evaluated the performance of 14 LLMs on maritime navigation exams, revealing that while these models show promise in onshore navigation assistance and onboard decision-making, they require fine-tuning to align with maritime regulations and operational complexities. Similarly, Agyei et al. [8]

investigated LLM integration in autonomous surface vehicles (ASVs), and found that LLM-driven systems can interpret maritime navigation rules, ensuring compliance with the Convention on the International Regulations for Preventing Collisions at Sea (COLREGs) [9] while maintaining explainability in complex scenarios.

LLMs have shown potential in maritime risk management by automating data collection and classification. Huang et al. [10] demonstrated that LLMs can enhance real-time risk assessment by extracting relevant data from news sources and by continuously updating risk databases. Their study compared GPT-4 and LLaMA-3.1, concluding that LLMs significantly improve the classification and summarization of maritime risks, supporting proactive risk mitigation strategies. Sanchez-Heres et al. [11] further assessed LLM effectiveness in decision support systems for maritime navigation, emphasizing their ability to interpret COLREGs in simulated traffic scenarios. While these findings highlight the potential of LLMs such as ChatGPT and GPT-4 in maritime operations, challenges remain regarding real-world applicability and decision robustness.

LLMs have also demonstrated effectiveness in maritime text processing and classification. Zhang et al. [12] proposed an LLM-based framework for maritime-context text classification using ConvBERT, a variant of BERT [1], to achieve a 99.97% accuracy in identifying marine-related texts. This approach outperformed standard BERT models in computational efficiency and accuracy. Additionally, Bach et al. [13] explored LLM applications in stakeholder communication, demonstrating their potential in automating professional correspondence in the maritime industry. However, their study also emphasized the need for further model refinement to fully meet industry-specific communication demands.

In addition to adapting existing models, novel LLM architectures specifically designed for maritime applications are emerging. Nguyen et al. [14] introduced TM-LLM, an LLM optimized for vessel trajectory prediction using Automatic Identification System (AIS) data [15]. Their model enhances situational awareness and maritime safety by accurately forecasting vessel movements in real-time, demonstrating the potential of domain-specific LLM adaptations.

4. CONCLUSIONS

The integration of LLMs in maritime operations remains in its early stages, yet recent studies highlight their significant potential in autonomous navigation, risk

management, and maritime communication. While LLMs demonstrate promising applications, several challenges must be addressed, particularly in fine-tuning for industry-specific tasks, ensuring regulatory compliance, and improving real-time adaptability. Future research should prioritize RAG and KAG methods to enhance maritime-specific performance before fine-tuning. Additionally, emerging models such as DeepSeek **[16]** should be compared with established architectures like GPT, BERT, and LLaMA to assess their suitability for maritime automation and decision-making.

Acknowledgments: This work has been supported by the University of Rijeka project uniri-mladi-tehnic-23-15, the project line ZIP UNIRI of the University of Rijeka for the project UNIRI-ZIP-2103-4-22, and the bilateral Croatian-Slovenian project "Predicting Anomalous Trajectories Using Machine Learning" funded by the Ministry of Science, Education and Youth of the Republic of Croatia.

REFERENCES

[1] Zhao, W. X., Zhou, K., Li, J., Tang, T., Wang, X., Hou, Y., Min, Y., Zhang, B., Zhang, J., Dong, Z., Du, Y., Yang, C., Chen, Y., Chen, Z., Jiang, J., Ren, R., Li, Y., Tang, X., Liu, Z., Liu, P., Nie, J.-Y., and Wen, J.-R. (2024). A Survey of Large Language Models. *arXiv preprint arXiv:2303.18223*.

[2] Jurdana, I., Lopac, N., Wakabayashi, N., and Liu, H. (2021). Shipboard Data Compression Method for Sustainable Real-Time Maritime Communication in Remote Voyage Monitoring of Autonomous Ships. *Sustainability*, 13(15), 8264. doi:10.3390/su13158264.

[3] Vaswani, A., Shazeer, N., Parmar, N., Uszkoreit, J., Jones, L., Gomez, A. N., Kaiser, Ł., and Polosukhin, I. (2017). Attention Is All You Need. In: *Proceedings of the 31st International Conference on Neural Information Processing Systems (NeurIPS)*, pp. 5998–6008. Curran Associates, Inc.

[4] Briganti, G. (2024). How ChatGPT works: a mini review. *European Archives of Oto-Rhino-Laryngology, 281*(5), pp. 1565–1569. doi: 10.1007/s00405-023-08337-7.

[5] Gao, Y., Xiong, Y., Gao, X., Jia, K., Pan, J., Bi, Y., Dai, Y., Sun, J., Wang, M., and Wang, H. (2024). Retrieval-Augmented Generation for Large Language Models: A Survey. *arXiv preprint arXiv:2312.10997*.

[6] Liang, L., Sun, M., Gui, Z., Zhu, Z., Jiang, Z., Zhong, L., Qu, Y., Zhao, P., Bo, Z., Yang, J., Xiong, H., Yuan, L., Xu, J., Wang, Z., Zhang, Z., Zhang, W., Chen, H., Chen, W., and Zhou, J. (2024). KAG: Boosting LLMs in Professional Domains via Knowledge Augmented Generation. *arXiv preprint arXiv:2409.13731*.

[7] Pei, D., He, J., Liu, K., Chen, M., and Zhang, S. (2024). Application of Large Language Models and Assessment of Their Ship-Handling Theory Knowledge and Skills for Connected Maritime Autonomous Surface Ships. *Mathematics, 12*(15), pp. 2381. doi: 10.3390/math12152381.

[8] Agyei, K., Sarhadi, P., and Naeem, W. (2024). Large Language Model-based Decision-making for COLREGs and the Control of Autonomous Surface Vehicles. *arXiv preprint arXiv:2411.16587*.

[9] International Maritime Organization (IMO). (1972). *Convention on the International Regulations for Preventing Collisions at Sea (COLREGs)*. Adopted on 20 October 1972; entered into force on 15 July 1977.

[10] Huang, D., Fu, X., Yin, X., Pen, H., and Wang, Z. (2024). Automating Maritime Risk Data Collection and Identification Leveraging Large Language Models. In: *Proceedings of the IEEE International Conference on Data Mining Workshops (ICDMW)*, pp. 1–8. Abu Dhabi, UAE: IEEE.

[11] Sánchez-Heres, L. F., Weber, R., Ahlgren, F., and Olsson, F. (2024). COLREG3: Exploring the potential of Large Language Models in marine navigation systems. *Lighthouse Reports*.

[12] Zhang, X., Lim, H., Fu, X., Wang, K., Xiao, Z., and Qin, Z. (2024). Maritime-Context Text Identification for Connecting Artificial Intelligence (AI) Models. In: *2024 IEEE Conference on Artificial Intelligence (CAI)*, pp. 899–904. IEEE. doi: 10.1109/CAI59869.2024.00165.

[13] Bach, T. A., Babic, A., Park, N., Sporsem, T., Ulfsnes, R., Smith-Meyer, H., and Skeie, T. (2024). Using LLM-Generated Draft Replies to Support Human Experts in Responding to Stakeholder Inquiries in Maritime Industry: A Real-World Case Study of Industrial AI. *arXiv preprint arXiv:2412.12732*.

[14] Nguyen, T. C. A., Tao, T. M., Lee, C., and Youn, C.-H. (2024). TM-LLM: Token-Motion Embedding Fusion for Large Language Model-Based Vessel Trajectory Prediction. In: *2024 15th International Conference on Information and Communication Technology Convergence (ICTC)*, pp. 115–120. IEEE. doi: 10.1109/ICTC62082.2024.10827542.

[15] Liu, H., Jurdana, I., Lopac, N., and Wakabayashi, N. (2022). BlueNavi: A Microservices Architecture-Styled Platform Providing Maritime Information. *Sustainability, 14*(4), pp. 2173. doi: 10.3390/su14042173.

[16] DeepSeek-AI. (2025). DeepSeek-R1: Incentivizing Reasoning Capability in LLMs via Reinforcement Learning. *arXiv preprint arXiv:2501.12948*.

The 17th Baška Conference
GNSS
Global Navigation Satellite Systems
Green Navigation and Smart Systems

DEVELOPING A TRANSPORT SUPPLY MODEL USING AIS DATA

Neven Grubisic*, David Brcic, Sanjin Valcic, Tomislav Krljan

University of Rijeka, Faculty of Maritime Studies, Rijeka, Croatia
* *Corresponding author:* Neven Grubisic (neven.grubisic@uniri.hr)

Abstract. *This research explores the potential of utilizing historical Automatic Identification System (AIS) data on ship tracking for transport network design, model development, and integrating elements within a supply model. Test data collected via a single Software Defined Radio (SDR) AIS receiver were pre-processed and imported into the PTV Visum software. After establishing the fundamental components of the supply model, internal and external zones representing real ports, terminals, or virtual areas of external demand, were constructed and integrated into the model. Finally, a test scenario incorporating traffic demand was developed to simulate traffic flows.*

Keywords: *AIS data processing; maritime model network; maritime traffic flow; PTV-Visum; transport modelling*

University of Zadar

1. INTRODUCTION

Transport models are widely used in road and urban transport for demand modelling, traffic flow simulations, traffic management, and evaluating the efficiency of transport networks [1]. However, their application in maritime transport is limited, as they are primarily designed to reflect the traffic flow dynamics and behaviours in inland transport systems.

Unlike road transport, maritime transport lacks a traditional infrastructure that physically guides vehicles, as well as standard network capacity limitations. Additionally, the dynamics and behaviour of traffic entities influence traffic flow differently than in road transport [8]. In practice, although the main waterways are defined – both general and ship-related, ships can follow multiple routes between origin and destination terminals, with several possible intermediate points where course adjustments occur. Although its primary purpose is ship-to-ship information exchange, the usage of maritime AIS enables the tracking of all ships obliged to carry the system.

The goal of the study was to construct the fundamental elements of a transport network model using AIS data on ship movements, and to propose a rudimental methodology frame for AIS data-driven transport modelling. Based on this data, the model elements, nodes and links, have been automatically generated through a programmed script, imported into the computational model, and their attributes adjusted accordingly.

2. METHODOLOGY

Records of ship movements were collected using a SDR AIS receiver over a period of two characteristic days. The SDR AIS receiver setup comprised a NESDR SMArt v5 SDR [4] connected to a computer via USB interface. This computer ran on a 64-bit Windows 11 operating system, powered by an Intel i5-1135g7 processor and equipped with 16 GB of RAM. The system utilized MathWorks MATLAB® R2022b, along with the Communications Toolbox™ and Communications Toolbox Support Package for RTL-SDR Radio, to control the NESDR SMArt v5 and execute the built-in "Ship Tracking Using AIS Signals" program [5]. On the antenna side, the NESDR SMArt v5 was linked via a male SMA to SO-239 nickel-plated adapter to a 40 m long RG 213/U coaxial cable. This cable was connected to a Marine VHF Glass Fiber Antenna (Scan Antenna VHF74), which is a full half-wave dipole [6]. The antenna was positioned at coordinates 45.3303 N,

14.436 E, at an elevation of 32 m above mean sea level (AMSL). Due to the antenna's position, the data covered the wider area of the Rijeka Bay, including the Port of Rijeka, the Bakar and Omišalj terminals, as well as the ferry terminals in Brestova, Porozina, Merag, and Valbiska.

For pre-processing and statistical data analysis, a script has been written in Python. The pre-processing involved data cleaning and filtering based on the MMSI number as well as screening according to time intervals in which the ship's position was recorded. This approach ensured that individual ship records could be mapped to corresponding objects in the model [7]. The Haversine formula was used to calculate the distance between points, as well as the ship's course and speed. To ensure proper link formation in the model, points located less than 300 meters apart or recorded with a time step of less than one minute were excluded from consideration.

Table 1. Filtering condition to reduce the number of points for selected MMSIs.

MMSI with number of points min =10	
number of ships (before)	47
number of ships (after)	18
average time interval	440

Table 2. Speed distributions for selected MMSIs.

Statistical measure	**Value (knots)**
count	1027
average	13.18
st. dev.	6.06
min	0
median	11.76
max	40

A key step in model development was a creation of the network model, specifically a script for transforming individual ship movement records into network model objects and attributes, namely: nodes, links, and permitted turns within the constructed network. A distinctive feature of this network is that each ship, through its sailing route, defines travel paths in the form of bundles of possible links that connect main nodes or terminals within the transport network.

Zones and connectors were added to the developed model to integrate ports and terminals into the transport network, enabling the generation of traffic demand between origin-destination (OD) pairs. In addition to internal zones, external virtual demand zones were introduced to allow for model testing. A demand matrix was created, representing an arbitrary number of daily ship journeys within the study area.

Finally, a procedure was carried out to assign the arbitrarily generated journeys to the transport network to test the model and visualize the distribution of traffic flows across the target network.

3. RESULTS AND DISCUSSION

The result of the developed model is represented by a digital network, in which 1,900 bidirectional links and 971 nodes were created, allowing for 3,916 interconnections. In the example, 50 journeys were generated and distributed between 9 internal zones (ports and terminals) and 2 external (virtual) zones. Part of it is visualized in **Fig. 1**. The traffic demand assignments are shown in **Fig. 2**. It can be observed that the generated ship journeys follow routes connecting ports and terminals, with maritime flows distributed according to the positions of internal and external centroids and their connectors.

Given the limited study area, it is not possible to fully demonstrate the model's capabilities on a macroscopic level. However, by expanding the coverage area, the model can be integrated into a broader multimodal transport network, which would be the greatest advantage of such a digital model. The model can be used for freight demand modelling [2] and maritime public transport modelling [3], including the analysis of cargo and passenger flows. Prior to this, link speeds and parameters must be calibrated to calculate traffic impedance on specific routes, which also includes impedance at key nodes (anchorages, ports, and terminals).

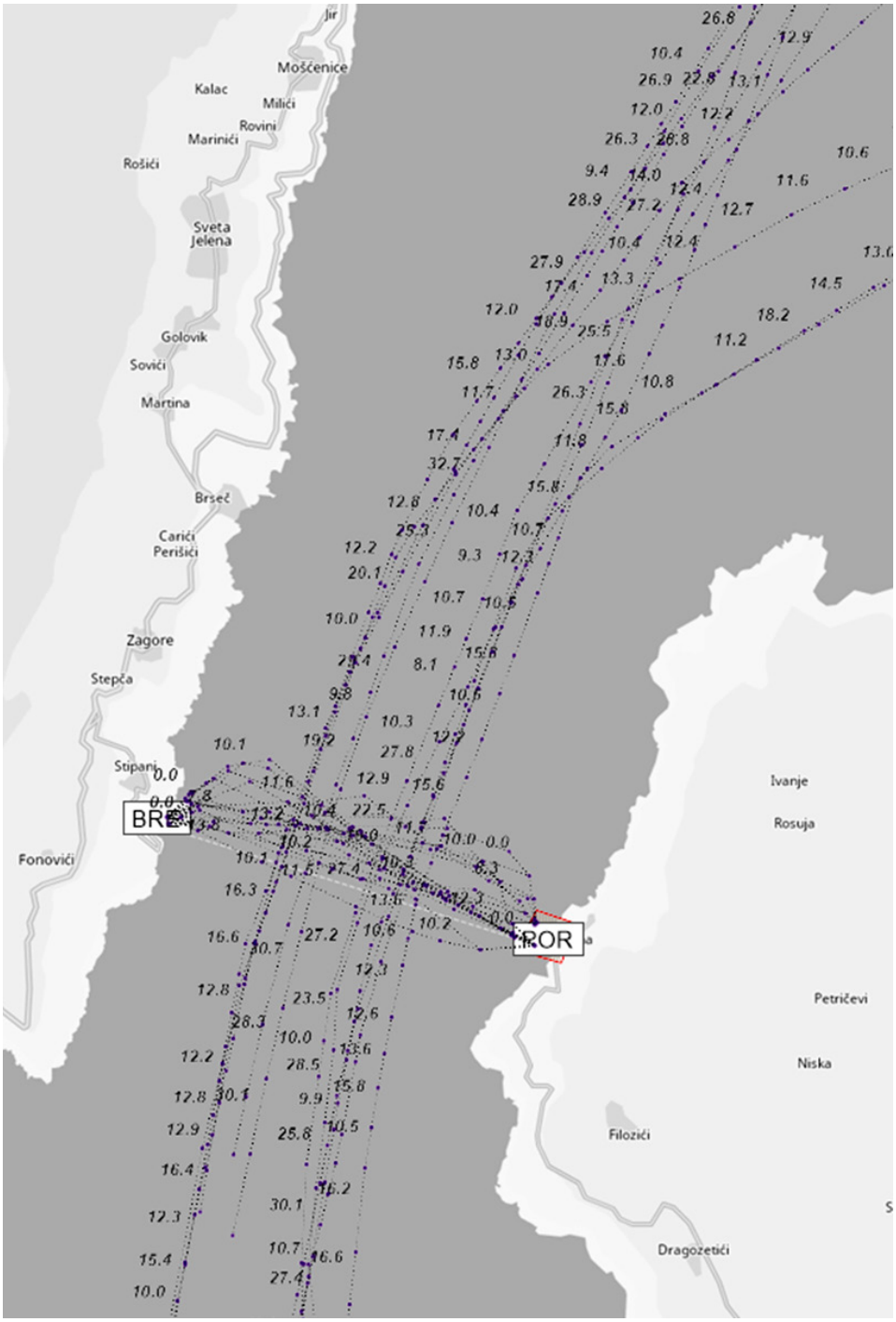

Figure 1. Nodes and links bundle for the selected part of network.

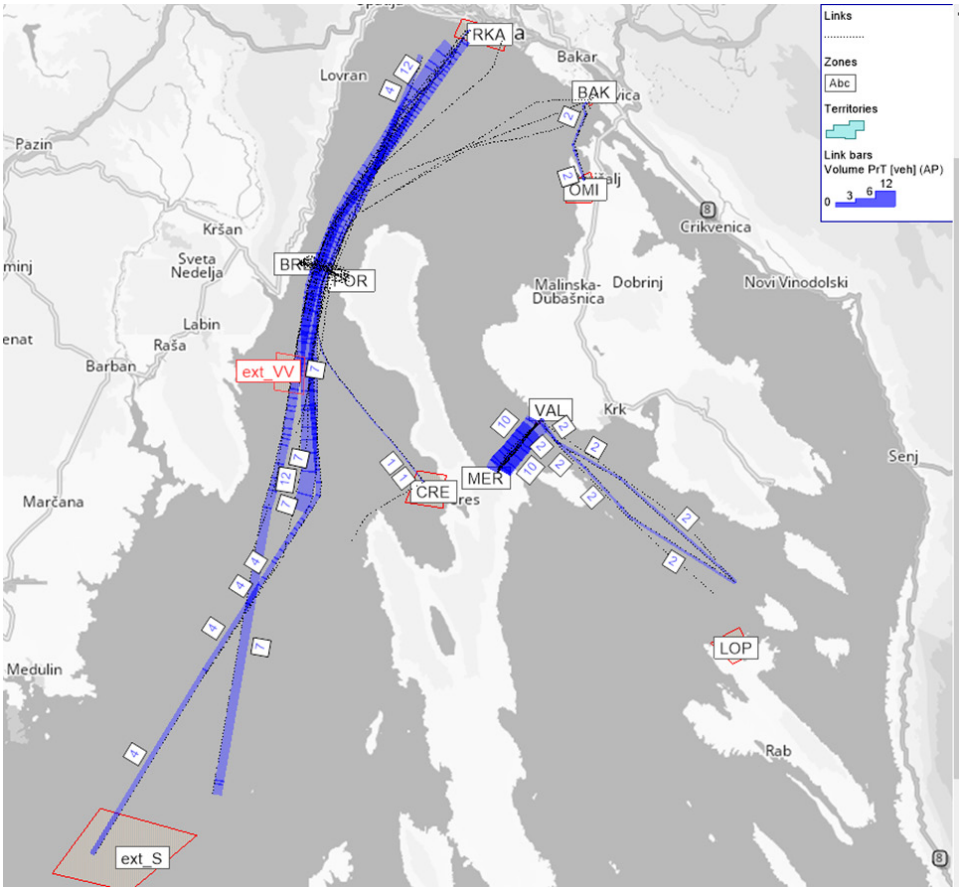

Figure 2. Transport model network with assigned demand.

4. CONCLUSION

This study demonstrates the possibility of utilizing AIS data to develop a maritime transport supply model. By pre-processing ship movement records and integrating them into a digital network, the model successfully simulates traffic flows and identifies key maritime routes. While the study area was limited, the model has the potential for broader applications, including freight demand analysis and maritime public transport planning. Future enhancements, such as improved calibration of link speeds and impedance factors, could further refine its accuracy and applicability within multimodal transport networks. Incorporating real-time AIS data and machine learning techniques could enhance predictive capabilities,

enabling dynamic traffic management and optimising route planning. Expanding the model to include port operations and hinterland connections would further improve its relevance for integrated transport planning.

Acknowledgments: This paper was funded under the project line ZIP UNIRI of the University of Rijeka, for the project UNIRI-ZIP-2103-12-22.

REFERENCES

[1] Barcelo, J., Casas, J., Garcia, D., Perarnau, J. (2005). Methodological Notes on Combining Macro, Meso and Micro Models for Transportation Analysis. *Workshop on Modeling and Simulation*, 2005.

[2] Flitsch, V., Brummerstedt, K. (2015). Freight Transport Modelling of Container Hinterland Supply Chains. *Operational Excellence in Logistics and Supply Chains: Optimization Methods, Data-driven Approaches and Security Insights*. Proceedings of the Hamburg International Conference of Logistics (HICL), Vol. 22 [ISBN:] 978-3-7375-4058-2 [Publisher:] epubli GmbH [Place:] Berlin [Year:] 2015 [Pages:] 233-266.

[3] Grubisic, N., Krljan, T., Biondic, P. (2023). Developing General Transit Feed Specification data for modelling of maritime public service network: The use case for Northern Adriatic Sea network selection. *16th Baska GNSS Conference: Technologies, Techniques and Applications Across PNT and The 3rd Workshop on Smart, Blue and Green Maritime Technologies*. Book of Extended Abstracts, ISSN 2939-1733 (Online).

[4] Nooelec. NESDR SMArt v5 SDR. Available online: https://www.nooelec.com/store/sdr/sdr-receivers/nesdr-smart-sdr.html (accessed on 28 February 2025).

[5] MathWorks®. Ship Tracking Using AIS Signals. Available online: https://uk.mathworks.com/help/comm/ug/ship-trackingusing-ais-signals.html (accessed on 28 February 2025).

[6] Scan-Antenna. VHF74 Datasheet. Available online: https://www.scan-antenna.com/umbraco/surface/product/GetProductForPDF?productId=5365 (accessed on 28 February 2025).

[7] Xiao, F., Ligteringen, H., Gulijk, C., Ale, B. (2015). Comparison study on AIS data of ship traffic behaviour. *Ocean Engineering* 95 (2015), pp 84-93. doi: 10.1016/j.oceaneng.2014.11.020.

[8] Zhou, Y., Daamen, W., Vellinga, T., Hoogendoorn, S. (2019). Review of maritime traffic models from vessel behaviour modelling perspective. *Transportation Research Part C: Emerging Technologies*, 105, pp 323-345, doi: 10.1016/j.trc.2019.06.004.

The 17th Baška Conference
GNSS
Global Navigation Satellite Systems
Green Navigation and Smart Systems

INVESTIGATION OF PIPELINE FLOW DISTRIBUTION FOR UV REACTORS IN SHIP BALLAST WATER TREATMENT SYSTEMS

Andro Rak[1*], Tomislav Mrakovčić[2], Lado Kranjčević[1,3]

[1] University of Rijeka, Faculty of Engineering, Department of Fluid Mechanics and Computational Engineering, Rijeka, Croatia

[2] University of Rijeka, Faculty of Engineering, Department of Thermodynamics and Energy Engineering, Rijeka, Croatia

[3] A Center for Advanced Computing and Modelling, Rijeka, Croatia

[*] *Corresponding author:* Andro Rak (andro.rak@riteh.uniri.hr)

Abstract. *Ballast water management is crucial for preventing the spread of invasive aquatic species and protecting marine ecosystems. This study presents a comprehensive Computational Fluid Dynamics (CFD) analysis of ballast water treatment units (BWTUs) installed in newly built engine rooms. The research focuses on evaluating fluid flow uniformity and volume-flow rate distribution through UV reactors in parallel arrangements. Simulations were conducted for both port and starboard layouts at various flow rates. The study revealed that current pipeline configurations at maximum volume flow rate values exceed manufacturer-recommended flow limits by 2.35% and 4.95% for port and starboard sides, respectively.*

Keywords: *Computational Fluid Dynamics (CFD); Ballast Water Treatment (BWT); UV reactors; RANS; Marine environment*

University of Zadar

1. INTRODUCTION

The global marine ecosystem faces significant challenges, with ballast water management emerging as a critical issue due to its role in introducing invasive species and harmful microorganisms, which cause irreversible ecological and economic impacts [1], [2]. The International Maritime Organization (IMO) has established strict regulations for ballast water treatment systems (BWTS), promoting several technological solutions [3], [4], [5], [6], [7] and methods such as UV irradiation [8], [9]. However, optimizing BWTS performance in confined engine room spaces remains a challenge. This study presents a detailed CFD analysis of BWTUs in a bulk carrier, focusing on flow uniformity and volume flow rate distribution through UV reactors [10].

2. METHODOLOGY

This study investigates fluid flow characteristics in BWTS installed in confined ship engine rooms using CFD. The examined BWTS consists of two BWTUs, each equipped with two parallel UV reactors, positioned on the port and starboard sides of a self-discharging bulk carrier engine room. Accurate distribution of seawater flow between parallel UVRs is crucial to avoid exceeding individual reactor capacities and to ensure adequate treatment efficiency.

To perform the CFD analysis, simplified 3D CAD models were developed, representing pipeline segments downstream from the filter outlet to at least three pipe diameters beyond the UVRs. Numerical simulations were conducted using ANSYS Fluent at nominal inlet flow rates of 1900, and 2000 m^3/h. The seawater was modelled with density, kinematic viscosity, and dynamic viscosity corresponding to a temperature of 30°C. Turbulent flow was simulated using Reynolds-Averaged Navier-Stokes (RANS) equations with the realizable k-ε turbulence model and included the wall function.

Mesh sensitivity study ensured numerical accuracy, resulting in meshes comprising approximately 2.8 million cells per case. Mesh quality metrics, such as skewness below 0.75 and orthogonal quality above 0.25, were maintained alongside appropriate wall y^+ values between 30 and 300. Simulations achieved convergence criteria with residuals for velocity reaching 10^{-5} and turbulence parameters stabilizing at approximately 10^{-3} to 10^{-4}. Results were averaged over the final simulation iterations to provide stable representations of flow conditions for subsequent analysis.

3. RESULTS AND DISCUSSION

The CFD analysis revealed significant challenges in achieving uniform seawater flow distribution within the existing pipeline layouts for both port and starboard BWTUs. At the maximum nominal volume flow rate of 2000 m³/h, both layouts exceeded the manufacturer's recommended limit of 1000 m³/h per UV reactor. Specifically, the starboard side exhibited a relative error of +4.95%, while the port side showed +2.35%. Consequently, an operational reduction of approximately 5% was required to remain within safe operational limits.

Table 1. Volume flow rate values at the UVR inlet surfaces with relative error for port and starboard pipeline layouts.

Nominal flow	Port side BWTU			Starboard side BWTU		
	Pipe Type	Q [m³/h]	ε_r [%]	Pipe Type	Q [m³/h]	ε_r [%]
2000 m³/h	Main Pipe	1023.54	2.35	Main Pipe	1049.49	4.95
	Side Pipe	973.06	-2.69	Side Pipe	947.35	-5.26
1900 m³/h	Main Pipe	972.54	-2.75	Main Pipe	996.96	-0.3
	Side Pipe	924.43	-7.56	Side Pipe	899.98	-10

Detailed visualization of velocity streamlines indicated that sharp geometrical transitions, such as abrupt T-junctions and bends, generated pronounced vortical structures and regions of high turbulence upstream of UVRs. For instance, in the starboard layout, a strong vortex formed immediately after a large T-junction due to a complex pipe geometry that included a curved lower pipe segment. This vortex persisted along the straight pipeline section, significantly disturbing flow uniformity before entering the UV reactors.

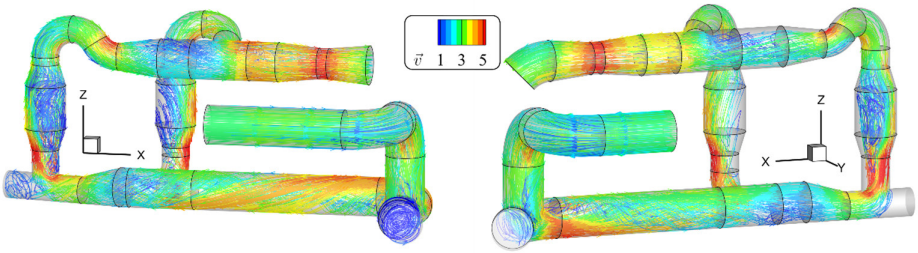

a) b)

Figure 1. Port and starboard side pipeline layout for BWTUs with streamlined representation of velocity magnitude for the nominal volume flow rate of 2000 m³/h.

The study demonstrated clearly that CFD simulations provide valuable insightinto practical engineering challenges faced during BWTS installation onboard ships. By highlighting specific geometric features responsible for turbulent disturbances and uneven flow distributions, this analysis offered actionable recommendations for more efficient solutions.

4. CONCLUSION

This CFD study evaluated fluid flow characteristics in ballast water treatment units (BWTUs) installed onboard a self-discharging bulk carrier engine room. Analyses revealed uneven seawater distribution between parallel UV reactors, exceeding recommended operational limits at maximum nominal capacities due to turbulent vortices generated by sharp pipeline geometries.

The findings underscore the critical role of CFD in diagnosing practical engineering problems related to ballast water management onboard ships. By using CFD tools with strategic geometric adjustments even within confined spaces, improvements can be made that align with environmental standards while reducing operational risks associated with ballast water treatment systems.

REFERENCES

[1] D. Minchin, "Aquaculture and transport in a changing environment: Overlap and links in the spread of alien biota," *Mar Pollut Bull*, vol. 55, no. 7–9, pp. 302–313, Jan. 2007, doi: 10.1016/J.MARPOLBUL.2006.11.017.

[2] J. L. Molnar, R. L. Gamboa, C. Revenga, and M. D. Spalding, "Assessing the global threat of invasive species to marine biodiversity," *Front Ecol Environ*, vol. 6, no. 9, pp. 485–492, Nov. 2008, doi: 10.1890/070064.

[3] B. Werschkun *et al.*, "Emerging risks from ballast water treatment: The run-up to the International Ballast Water Management Convention," *Chemosphere*, vol. 112, pp. 256–266, 2014, doi: 10.1016/J.CHEMOSPHERE.2014.03.135.

[4] R. Balaji, O. Yaakob, and K. K. Koh, "A review of developments in ballast water management," *Environmental Reviews*, vol. 22, no. 3, pp. 298–310, 2014, doi: 10.1139/ER-2013-0073.

[5] G. Bakalar, "Comparisons of interdisciplinary ballast water treatment systems and operational experiences from ships," *Springerplus*, vol. 5, no. 1, pp. 1–12, Dec. 2016, doi: 10.1186/S40064-016-1916-Z.

[6] A. Vorkapić, R. Radonja, and D. Zec, "Cost efficiency of ballast water treatment systems based on ultraviolet irradiation and electrochlorination," *Promet - Traffic and Transportation*, vol. 30, no. 3, pp. 343–348, Jun. 2018, doi: 10.7307/PTT.V30I3.2564.

[7] B. Sayinli, Y. Dong, Y. Park, A. Bhatnagar, and M. Sillanpää, "Recent progress and challenges facing ballast water treatment – A review," *Chemosphere*, vol. 291, Mar. 2022, doi: 10.1016/J.CHEMOSPHERE.2021.132776.

[8] E. Tsolaki and E. Diamadopoulos, "Technologies for ballast water treatment: A review," *Journal of Chemical Technology and Biotechnology*, vol. 85, no. 1, pp. 19–32, Jan. 2010, doi: 10.1002/JCTB.2276.

[9] B. Werschkun, Y. Sommer, and S. Banerji, "Disinfection by-products in ballast water treatment: An evaluation of regulatory data," *Water Res*, vol. 46, no. 16, pp. 4884–4901, Oct. 2012, doi: 10.1016/J.WATRES.2012.05.034.

[10] N. D. Thach and P. Van Hung, "Development of UV reactor controller in ballast water treatment system to minimize the biological threat on marine environment," *J Sea Res*, vol. 198, Apr. 2024, doi: 10.1016/J.SEARES.2023.102465.

The 17th Baška Conference
GNSS
Global Navigation Satellite Systems
Green Navigation and Smart Systems

WI-FI VULNERABILITIES IN MARITIME OPERATIONS: RISK ASSESSMENT AND DETECTION STRATEGIES

Marko Vukšić*, Jasmin Ćelić, Ivan Panić, Aleksandar Cuculić

University of Rijeka, Faculty of Maritime Studies, Rijeka, Croatia
* *Corresponding author:* Marko Vukšić (marko.vuksic@pfri.uniri.hr)

Abstract. *The maritime industry is becoming more reliant on digital connectivity, making cybersecurity a serious concern. This study investigates vulnerabilities in marine Wi-Fi networks, focusing on threats such as Man-in-the-Middle (MitM) attacks and rogue access points. Using WiFi Pineapple Mark VII, real-world cyber threats were simulated to assess risks and demonstrate the value of proactive security measures. The findings confirm the effectiveness of penetration testing in detecting network problems. However, physical proximity restrictions limit the possibility of an attack at sea. To improve security, the marine sector should implement industry best practices such as network segmentation, intrusion detection systems, and regular security audits.*

Keywords: *Cyber security; Cyber resilience; Navigation System Hacking; Wi-Fi; WiFi Pineapple*

University of Zadar

1. INTRODUCTION

The maritime sector is undergoing major changes, driven by digitalization, automation, and system integration that aim to improve safety, efficiency, and sustainability [1]. However, this shift also increases vulnerability to cyber risks, affecting both operational safety and economic aspects. Ships rely heavily on connectivity via VSAT, GSM/LTE, and Wi-Fi, making their networks exposed to similar threats as land-based systems. Rough sea environments make protection even more difficult. Despite progress, regulation gaps and limited awareness often prevent effective cybersecurity implementation [2].

2. METHODOLOGY

Wi-Fi networks in maritime operations are exposed to similar vulnerabilities to those found in shore – based systems, with slight difference regarding the connectivity issues experienced on vessels. The most significant threats are Man-in-the-Middle (MitM) attacks and rogue access points (APs), that can be easily detected through the use of tools such as WiFi Pineapple Mark VII [3]. A rogue AP attack, using the "evil twin" tactic (**Fig. 1**), when an unauthorized device mimics a legitimate Wi-Fi network to lure users into connecting, enables attackers to intercept sensitive data, inject malicious payloads, or steal credentials. The WiFi Pineapple works in a way that it allows deauthentication attacks through automated MitM techniques that force devices to reconnect through a rogue AP [3].

Another threat that maritime Wi-Fi is vulnerable to is jamming caused by interference with shipboard communication and security systems. Moreover, as part of a larger cyber-physical assault, multi-frequency jammers can render networks inoperable [5]. Conversely, passive eavesdropping tools like Wireshark allow attackers to capture and analyse unencrypted data packets for the purpose of revealing credentials and sensitive information [6]. A wide range of tools is used by cybersecurity experts to evaluate these threats. Some of those tools are used for detecting rogue APs and unauthorized devices like wireless monitoring solution Kismet detect [7], while on the other hand the Aircrack-ng suite tests Wi-Fi encryption strength through WPA handshake capture and decryption attempts [8]. These tools emphasize the need for proactive security measures through network segmentation and intrusion detection systems [9]. The authors used an outside-in approach with the aim of detecting Wi-Fi vulnerabilities by using WiFi Pineapple Mark VII tool. The method focuses on external exploration

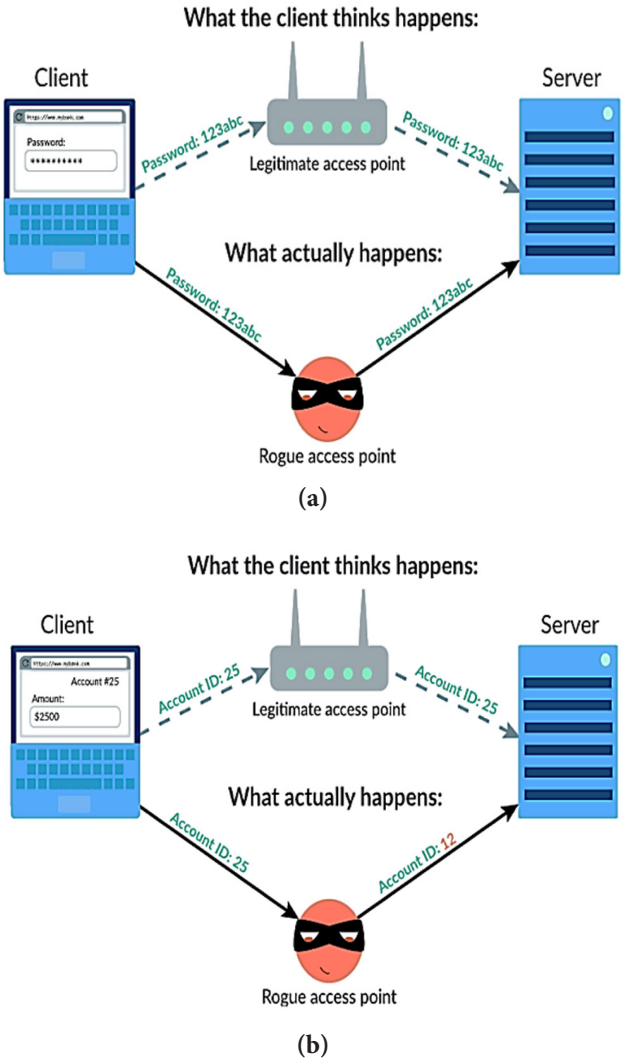

Figure 1. Two techniques rogue access points use to capture data: (a) Passive interception; (b) Active interception [4].

and exploitation through simulation of real-world adversary tactics. For that reason, because of its ability to identify auto-connect behaviours, execute targeted deauthentication attacks, and establish MitM positions for traffic interception, the WiFi Pineapple was chosen [10]. Given the increasing reliance of modern vessels on VSAT, LTE, and onboard Wi-Fi, it is essential to recognize wireless networks as potential attack vectors. Industry guidelines emphasize the importance of treating all wireless networks as unsecured and keeping them

separate from critical shipboard systems [11]. To protect maritime digital infrastructure, it is crucial to enhance security through advanced monitoring tools and a defence-in-depth approach.

3. RESULTS AND DISCUSSION

As a result of an outside – in approach WiFi Pineapple Mark VII has proven its effectiveness in determining main vulnerabilities within maritime Wi-Fi networks. Through testing, this device has proven its ability to detect auto-connect behaviours, execute deauthentication attacks, and establish a Man-in-the-Middle (MitM) position to intercept and manipulate network traffic. These findings highlight serious security risks posed by unsecured wireless systems onboard vessels. The goal of these methods was to simulate real-world adversary actions, to emphasize the need for proactive cybersecurity measures in maritime operations (**Fig. 2**).

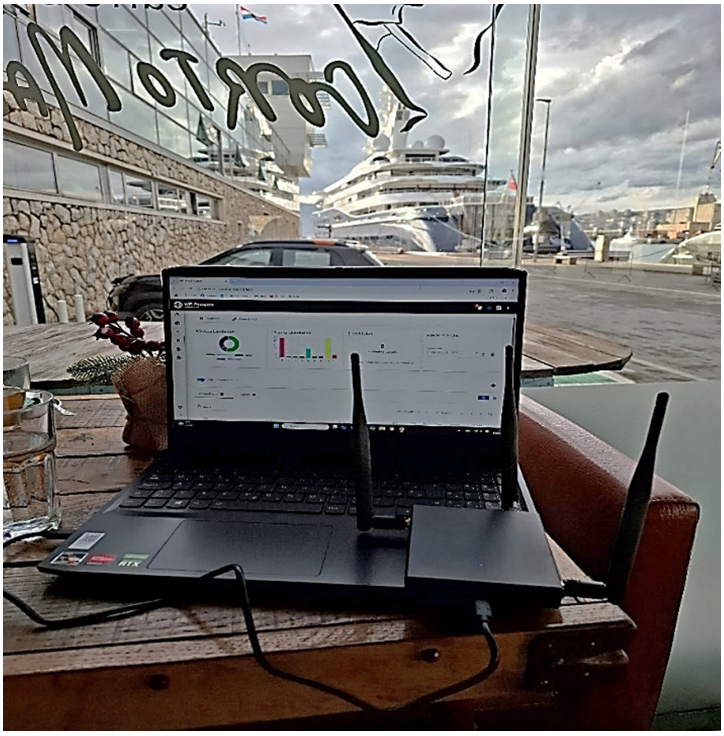

Figure 2. Detection of Ship's Wi-Fi Network Vulnerabilities Using WiFi Pineapple Mark VII at the Rijeka Terminal.

Regardless of its effectiveness, the WiFi Pineapple's problem lies in reliance on physical proximity, which means that an attacker needs to be close to the target, which is quite difficult in open sea environments. Moreover, the ship's metal structure can obstruct signals, therefore, attackers may need to deploy multiple devices or focus efforts on specific areas of the vessel. Although tools like the WiFi Pineapple can reveal vulnerabilities, the success of a cyberattack ultimately depends on user practices and system configurations. Identifying rogue access points requires compliance with industry guidelines, such as those from NIST and BIMCO, that put emphasis on the importance of isolating critical systems from general Wi-Fi access and implementing wireless intrusion detection systems (WIDS/WIPS) **[10-14]**. To better contextualize these risks, it is important to understand the communication standards and technical limitations of the tested onboard equipment. Tested shipboard devices operated under widely used IEEE 802.11 standards, including 802.11n and 802.11ac. These standards support substantial ranges in optimal conditions—up to 600 feet (approximately 180 meters) for 802.11ac in open environments. However, test results confirmed that metallic ship structures significantly reduce range and signal stability, further complicating the execution of attacks like MitM or rogue APs without close proximity. Recognizing these limitations supports the case for using specialized tools such as WiFi Pineapple, which can identify these vulnerabilities early. A comprehensive risk management approach combining proactive detection, regular security audits, and real-time monitoring is essential for improving cybersecurity onboard modern vessels.

4. CONCLUSION

The growing use of Wi-Fi on cruise ships brings notable cybersecurity challenges that require structured protection. Industry frameworks exist, yet practical vulnerabilities are still present. Passengers, for example, might exploit network weaknesses through rogue access points or Man-in-the-Middle (MitM) attacks. While rare, such threats should not be ignored. Crew members, though not malicious, could unintentionally connect to these networks. If compromised, their devices might later access sensitive systems. Regular penetration testing, monitoring, and network segmentation—combined with crew training and awareness—are key steps in reducing cyber risks and protecting both operations and data.

REFERENCES

[1] Hirata, E.; Watanabe, D.; Lambrou, M. Shipping Digitalization and Automation for the Smart Port. Supply Chain - Recent Advances and New Perspectives in the Industry 4.0 Era. IntechOpen. 2022, n. pag. https://doi.org/10.5772/intechopen.102015.

[2] Kavallieratos, G.; Katsikas, S.; Gkioulos, V. Cyberattacks against the autonomous ship. In Computer Security; Springer: Berlin/Heidelberg, Germany, 2018; pp. 20–36. https://doi.org/10.1007/978-3-030-12786-2_2.

[3] Lutkevich, B. (2022, October 14). Wi – Fi PineApple. Search Security. https://www.techtarget.com/searchsecurity/definition/Wi-Fi-Pineapple#:~:text=A%20Wi,company%E2%80%99s%20system%2C%20network%20or%20infrastructure (accessed on 2 February 25).

[4] Khan Academy. (n.d.). https://www.khanacademy.org/computing/computers-and-internet/xcae6f4a7ff015e7d:online-data-security/xcae6f4a7ff015e7d:cyber-attacks/a/rogue-access-points-mitm-attacks (accessed on 17 February 25).

[5] Editor. (2021, October 21). Jamming - It's not just for GPS anymore! - RNTF. RNTF. https://rntfnd.org/2021/01/06/jamming-its-not-just-for-gps-anymore/#:~:text=It%20is%20the%20professional%20car,Even%20a%20police%20car (accessed on 20 February 25).

[6] What is Wireshark and how to use it | Cybersecurity | CompTIA. (n.d.). CompTIA. https://www.comptia.org/content/articles/what-is-wireshark-and-how-to-use-it#:~:text=Wireshark%20is%20a%20network%20protocol,in%20a%20typical%20Ethernet%20network (accessed on 20 February 25).

[7] Kismet | CISA. (n.d.). Cybersecurity and Infrastructure Security Agency CISA. https://www.cisa.gov/resources-tools/services/kismet#:~:text=Kismet%20is%20a%20console%20%28ncurses%29,estimated%20ranges%20on%20downloaded%20maps (accessed on 15 February 25).

[8] Aircrack-ng. (n.d.). https://www.aircrack-ng.org/#:~:text=Aircrack,to%20assess%20WiFi%20network%20security (accessed on 10 February 25).

[9] ShipUniverse.com. (n.d.). Maritime Cybersecurity Threats in 2025: Top 10 ways Hackers are targeting your fleet – Ship Universe. https://www.shipuniverse.com/maritime-cybersecurity-threats-in-2025-top-10-ways-hackers-are-targeting-your-fleet/#:~:text=,of%20critical%20data%20and%20systems (accessed on 10 february 25).

[10] WiFi PineApple Mark VII | WiFi PineApple Mark VII. (n.d.). https://docs.hak5.org/wifi-pineapple (accessed on 20 February 25).

[11] Bimco. (2021, January 4). The guidelines on cyber security onboard ships. Bimco. chrome-extension://efaidnbmnnnibpcajpcglclefindmkaj/https://www.ics-shipping.org/wp-content/uploads/2021/02/2021-Cyber-Security-Guidelines.pdf (accessed on 15 february 2025).

[12] Bothur, D., Zheng, G., & Valli, C. (2017). A critical analysis of security vulnerabilities and countermeasures in a smart ship system.

[13] ClassNK. (2022). Guidelines for designing cyber security onboard ships (2nd ed.). ClassNK. chrome-extension://efaidnbmnnnibpcajpcglclefindmkaj/https://www.nextdeal.gr/sites/default/files/sitefiles_2020-07/guidelines_for_designing_cyber_security_onboard_ships.pdf (accessed on 20 February 25).

[14] International Maritime Organization (IMO). (2021). Guidelines on maritime cyber risk management (MSC-FAL.1/Circ.3). IMO. https://portswigger.net/daily-swig/secure-by-design-classnk-updates-maritime-cybersecurity-guidelines (accessed on 25 February 2025).